

December 2018

Novel Engineered Porous Materials for the Removal of Lead from Water

Mohsen Hajipour Hajipour Manjili
University of Wisconsin-Milwaukee

Follow this and additional works at: <https://dc.uwm.edu/etd>

 Part of the [Materials Science and Engineering Commons](#)

Recommended Citation

Hajipour Manjili, Mohsen Hajipour, "Novel Engineered Porous Materials for the Removal of Lead from Water" (2018). *Theses and Dissertations*. 1991.
<https://dc.uwm.edu/etd/1991>

This Dissertation is brought to you for free and open access by UWM Digital Commons. It has been accepted for inclusion in Theses and Dissertations by an authorized administrator of UWM Digital Commons. For more information, please contact open-access@uwm.edu.

**NOVEL ENGINEERED POROUS MATERIALS FOR THE REMOVAL OF
LEAD FROM WATER**

by

Mohsen Hajipour Manjili

A Dissertation Submitted in
Partial Fulfillment of the
Requirements for the Degree of

**Doctor of Philosophy
in Engineering**

at

The University of Wisconsin-Milwaukee

December 2018

ABSTRACT

NOVEL ENGINEERED POROUS MATERIALS FOR THE REMOVAL OF LEAD FROM WATER

by

Mohsen Hajipour Manjili

The University of Wisconsin-Milwaukee, 2018
Under the Supervision of Dr. Nidal Abu-Zahra and Dr. Marcia Silva

The estimated average blood lead level for the population younger than 5 years in the United States is approximately 100 times higher than ancient background levels, indicating that substantial sources of lead exposure exist in the environment. This research is focused on the removal of lead from water with a functionalized zeolite. Functionalization improves adsorption behavior to achieve adsorbent materials with high capacity and stability with potential multiple re-uses.

The lead sorption from water onto an Australian zeolitic mineral (clinoptilolite) unmodified and modified with sulfide-based reagents is investigated with batch and fixed bed column experiments. The effect of solution pH, functional groups' concentration, and competing ions are studied on the adsorption behavior.

Functional groups stability and particles regeneration are also examined. The idea of functionalizing zeolite with sulfides for the removal of lead is able to develop a unique adsorbent material. The use of reactive sulfides attached to zeolite is a novel development.

The functionalized zeolite was characterized by Fourier transform infrared spectroscopy (FTIR), thermogravimetric analysis (TGA), scanning electron microscope (SEM) and energy disperse spectroscopy (EDS). The reactivity, sorption kinetics behavior, and retention isotherms for lead were determined to permit modeling and design of processes for optimum contaminant removal.

The significance of this research work is realized by its ability to create an engineered mesoporous-macroporous medium for lead adsorption by incorporating the functionality into the natural zeolite; this is accomplished using sulfides-based reagents. Sulfide-based reagents are ideal candidates for heavy metal remediation applications because of their soft basic frameworks, which should show increased affinity toward softer Lewis acids. The functional design and data analysis are significant to the scientific community, and are fundamental for the water industry, as they provide the knowledge necessary for developing next-generation water

filtration media using zeolite materials.

Dedication

Every challenging work needs self-efforts as well as guidance of elders especially those who were very close to our heart.

My humble effort I dedicate to my sweet and loving

Mother & Father & Wife

Whose affection, love, encouragement, and prays of day and night make me able to get such success and honor,

Along with all hard working and respected

Teachers

TABLE OF CONTENTS

Chapter 1: Introduction and Literature Review.....	1
Introduction	2
Literature Review	4
Zeolites	6
Removal Technologies for Heavy Metals from Water.....	17
Ion Exchange Materials Properties.....	18
Adsorption	20
Metal ion complexation references should be updated	20
Lead Complexation Forms	23
Theory of Adsorption	25
Adsorption Kinetics and Mechanisms.....	27
Langmuir Model.....	29
Freundlich Model	30
Pseudo Model (n-order).....	30
Adsorbents.....	31
Chapter 2: Research Objectives and Novelty.....	37
Research Principles	38

Project Objectives.....	38
Project Hypothesis.....	39
Research Novelty and Significance.....	39
Chapter 3: Materials and Methods and Experimental Design.....	41
Materials.....	42
Zeolite functionalization.....	42
Cystamine Dihydrochloride Ceolite.....	42
Zinc Sulfide Zeolite.....	42
Characterization of Materials.....	43
Adsorption Experiments.....	44
Lead Sorption Isotherms.....	44
Lead Sorption Kinetics.....	44
Column Test and Particles Regeneration.....	45
Chapter 4.....	47
Zeolite processing.....	48
Zeolite physical properties.....	49
Equilibrium Adsorption Experiments for Lead.....	58
Adsorption Isotherms.....	63

Mechanism and Kinetics: Pseudo Model and Diffusion Studies	69
Effect of Cystamine Loadings on Removal Efficiency	76
Leaching of Cystamine Groups from Functionalized Zeolites.....	78
ZnS-Z Fabrication	81
Zeolite Functionalization with Sulfide Nanostructures	82
Effect of Competing Ions on ZnS-S' Removal Efficiency.....	85
ZnS-Z Particles Regeneration.....	87
Chapter 5: Application of Isotherm Models to Predict: Equilibrium Concentration, Removal Efficiency, Adsorption Capacity, and Required Amount of Adsorbent ..	91
Langmuir Isotherm	92
Modified Langmuir Equation	97
Freundlich Isotherm.....	102
pH-dependent Model	105
Chapter 6: Conclusions.....	110
Conclusions	110
References	113
Curriculum vitae.....	137

LIST OF FIGURES

Figure 1. An example of complex ion.....	21
Figure 2. Holodirected coordination environment of Pb (left) and hemidirected environment of (right) [77].....	24
Figure 3. Acid and base categories in the periodic table.....	48
Figure 4. SEM images for: (a) CZ and (b) CDHZ ¹ : no significant change in structure is seen after functionalization process.....	55
Figure 5. Sulfur distribution on CDHZ ¹ : sulfur distribution on CDHZ ¹	56
Figure 6. FTIR spectra of CDHZ ¹	57
Figure 7. TGA plot of: (a) CZ and (b) CDHZ ¹	58
Figure 8. Pourbaix diagram for Pb.....	60
Figure 9. Zeta potential of CDHZ ¹ at different pH values.....	61
Figure 10. pH effect on residual concentration of lead for CDHZ ¹	62
Figure 11. Isotherm plot of CZ and CDHZ ¹	65
Figure 12. The four main shapes of isotherms [142].....	66
Figure 13. Isotherm models: (a) and (b) show Longmuir model for CZ and CDHZ ¹ , respectively. (c) and (d) show Freundlich model for CZ and CDHZ ¹ , respectively.	67
Figure 14. Pb adsorption schematics on CDHZ ¹	69

Figure 15. Pseudo isotherm models: (a)-(b) Pseudo first order model before and after the interruption, (c)-(d) Pseudo second order model before and after the interruption, respectively.....	70
Figure 16. Diffusion model schematics.....	71
Figure 17. Interruption test results for: (a) CZ, (b) CDGHZ ¹	74
Figure 18. Particle diffusion model plot.....	75
Figure 19. ZnS-Z fabrication schematic.....	82
Figure 20. SEM images of ZnS-Z: ZnS nano particles.	84
Figure 21. EDS plot for ZnS-Z: zinc and sulfur in ZnS-Z.	84
Figure 22. Column test schematic.	88
Figure 23. Regeneration cycles for Pb removal by using ZnS-Z.	90
Figure 24. Isotherm plot for lead removal tests by using ZnS-Z at pH = 5.....	93
Figure 25. Langmuir plot for lead removal tests by using ZnS-Z at pH = 5.....	94
Figure 26. Calculated versus experimental values of C_e , by using Langmuir model.	96
Figure 27. Freundlich plot for lead removal tests by using ZnS-Z at pH = 5.	103
Figure 28. Calculated versus experimental values of C_e , by using Freundlich model.	105
Figure 29. Langmuir plots for lead removal tests by using ZnS-Z: (a) pH = 3, (b) pH = 4.....	107
Figure 30. Langmuir constant (K_L) vs. pH for lead adsorption on ZnS-Z.	108

Figure 31. Predicted versus experimental values of C_e : (a) pH = 3, (b) pH = 4, (c) pH = 5.109

LIST OF TABLES

Table 1. The maximum contaminant limit (MCL) of heavy metals, reported by US-EPA [2].	2
Table 2 Literature review of heavy metal removal from wastewater.	14
Table 3. Principal valence and coordination number of selected metals.	21
Table 4. Metal complexes schematics.	22
Table 5. Summary of experimental design for the objectives.	45
Table 6. Porosity parameters of zeolite.	49
Table 7. EDS analysis for CZ and salt treated zeolites.	50
Table 8. Required number of sulfur atoms in lead adsorption.	52
Table 9. EDS analysis for zeolite and cystamine functionalized zeolites.	54
Table 10. Expected improvement in the zeolite's adsorption capacity.	55
Table 11. Experimental factors.	58
Table 12. Isotherm constants for CZ and CDHZ ¹ .	67
Table 13. Pseudo model parameters.	70
Table 14. Particle diffusion parameters.	76
Table 15. EDS analysis for CDHZ ¹ and CDHZ ² .	77
Table 16. Cystamine dihydrochloride and sulfur loadings on zeolite.	79
Table 17. Sulfur concentration in Ultra-high purity water batch.	80
Table 18. Cystamine groups loss in Ultra-high purity water batch.	80

Table 19. Sulfur concentration in lead removal batch.....	80
Table 20. Cystamine groups loss in lead removal batch.	81
Table 21. Reactant amounts and experimental parameters for sonochemical preparation of ZnS-Z.	83
Table 22. Atomic percent of O, Si, Zn, and S in CZ and ZnS-Z.....	85
Table 23. Removal efficiency and distribution coefficient at equilibrium time.....	87
Table 24. Column test parameters.	89
Table 25. Removal efficiency for regenerated ZnS-Z particles.	90
Table 26. Langmuir model parameters for lead removal tests by using ZnS-Z at pH = 5.....	94
Table 27. Calculated values of the modified Langmuir model for ZnS-Z at pH = 5.	101
Table 28. Freundlich isotherm constants for ZnS-Z at pH = 5.....	104
Table 29. Langmuir isotherm parameters for lead adsorption on ZnS-Z at pH = 3 and pH = 4.	107

LIST OF ABBREVIATIONS

1/n	Degree of nonlinearity between solution concentration and adsorption
AC	Activated carbon
C ₀	Initial concentration
CEC	Cation Exchange Capacity
CDB	Contaminants disinfection byproducts
CDHZ*	Cystamine hydrochloride zeolite with no pretreatment
CDHZ ¹	Cystamine hydrochloride zeolite with, 1 mmol
CDHZ ²	Cystamine hydrochloride zeolite with, 2 mmol
C _e	Equilibrium concentration
CNT	Carbon nanotube
c _t	Concentration at time t
CZ	Clean zeolite
D	Diffusion coefficient
EDS	Energy dispersive spectroscopy
EPA	Environmental Protection Agency
FTIR	Fourier Transform Infrared Spectroscopy
HDTMA	hexadecyltri-methylammonium
HSAB	hard and soft acids and bases
ICP-MS	Inductively coupled plasma mass spectrometry

J	Diffusion flux
K_d	Distribution coefficient
K_F	Freundlich constant
K_L	Langmuir constant
KML	Modified Longmuir constant
K_p	Pseudo constant
K_{P1}	Pseudo first order
K_{P2}	Pseudo second order
LC-MS	Liquid chromatography mass spectrometry
M	Adsorbent mass
MCL	Maximum contaminant limit
MCLG	Maximum Contamination Level Goals
ppb	parts per billion
ppm	parts per million
q	Surface coverage
q_e	Equilibrium adsorption capacity
q_{max}	Maximum adsorption capacity
q_t	Adsorption capacity at time t
R	Removal efficiency
r	Adsorbent radius

R^2	R-squared
r_a	Rate of adsorption
r_d	Rate of desorption
SEM	Scanning electron microscope
t	Time
TGA	Thermogravimetric analysis
USGS	United States Geological Survey
V	Solution volume
WHO	World Health Organization
ZnS-Z	Zinc sulfide zeolite

ACKNOWLEDGMENTS

Firstly, I would like to express my sincere gratitude to my advisors Dr. Nidal H. Abu-Zahra and Dr. Marcia Silva for the continuous support of my Ph.D. study and related research, for their patience, motivation, and immense knowledge. Their guidance helped me in all the time of research and writing of this thesis. I could not have imagined having better advisors for my Ph.D. study.

Besides my advisors, I would like to thank the rest of my thesis committee: Dr. Benjamin Church, Dr. Junjie Niu, Dr. David Garman, and Dr. Peter Hinow, for their insightful comments and encouragement, but also for the hard questions which incited me to widen my research from various perspectives.

My sincere thanks also go to Patrick Anderson from the School of freshwater Sciences for scheduling and setting up the ICP-MS which was significant for the performance analysis in this research work. I am also grateful to Dr. Anna Benko from the Shimadzu Center and Dr. Heather Owen from the Biology Department for their guidance and assistance in the LC-MS and SEM-EDS analysis, respectively.

I would also like to thank my industry mentors from A.O. Smith, Pentair, KX

Technologies, Graver Technologies, Veolia, Wattswater, Ecolab, and MWRD companies who participated in my research work.

Last but not least, I must express my very proudful gratitude to my parents, to my sisters, to my brother, and to my wife for providing me with unfailing support and continuous encouragement throughout my years of study and through the process of researching and writing this thesis. This accomplishment would not have been possible without them. Thank you.

This project was supported by National Science Foundation Industry/University Cooperative Research Center on Water Equipment & Policy located at University of Wisconsin-Milwaukee (IIP-1540032) and Marquette University (IIP-1540010)

Mohsen Hajipour Manjili

Chapter 1

Introduction and Literature Review

Introduction

The term heavy metal has particular application to elements having atomic weight between 53.5 and 200.6 g/mol such as cadmium (Cd), mercury (Hg), lead (Pb), and arsenic (As) [1].

Lead is a naturally occurring toxic heavy metal with significant adverse impacts on the environment, human health, and ecological systems. The United States Environmental Protection Agency (EPA) and the World Health Organization (WHO) list lead and its compounds as toxic pollutants. The maximum contaminant limit (MCL) of heavy metals, reported by the EPA [2] is summarized in Table 1. Human body and its organisms require known trace amounts of some heavy metals, such as cobalt, copper, iron, manganese, molybdenum, vanadium, strontium, and zinc. Excess levels of essential metals, however, can be detrimental to organisms, particularly humans [3].

The main sources of the heavy metals in the environment can be divided into three major groups: (a) natural sources of heavy metals, (b) agricultural sources of heavy metals, and (c) industrial sources of heavy metals [4].

Table 1. The maximum contaminant limit (MCL) of heavy metals, reported by US-EPA [2].

Heavy metal	Human Toxicity impacts	MCL (ppm) water
Arsenic	Skin manifestation, visceral cancers, vascular diseases	0.050
Cadmium	Kidney damage, renal disorder, human carcinogenic	0.01
Chromium	Headache, diarrhea, nausea, vomiting, carcinogen	0.05
Copper	Liver damage, Wilson disease, insomnia	0.25
Nickel	Dermatitis, nausea, chronic asthma, coughing, human carcinogen	0.20
Zinc	Depression, lethargy, neuroglial signs and increased thirst	0.80
Lead	Damage to fetal brains, disease of the kidneys, circulatory system, and nervous system	0.006
Mercury	Rheumatoid arthritis, and diseases of kidneys, circulatory system, and nervous system	0.00003

The EPA developed Surface Water Treatment Rules (SWTR) to improve the qualities of drinking water in November 2016. The regulations provide protection

from disease-causing pathogens and contaminants, as well as protection against disinfection byproducts (DBP) that can form during drinking water treatment. They also provide guidance documents to help public water utilities implement the contamination management rules [6]. The recommended treatment technologies remove or destroy pollutants in water. Federal laws require the EPA to provide a cost estimation for new drinking water standards. There are three major components of the final cost: treatment, monitoring, and administrative costs. Several engineering models have been developed to estimate the treatment costs using a bottom-up approach [7].

Literature Review

A naturally occurring low-cost material that is suitable for modification with a wide range of appropriate physical properties, would appear to have the greatest potential for the fabrication of filter materials to capture heavy metals from water.

Natural zeolites are a class of hydrated aluminosilicate materials that are environmentally and economically desirable as adsorbent materials. They have attracted attention due to their unique characteristics such as environmentally sound and nontoxic, being available in big quantities in the world, having high sorption

capacity, being able to modestly adjust the pH of systems, not introducing additional pollution in the environment, providing adsorption sites with exchangeable cations for heavy metal ions and porosity for free metals, and having a great potential for modification [8]. Due to excess negative charge on the surface, the natural zeolite is a cationic exchanger. However, the zeolite can be chemically modified by inorganic salts or organic surfactants, and this generates a positively charged oxi-hydroxides, or surfactants micelles. As a result, the zeolite is enabled to bind to anions, as well [9].

Zeolites have a great stability in various environmental condition and this can challenge other materials. Its high melting point ($> 1,000^{\circ}\text{C}$) causes a high thermal stability. They also resist high pressures, do not dissolve in water or other inorganic solvents, and they do not oxidize in the air. Zeolites do not cause health problems, for example, from skin contact or inhalation (unless very fine). Since they are unreactive and based on naturally occurring materials, they do not have any harmful environmental impacts [10]. This project uses the zeolite that is a naturally occurring material as an adsorbent, it has advantages over other materials mentioned above, and additionally has a low-cost processing.

Prices for natural zeolites can vary based on the zeolite content and processing. Unit values collected through the United States Geological Survey (USGS) census of domestic zeolite producers, ranged from \$85 per metric ton to \$320 per metric ton [11]. The unmatched properties of zeolites and the possibility of adjusting acidic and basic sites, or incorporation of other elements in its framework, as well as structure modification open a wide range of application of zeolites. Zeolites belong to a well-known family of crystalline aluminosilicates displaying a unique combination of properties such as high surface area, well-defined microporosity, high (hydro) thermal stability, and the ability to confine active metal species in their pores [12]. The following section provides a detailed discussion of the zeolitic material properties.

Zeolites

Zeolites based on their ion-exchange properties, have been used as adsorbents and ion-exchangers for different environmental friendly applications and water treatment [13]. Different factors such as the process temperature, the solution pH, the solution initial concentration, the presence of competing cations and complex agents, and the process time can affect the uptake of the metal cations from solutions

[14].

The application of zeolites in the purification of wastewater and treatment of industrial urban wastewater is the subject of numerous studies.

In addition to energy conservation, agriculture and aquaculture, odor control, mining and metallurgy, environmental pollution control is one of the main applications of the natural zeolites [15]. Ion exchange and molecular sieve properties are the two most important reasons which make the natural zeolite a potential choice in the environmental remediation processes [16, 17]. Traditionally, the ion exchange equilibrium in zeolites has been expressed by a thermodynamic equilibrium constant (K) for the exchange reaction between the ions in solution, and those exchanged on the zeolite sites [18, 19].

Adinehvand et. al [20] employed zeolite to capture zinc from water. They used natural zeolite (clinoptilolite), and sulfuric acid treated zeolite as the adsorbent. Due to the predominant role of hydrogen ions as an exchangeable ion in the zeolite, the acid treated zeolite showed higher adsorption results. In a study of pH effect, the maximum removal efficiency happened at a pH level of 6. pH affects the surface

electrical charge of the adsorbent as well as the existing zinc species. Therefore, different charge values and zinc species at different pH levels affected the adsorption process. In solutions containing heavy metals, natural zeolites prefer adsorbing H^+ better than adsorbing heavy metals ions [21, 22]. As a result, more H^+ ions will be adsorbed under acidic conditions. At pH levels toward a neutral level, in a range of 6.5 to 7.5, the free H^+ ion concentration is lower, causing more heavy metal ions being adsorbed from the solution. An increase in pH from 2.5 to 3.5 showed an increase in adsorption capacity, q_e , by 49%, 38% and 20% for Mn^{2+} , Zn^{2+} , and Cu^{2+} ; respectively [16].

Most of the aqueous solutions contain a mixture of heavy metal ions requiring investigation of the influence of competing cations on the individual adsorption characteristics by natural zeolite. Different adsorption mechanisms can be involved in the adsorption of each cation from solution [23]. Experiments were conducted [24] to study the effect of competing Ca^{2+} ions on the uptake of Pb^{2+} , Zn^{2+} , and Cd^{2+} . Results showed that the Pb^{2+} uptake was only affected slightly, while Zn^{2+} and Cd^{2+} adsorption decreased strongly in the presence of Ca^{2+} . Different preferences of the clinoptilolite for different cations were used to explain these findings. Due to a high

Si:Al ratio, clinoptilolite has a low structural charge density. So, cations with lower hydration energy are preferred to be adsorbed compared with cations with higher hydration energies [25].

Surface treated zeolites were fabricated as filter materials by combining the cation adsorption property of natural zeolite and with anion adsorption property of functional groups. These materials have applications as decontamination agents for soil and water basins [26]. Mercury adsorption was found to be maximized for sulfur treated zeolites [27]. The adsorption capacity was increased from 0.084 mg Hg/g for natural zeolite to 0.092 mg Hg/ g for zeolite treated with organic sulfur compound at initial mercury solution concentration of 6.22 ppm. Results revealed highest mercury retention for the modified zeolites when it was in contact with the highest initial concentration of 62.19 ppm. The mercury adsorption isotherms showed the best fit to the Langmuir model, and the Langmuir maximum adsorption capacity (q_m) of zeolite minerals increased from 2.15 to 10.23 mg Hg/g.

Another study [28] focused on the application of natural zeolite from clinoptilolite group in the removal of mercury from industrial wastewater. They also showed that

the ion exchange mechanism was the dominating mechanism of the sorption with a maximum adsorption capacity of 1.21 meq/g sorbent. The adsorption behavior of natural and Fe-modified zeolites [29] was extensively studied. Due to its specific surface area and the presence of the amorphous Fe-oxide phase, for the range of concentrations studied, the percentage of total metal adsorption on the Fe-modified zeolite system was almost twice as high as natural zeolite. For Cu, Zn, and Mn concentrations up to 80 ppm, the Fe-modified zeolite system was capable of adsorbing more than 80% of the total concentration of the contaminants. On the other hand, for the metal concentrations up to 35 ppm, the adsorption reached almost 100%. In the same concentration region, zeolite adsorbed between 45% and 80% of metals.

Another study has been conducted by Luiz et al. [30] to investigate the adsorption features of zeolites combined with the magnetic properties of iron oxides to produce a novel magnetic adsorbent. The goal of the study was to fabricate a magnetic composite as an adsorbent material that can subsequently be separated from the medium by a simple magnetic process. They fabricated a zeolite: Fe oxide composite with a ratio of 3:1, and studied the adsorption of Cu^{2+} , Cr^{3+} , and Zn^{2+} from aqueous

solution. Selectivity sequence was found to be in the order of $\text{Cr}^+ < \text{Cu}^{2+} < \text{Zn}^{2+}$. The adsorption tests showed adsorption capacities of 49, 87, and 114 mg/g of Cu^{2+} , Cr^{3+} , and Zn^{2+} for the fabricated adsorbent, respectively. For pure NaY zeolite, the adsorption capacities of Cu^{2+} , Cr^{3+} , and Zn^{2+} were 45, 88, and 111 mg/g, respectively; suggesting that the presence of Fe oxide in the composite is not inhibiting the adsorption of metals.

Natural and NaCl modified clinoptilolite have been used as Zn ion sorbents [31] resulting in the modified clinoptilolite achieving up to 100% higher effective sorption capacity than the natural material. Due to dust formation during the natural clinoptilolite treatment, pore volume and pore surface area ($0.0546 \text{ cm}^3 \cdot \text{g}^{-1}$ and $9.13 \text{ m}^2 \cdot \text{g}^{-1}$) of the treated material are smaller to the natural one ($0.0706 \text{ cm}^3 \cdot \text{g}^{-1}$ and $14.5 \text{ m}^2 \cdot \text{g}^{-1}$). The average pore diameters of natural and modified clinoptilolite were measured to be 195 Å and 239 Å; respectively. This is evident that the treated clinoptilolite surface and pore openings are partially covered by the dust, resulting in pores clogging, causing a smaller ion exchange capacity and slower ion exchange rates. However, pore-clogging alone is not able to explain the effective performance of treated clinoptilolite compared to the natural form. Differences in surface charge

between the natural modified clinoptilolite at the same pH are proposed as another reason for the increase in the ion exchange rate.

As an adsorbent, synthetic zeolites are found to be very effective in heavy metal removal from solutions. A comparison of the adsorption behavior for natural and synthetic zeolites shows that synthetic zeolites perform considerably better than natural zeolites, because of their higher aluminum content. There are also higher amounts of released sodium from the synthetic zeolite that can address the higher metal removal compared to the natural zeolite [32]. In their work, the synthetic zeolite was found to be very effective in removing 100%, 98.4%, 96.8% and 100% of Pb^{2+} , Cu^{2+} , Zn^{2+} , and Cd^{2+} , respectively. Whereas the percent removal of the natural zeolite was 89.2%, 53.4%, 41.8% and 45.0% for Pb^{2+} , Cu^{2+} , Zn^{2+} and Cd^{2+} ; respectively. It is notable that, due to hydronium ion exchange reducing the concentration of proton in solution, the pH level of the solution after contact with the synthetic zeolite increased to 8.5-9.0 regardless of the initial pH.

Zeolite synthesized from coal fly ash showed a higher adsorption capacity for Pb by a factor of 3-5 times compared to natural zeolite, because of its higher affinity for

metal ions [33]. Artificial zeolites prepared from fly ash are capable of showing high cationic exchange capacities, due to their large surface area and high residual carbon contents; conversion of fly ash into zeolites has become an important issue for waste management in recent years [34-38].

Synthesized zeolites type A and X have been used as adsorbents to capture Cu^{2+} and Zn^{2+} . The Si:Al molar ratio of zeolite A is between 1.0 to 1.2, and for zeolite X is in the 1.0-1.5 range. Zeolite X has bigger pore channels than zeolite A. For zeolite X, the adsorbed amount of Cu^{2+} was higher than that for Zn^{2+} . The adsorption property is explained by (a) the nature of heavy metal cations and (b) the microstructure of zeolites [39].

Zeolite A was synthesized and used as an adsorbent material to uptake Zn and Cd from wastewater solutions [40]. Investigations on the rate of uptake of both Zn and Cd ions indicated that 60-70% of the ultimate sorption of each ion occurred within the first 20 minutes of contact with saturation reached in around 45 minutes. The data also showed that the adsorbed amount of Zn^{2+} and Cd^{2+} increased with an increase in the temperature, indicating an endothermic nature of the process with the

time required to reach saturation remaining practically unaffected. This increase in sorption capacity with temperature suggests that the active surfaces available for sorption have increased with temperature. This was attributed to the change in pore size and enhanced rate of intraparticle diffusion of solute, as diffusion is an endothermic process. The kinetics study showed that the pseudo second-order sorption mechanism is predominant. The adsorption capacity of the synthesized zeolite at 333 K was calculated to be 421.01 and 353.19 mg/g for Zn^{2+} and Cd^{2+} ; respectively.

Table 2 lists a selected number of studies investigating heavy metal removal from water by using different types of zeolites. In order to be comparable easier, all the results in Table 2 are converted to the same unit, mg/g.

Table 2 Literature review of heavy metal removal from wastewater.

Reference	Material	Results
Li Liu, 2012 [41]	Graphene Oxide (GO)	108.342 mg/g Au 80.775 mg/g Pd 71.378 mg/g Pt
Yang Yu, 2013 [42]	GO modified zeolite (clinoptilolite)	50 mg/g Natural zeolite 55 mg/g GO zeolite 67 mg/g GO/acid treated zeolite, cationic dye removal

Junyong, 2014 [43]	Zeolite (synthesized)- reduced graphene oxide (r-GO)	53 mg/g methyl blue 48 mg/g malachite green
Vernon, 2006 [44]	Fly ash zeolite (synthesized)	0.000153 mg/g Pb 0.000015 mg/g Hg
Meili Yin, 2011[45]	mesoporous zeolite nanocomposite (synthesized)	25 mg/g Hg
T. Gebremedhinhalie, 2002 [27]	Natural zeolite (clinoptilolite- heulandite) Sulfide treated zeolite	2 mg/g Hg 10 mg/g Hg
A. Chojnack, 2004 [28]	Natural zeolite (clinoptilolite)	2.42 mg/g Hg
Shunli Wan, 2016 [46]	Hydrated manganese oxide on GO	553 mg/g Pb
J. Adinehvand, 2016 [20]	Acid treated zeolite (clinoptilolite)	28 mg/g Zn
Do-Gun Kim, 2015 [47]	Nano Biogenic Manganese Oxide on natural zeolite	98 mg/g Pb 92.5 mg/g Cd 89.57 mg/g Zn
Mojgan Zendehdel, 2016 [48]	Hydroxyapatite/zeolite nanocomposite (synthesized)	55.55 mg/g Pb 40.16 mg/g Cd

Ruchi Shaw, 2016 [49]	ZnO engineered zeolite (zeolite Y)	78.85 mg/g Pb
Sharifpour, 2015 [50]	Sepiolite	31.5 mg/g Pb
	Zeolite	25.3 mg/g Pb
Gupta, 2008 [51]	Wyoming bentonite	31.1 mg/g Pb
	Georgia kaolinite	11.5 mg/g Pb
Sprynsky, 2006 [21]	Natural zeolite (clinoptilolite)	27.7 mg/g Pb
Potgieter, 2006 [52]	Palygorskite	62.1 mg/g Pb
Bektas, 2004 [53]	Turkish sepiolite	93.4 mg/g Pb
Shaheen, 2012 [54]	Clinoptilolite	1.2 mg/g Pb
Corner, 2015 [55]	Synthetic zeolite A4	0.4554 mg/g Pb
Buasri, 2008 [56]	Zeolite Clinoptilolite	52 mg/g mg/g Pb
Payne, 2004 [57]	Zeolite Clinoptilolite	25 mg/g mg/g Pb
Dursun, 2007 [58]	Natural zeolite (clinoptilolite)	0.0664 mg/g Pb
Chibuzo, 2016 [59]	Synthetic zeolite	200 mg/g Pb

The improved and long-term chemical and physical stability of the modified zeolites, the combination of their sorption properties with low operational costs, and

regeneration of the contaminant loaded zeolitic materials have increased their environmental application possibilities. Although in some cases the adsorption capacity of the raw and modified natural zeolites cannot be compared with those of the synthetic materials, this drawback can be compensated by the low-cost of the natural zeolitic materials and their availability in big quantities all over the world.

Removal Technologies for Heavy Metals from Water

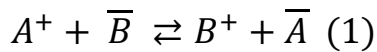
Several treatment technologies are available to capture heavy metals from contaminated solutions including sulfide precipitation, membrane filtration, bioremediation, and adsorption/ion exchange. Sulfide precipitation is the most common method for aqueous mercury removal. To remove this insoluble salt, additional treatment such as pH adjustment, coagulation, flocculation, and gravity settling, or filtration is necessary. Mercury re-solubility, difficulties monitoring sulfide levels, and residual sulfide in the effluent are some of the disadvantages of this method. Coagulation/coprecipitation is used as an alternative to sulfide precipitation. In this treatment, aluminum or iron salts are used as the coagulator [60]. Other innovations have used supported liquid membranes containing chemicals such as trioctylamine as a carrier and coconut oil as a diluent [61-63].

Ion Exchange Materials Properties

Ion exchange processes have received considerable interest because of their high efficiency and low operational costs. The most important advantages of ion exchange compared with chemical precipitation are the ability to recover the heavy metals, selectivity, and less by products [64]. There are numerous investigations of heavy metal removal by ion exchange resins [65-69]. In this process, a cationic or anionic specialized ion exchange material is used to remove metal ions from the solution. Commonly used ion exchangers are synthetic organic ion exchange resins made from polystyrene and divinylbenzene which are modified by an acid or alkali treatment. The resins are usually water-insoluble solid substances that can adsorb cations or anions from the solution with the release of other ions with the same charges into solution in an equivalent amount. It is notable that the valences of the exchanging ions have a strong effect on ion exchange equilibrium, and thus on the removal efficiency of any type of an ion exchange process [70].

As an adsorbent, ion exchange resins are used in order to exchange contaminant cations and anions with hydrogen and hydroxyl ions; respectively. Resins are classified based on the type of functional groups they contain. Cationic exchangers

are categorized into two groups: (a) strongly acidic with functional groups derived from strong acids e.g., R-SO₃H (sulfonic); (b) weakly acidic with functional groups derived from weak acids, e.g., R-COOH (carboxylic). Anionic exchangers are also categorized into two groups: (a) strongly basic with functional groups derived from quaternary ammonium compounds, R₃-NH-OH; (b) weakly basic with functional groups derived from primary and secondary amines, R-NH₃OH or R-R'-NH₂OH. Preference of ions for resins is often expressed by the selectivity coefficient. For the cation A⁺ in a solution being exchanged with cation B⁺ on the ion exchanger:



the barred terms show the occupied position on the ion exchanger (solid phase) as opposed to the solution phase. For this exchange, an operational equilibrium constant can be defined as:

$$K_{B^+}^{A^+} = \frac{[\bar{A}][B^+]}{[A^+][\bar{B}]} \quad (2)$$

where [A⁺], [B⁺] are moles of A⁺, B⁺ per liter of liquid, and [\bar{A}], [\bar{B}] are moles of A⁺, B⁺ on resin per liter of resin; respectively. The superscript and subscript on the selectivity coefficient show the direction of the reaction. The superscript is the reaction side, and the subscript is the product side of the exchange reaction.

Adsorption

Adsorption of pollutants on a solid surface of a material, an adsorbent, is now recognized as one of the most effective, comprehensive, and economic methods. Flexibility in design and operation, along with high quality treated effluent, and a possibility of recovering the adsorbent and pollutant itself are some advantages of this technique.

Metal ion complexation references should be updated

When a metal ion combines with an electron donor, the resulted substance is called to be a complex, or coordination compound. In a complex environment, there is always an atom in the center which is surrounded by multiple other molecules or ions [71]. Nitrogen, oxygen, and sulfur are common examples of these donor atoms [72]. Atoms may combine with a known maximum number of other atoms, molecules, or radicals. This number is called as the coordination number. For example, as shown in Figure 1, in hexamine platinum chloride, $[\text{Pt}(\text{NH}_3)_6]\text{Cl}_4$, the six ammonia molecules are strongly attached to platinum atom. The chlorine atoms are less strongly attached to the atoms of the central complex. The weakly bounded groups may be easily exchanged under conditions that would not affect strongly attached atoms [72].

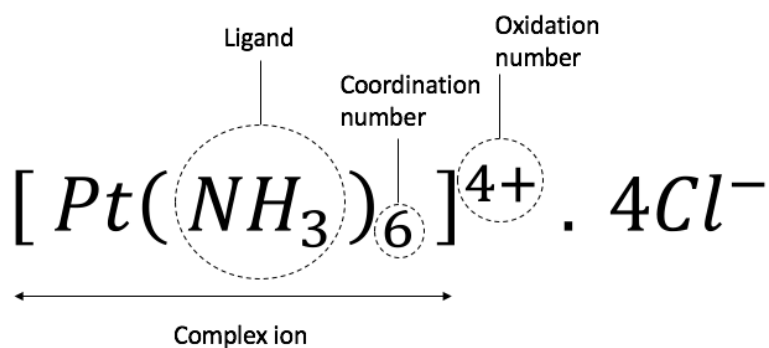


Figure 1. An example of complex ion.

Table 3 shows the principal valence and coordination numbers of some metals.

Table 3. Principal valence and coordination number of selected metals.



M ⁺	Coord. No.	M ²⁺	Coord. No.	M ³⁺	Coord. No.
Cu ⁺	2,4	Mn ²⁺	4,6	Sc ³⁺	6
Ag ⁺	2	Fe ²⁺	6	Cr ³⁺	6
Au ⁺	2,4	Co ²⁺	4,6	Co ³⁺	6
		Pb ²⁺	2,4	Au ³⁺	4
		Cu ²⁺	4,6		
		Zn ²⁺	4,6		




The tendency for complex formation can be explained as the tendency for metal ions to fill up unoccupied orbitals, and therefore approach the electric configuration of an inert gas [72]. For example, if we consider trivalent cobalt, it has 14 electrons in its

two outer shells. So, a donation of 12 electrons by 6 ammonia molecules, the cobalt atom acquires the stable krypton configuration with 18 and 8 electrons in the M and N shells, respectively. As already discussed, the coordination number of the metal can be used to determine the number of molecules or ions of complexing agents that will be attached to a single metal ion.

In some of the complexes, each ligand only forms one bond with the central metal ion, which a ligand is said to be unidentate. Some ligands, on the other hand have two or more lone pairs which can bond to the central metal ion. These are known as multidentate or polydentate ligands. Table 4 shows schematics of metal complex schematics.

Table 4. Metal complexes schematics.

Type of ligand	Complex schematic
Monodentate (Unidentate)	
Bidentate	

Tridentate	
Quadridentate	
Hex dentate	

Lead Complexation Forms

Among the different oxidation states of lead ion, the lead (IV) form is easily reduced, but the Lead (II) is stable and is the most common form of lead in the environment. Therefore, lead (II) attracted most interests to the coordination compounds involving the 2+ oxidation state [73].

Observed coordination numbers from 2 to 12 for lead (II), results in a large variety of configurations of its complexes and compound [74, 75]. Based on valence bonds theory, the inert electron pair can have the following forms: (a) occupy a hybrid orbital formed by mixing the 6S and 6P orbitals and becoming stereochemically active, or (b) be a pure s^2 electron pair and thereby stereochemically inactive.

There are two main structure types of lead (II) complexes that are identified as hemidirected and holodirected, introduced by Shimoni-Livny et al [76]. In the first one, the electron distribution around the metal ion is greatly uneven, on the other hand in the second one the electron distribution is symmetric. Figure 2 shows holodirected and hemidirected environment of Pb.

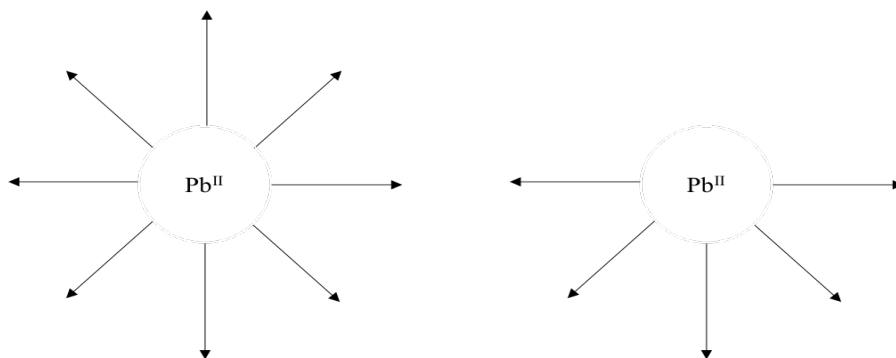


Figure 2. Holodirected coordination environment of Pb (left) and hemidirected environment of (right) [77].

There are different parameters determining whether the attitude of the s^2 electron pair is stereochemically active or inactive in a complex: (a) the stereochemical activity of the lone pair depends strongly on the nature of the donor atoms (soft or

hard), the charge of the donor, and also the interactions between coordinated ligands [72], (b) the denticity of the ligand and the charge of the donor atoms; in complexes with high denticity ligand hemidirected geometries were found in the presence of donor atoms with high affinity towards Pb (II). In fact, it has been observed that a soft donor atom such as sulfur, which is usually formed in holodirected Pb (II) complexes, was able to enforce a hemidirected structure, in cases that it was part of an anionic group in a polydentate molecule [72]. (c) another observation showed that the stereoactivity of the lone pair correlates with the coordination number. It was found that lead (II) compounds are hemidirected when the coordinating donor atoms are <6 in number, and holodirected if it is as high as 9-10. Both of these complex environment are seen for coordination numbers 6-8 [72].

Theory of Adsorption

Adsorption is a surface phenomenon in which molecules, atoms or ions are attracted to active sites on the surface of the adsorbent. Adsorption can be occurring in a form of a chemical or physical process, or a combination of both. Van der Waals forces are in charge for physisorption while chemisorption occurs via electrons redistribution between adsorbent and adsorbate with a resulting strong chemical bond [78-81].

The adsorption process on a porous adsorbent is generally defined with three main

steps. First, the cation (or anion) is moving from bulk solution to the external surface of the adsorbent material (film-diffusion or external-diffusion). Next, the adsorbate transports within the pores of the adsorbent (internal diffusion). In this rate-limiting step, a small amount of adsorption occurs on the external surface. In the last step, the adsorbate is adsorbed on the inner surface of the adsorbent pores and capillary spaces. The interaction between the adsorbate, matrix, and surface of adsorbent influences these stages and the resulting metal adsorption. Parameters that could influence the adsorption process are: conductivity, the solution pH, the process temperature, ionic strength, initial concentration of cations and anions in the solution, adsorbent mass, adsorbent particle size, and presence of competitive ions of the adsorption matrix, chemical and physical properties of adsorbate such as ionic radius and solubility, and adsorbent surface chemistry and characteristics [82-85].

The selectivity can be considered as an important property of the adsorbent in adsorption process. Zeolites with higher Si:Al ratio, such as clinoptilolite, are more selective for cations with lower charge density (K^+ , NH_4^+ , Ag^+ , Cs^+). Zeolites with lower Si:Al ratio, are more selective toward the high charge density cations (Na^+ ,

Li⁺). With increasing the concentration of the solution, the difference in ion exchange affinities of different charges is reduced. If the solution contains different ions of the same charge, the selectivity increases with increasing the atomic number (Li⁺, Na⁺, NH₄⁺, K⁺). The selectivity of clinoptilolite toward alkali metals exist in the sequence: Cs⁺> K⁺> Rb⁺> Na⁺> Li⁺, and the alkaline earth metals: Ba²⁺> Sr²⁺> Ca²⁺> Mg²⁺. The selectivity sequence of clinoptilolite toward heavy metal ions (cations) is found as: Pb²⁺> Cd²⁺> Cu²⁺> Co²⁺> Cr²⁺> Zn²⁺> Mn²⁺> Hg²⁺ and selectivity by anions exists in the series: SO₄²⁻> I⁻> NO₃⁻> HCrO₄⁻> Br⁻> Cl⁻> OH⁻ [86, 87].

Adsorption Kinetics and Mechanisms

In order to investigate the adsorption mechanism of the studied adsorbents for removing lead, the rate of adsorption should be modeled by proper reaction models.

In the past, several mathematical models have been developed to describe adsorption mechanisms. These models can generally be classified as adsorption diffusion models, and adsorption reaction models. Both models are used to discuss the kinetics process of adsorption, but they are quite different. In the diffusional models, the

assumption is based on the point that the diffusion is the rate-limiting step. There are two separate diffusions happening: the external mass transfer during which diffusion across the liquid film surrounding the adsorbent particles happens. And the internal mass transfer during which mass transfer into the interior of the particles happens. The effect of external mass transfer is eliminated by mechanical mixing in the batch experiments [88].

In the adsorption models, the adsorption reaction is considered as the rate-limiting step. If the adsorbent and adsorbate are in contact for enough period of time, an equilibrium will be reached between the amount of contaminant on the adsorbent and the amount of contaminant in the solution. The equilibrium relationship is then addressed by adsorption isotherms. Adsorption isotherms are analysis method to relate the equilibrium concentration of a cation (or anion) on the solid phase, q_e , to the concentration of the cation (or anion) in the liquid phase, C_e .

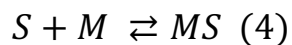
Simple batch experiments are used to generate the adsorption isotherms. The equilibrium concentration, C_e , is determined by the remaining amount of the solute in the solution by analytical methods. The equilibrium concentration of the solute on the adsorbent, q_e in mg/g is determined by equation (3):

$$q_e = \frac{(C_0 - C_e)V}{M} \quad (3)$$

where C_0 is the initial solution concentration in mg/L, V is the volume of the solution in liters, and M is the mass of adsorbent in gram.

Langmuir Model

The adsorption of metal ions is described by the Langmuir model using a reversible reaction shown in Equation (4):



where S is adsorption sites and M is the adsorbate. There are four assumptions in this model: (1) sorption occurs at localized sites and involves no interaction between the sorbed ions, (2) the energy of adsorption is not dependent on surface coverage, (3) maximum adsorption corresponds to a saturated monolayer of adsorbates on the adsorbent surface, and (4) the concentration of M is considered to be constant. The rate of desorption in this model is comparable to the rate of adsorption. This model is represented by Equation (5):

$$q_e = \frac{q_m K_L C_e}{1 + K_L C_e} \quad (5)$$

where q_m is the maximum adsorption per unit mass and K_L is the affinity parameter [88,89].

Freundlich Model

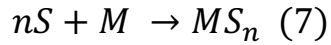
The Freundlich isotherm is a model that has been derived empirically to address heterogeneous systems and is not restricted to monolayer formation. This isotherm can be written as Equation (6):

$$q_e = K_F C_e^{1/n} \quad (6)$$

where K_F and n are Freundlich isotherm constants, indicative of the extent of the adsorption and the degree of nonlinearity between solution concentration and adsorption, respectively [90].

Pseudo Model (n-order)

The Pseudo (n-order) model is described by the non-reversible reaction shown as Equation (7):



The metal ion uptake on the adsorbent surface is governed by an n-order equation.

Then the sorption rate can be written as equation (8):

$$\frac{dq_t}{dt} = k_P(q_e - q_t)^n \quad (8)$$

where q_e and q_t (mg/g) are the adsorption capacities at equilibrium and time t (min); respectively. k_P is the Pseudo n-order rate constant for the kinetic model.

Adsorbents

Among different adsorbent materials, activated carbon (AC) has been used as the most common adsorbent for removing heavy metals from industrial effluent. However, its application (mainly in large adsorption systems) is limited due to several disadvantages such as high cost, and the difficulty in preparation and regeneration process [91, 92]. A growing number of studies in recent years have suggested various low-price sorbents [93-98]. These materials could potentially substitute AC in the water treatment process to remove heavy metals from water. Zeolites are valuable materials with an extensive application as adsorbents and

molecular sieves. Various zeolites have been used as a favorable material in environmental applications and wastewater treatments [93-98].

A significant number of researchers have worked with zeolitic minerals, and have determined selective sequences of these minerals for a range of metals [27]. This mineral is selective to toxic metals. In some publications [99, 100], a thiol (thiols are sometimes referred as *mercaptans* because the thiolate group bonds very strongly with mercury compounds [101]) functional group has been tested to remove heavy metals from aqueous acidic solutions.

AC is a well-studied material for the task of heavy metal removal from wastewater because of its exceptionally high surface area, a well-developed internal microporous structure as well as the presence of a wide spectrum of surface functional groups. The principle of adsorption of heavy metals on the activated carbon surface is attributed to bonding with van der Waals forces with the contribution of London dispersion forces [102]. A more acidic surface charge density that results in higher capacity for reduction of heavy metals such as lead, cadmium and mercury would be a good example. New technologies such as plasma

processing are being studied to modify the surface of AC. In Plasma techniques there is the ability to create the desired charge on the surface of ACs. Also, their extraordinary properties and environmentally friendly nature, have made graphene an attractive material due to its potential applications in wastewater treatment. Because of its impermeability to gases and liquids, graphene is considered as a proper water filtration material [103, 104].

Carbon nanotubes (CNTs) with a high specific surface area possess highly accessible adsorption sites and adjustable surface chemistry. Chemical bonding and electrostatic attraction cause metal ions to be adsorbed by CNTs [105]. Polymeric nanoadsorbents are another material that are utilizable for removing heavy metals from water. Tailored exterior branches can adsorb the heavy metals [106-108]. The costly CNTs production process and the need for additional technical devices (to make sure that there are no nanoparticles discharged into the aqueous environment) are the main concerns that offset their advantages [109].

Zeolite are categorized as aluminosilicates containing micro-macro size pores. Their structure consists of $[\text{SiO}_4]^{4-}$ and $[\text{AlO}_4]^{5-}$ tetrahedra structures that are connected by

sharing oxygen atom. [110, 111]. In addition, the negative potential that is resulted from the substitution of Si (IV) by Al (III) in the structure, is neutralized by the exchangeable cations. This results in the weakly connected cations and in the pores and channels of zeolite structure and causes the significant characteristics of zeolites to exchange cations of heavy metal with external medium or/and adsorb cations, anions, and organic compounds from the aquatic solutions [48]. In addition to the numerous types of natural zeolites, there are many more types of synthetic zeolites which are produced using different precursors [112-119].

Pure natural clinoptilolite has an ideal chemical composition of $[\text{Na}_{1.84}\text{K}_{1.76}\text{Mg}_{0.2}\text{Ca}_{1.24}(\text{H}_2\text{O})_{21.36}] [\text{Si}_{29.84}\text{Al}_{6.16}\text{O}_{72}]$ [120]. Multiple research work are available in the literature that are focused on the applications of zeolites in adsorption of heavy metals from water [28, 121].

Natural and synthetic zeolites can be modified chemically using acid/base treatment, impregnation, or ion exchange methods. Theoretically, it should be possible to modify a zeolite surface to produce an adsorbent with improved properties that is tailored for a specific function. Selecting a proper modification process to provide

selective removal is of great importance, since it may affect the mechanism and kinetic of adsorption process [122]. Acid/base treatment and surfactant impregnation by ion exchange are among the common methods to change the hydrophilic/hydrophobic properties for adsorption of various ions or organics [112].

To improve the adsorption properties of zeolite, chemical modification with inorganic materials (NaCl, CaCl₂, BaCl₂, NH₄Cl, FeCl₃) or a cationic surfactant (hexadecyltri-methylammonium (HDTMA) - bromide) was used [123, 124]. After treating zeolite with a salt solution, such as sodium chloride, exchange of cations (H⁺ or Na⁺) from solution with exchangeable cations (Na⁺, K⁺, Ca²⁺, Mg²⁺) from the zeolite structure occurs. To remove anions from the water, the zeolite surface has to be modified with a solution of inorganic salts (for example FeCl₃) whose adsorption on the zeolite surface leads to the formation of oxy-hydroxides, which then form stable complexes with anions in solution [125, 126]. Adsorbents functionalized with sulfur or organic compounds contacting sulfur have been reported in several publications [99, 127-129]. The presence of thiol groups in the adsorbent increased the loading capacities for heavy metals. This can be

addressed since the reaction between the heavy metal ions and the thiol groups is the most thermodynamically favorable.

The main goal of this research is to increase the lead adsorption performance of natural zeolite by surface functionalization. The project is focused on developing an adsorbent by functionalizing zeolite with sulfide agents materials to increase the removal efficiency of heavy metals. Natural zeolite is used as the starting adsorbent material. Various functionalization processes derived from literature are selectively considered as reference methods prior to developing new modifications to further improve the material performance for metal ion removal.

Chapter 2

Research Objectives and Novelty

Research Principles

The Maximum Contamination Level Goals (MCLG)¹ set by the EPA for lead is 2 ppb [130]. The limitations of commercial ion exchange resin beds, in terms of operational and regeneration costs, have opened a gateway to research and development of new filtration systems based on natural zeolite materials.

The main goal of this research is to increase the lead adsorption performance of natural zeolite by surface functionalization. Due to its high specific surface area, low cost, and ease in chemical functionalization, zeolite is selected as the adsorbent base material in this research. Sulfide materials are chosen as the functionalization agents because of their high affinity to lead, as explained in Chapter One.

Project Objectives

The objectives of this research work are defined as:

- 1- To investigate the relationship between the structure, properties, and performance of the fabricated adsorbents.

¹ Maximum Contaminant Level Goal (MCLG): The maximum level of a contaminant in drinking water at which no known or anticipated adverse effect on the health effect of persons would occur, and which allows for an adequate margin of safety. MCLGs are non-enforceable public health goals.

- 2- To determine the kinetic and isothermal parameters for the zeolitic adsorbent, in order to predict the conditions required for a continuous adsorption system.

Project Hypothesis

- 1- Functionalized zeolite will be used to remove lead from environmental waters.
- 2- The modification of natural zeolite with sulfur-based reagents will improve zeolites lead-removal efficiency.
- 3- Modifying the structure of zeolite will directly affect its performance in lead removal from environmental waters.

Research Novelty and Significance

The idea of functionalizing zeolite with sulfides for the removal of lead is to develop a unique adsorbent material. The use of reactive sulfides attached to zeolite is a novel development. This research evaluates the engineered zeolite particles and their subsequent enhancements for the removal of lead from water by using batch and fixed-bed column experiments.

The significance of this research work is realized by its creation of an engineered mixture of mesoporous-macroporous medium for lead ion adsorption by

incorporating the functionality of sulfides into natural zeolite. The functional design and data analysis are significant to the scientific community, and are especially of interest to the water industry, as they provide the knowledge necessary for developing next-generation water filtration media using zeolite materials.

Chapter 3

Materials and Methods and Experimental Design

Materials

Escott zeolite (0.7-1.0 mm) was purchased from Zeolite Australia PTY (57.0 wt% clinoptilolite). Cystamine dihydrochloride (96%) (Sigma-Aldrich), Thioacetamide (Sigma Aldrich), Zinc Acetate Dihydrate (Acros Chemicals) were used without further modifications. NaCl, KCl, MgCl₂, and CaCl₂ (Sigma Aldrich) were used to prepare salt solutions. Lead Nitrate (99%) was purchased from Fisher Chemicals and was used to prepare initial solutions. Deionized water (DI-water) and ultra-high purity water were prepared in the laboratory. HNO₃ and NaOH solution were used to adjust the solution pH. pH was measured by using OAKTON pH 700 benchtop meter equipped with a single junction pH electrode.

Zeolite functionalization

Cystamine Dihydrochloride Zeolite

A 0.05 M solution was prepared by adding 2.25 g (10 mmol) of cystamine dihydrochloride crystals to 200 mL DI water. 10 g of sodium-treated zeolite (NaCl-Z, see the supporting document) was added to the solution and refluxed at 85 °C for 48 hours. Treated zeolite was washed with DI water and dried at 100 °C for 12 hours.

Zinc Sulfide Zeolite

A stoichiometric ratio of zeolite, zinc acetate dihydrate, and thioacetamide was sonicated in an aqueous medium. Ultrasonic irradiation was accomplished with a

high-intensity ultrasonic probe. A Pyrex beaker was used, which was kept in a water bath to control the temperature of the batch.

Characterization of Materials

The specific surface area, pore volume, and average pore radius of zeolite were measured by Brunauer – Emmett – Teller analysis (BET), Quantachrome Instruments. The FTIR spectrum of each sample was obtained at room temperature by using the Shimadzu FTIR Tracer-100 and LabSolution IR software. Infrared spectra were recorded in the range of 4000 to 400 cm^{-1} . Thermogravimetric analysis (TGA) was performed using TA Instruments (Shimadzu DTG-60AH) from 25 °C to 850 °C under nitrogen atmosphere. Scanning electron microscopy (SEM) and energy dispersive spectroscopy (EDS) were performed with a Hitachi S-4800 equipped with a Bruker EDS detector, generating images and providing chemical composition of the samples. Electron microscopy was performed under 15.0 kV accelerating voltage with an extraction current of 15 μA . Liquid chromatography mass spectroscopy (LC-MS) was used to identify the lead complex when reacting with cystamine dihydrochloride (Shimadzu LCMS-2020). Lead concentration in the solution was analyzed by using the Inductively coupled plasma mass spectrometry (ICP-MS), Thermo Element 2 High Resolution with a lead detection limit of 0.1 ppb. All samples were diluted and acidified by putting 0.2% nitric acid before ICP-MS

analysis. Surface potential of the adsorbent was measured by Malvern Zetasizer nano series. Particles hardness was measured by TQC Hardness Pen.

Adsorption Experiments

In order to investigate the effect of the solutions' pH on adsorption behavior, adsorption experiments were performed in initial lead concentrations of 560 ppb. The pH value of 560 ppb solutions were adjusted to 4,7, and 10 by using HNO₃ and NaOH. In a batch experiment, 0.50 g of adsorbent was added to 100 mL of the solution and placed on a shaking table at 200 rpm for 4 hours. Samples were collected over time, and the residual concentration of lead was determined by ICP-MS.

Lead Sorption Isotherms

Adsorption experiments were performed in six different initial compositions: 10, 25, 50, 100, 250, and 500 ppm. The pH level in the initial solutions was adjusted to 5. Isotherm experiments were conducted by adding 0.20 g of adsorbent to 200 mL of the initial solutions while on the shaking table at 200 rpm. Samples were collected after 24 hours and the residual concentration of lead was determined by ICP-MS.

Lead Sorption Kinetics

In this experiment, 0.20 g of adsorbent was added to 1000 mL of Pb solution with a concentration of 12 ppm at pH 5. The batch was stirred on a shaking table for 72 hours. The adsorbent materials were removed from the solution for a brief period of

time (about two minutes) and were then immersed in a fresh lead solution and stirred on a shaking table (200 rpm) for another 72 hours.

Column Test and Particles Regeneration

Column test was employed to saturate the adsorbent particles with Pb. A column with a height of 200 mm and an internal diameter of 10 mm was used in this test. The column was packed with 4.00 g of ZnS-Z to make a height of 50 mm. The column was then operated in such a manner that 1,000 mL of 100 ppm lead solution was constantly added to it by using a peristaltic pump (Cole-Parmer variable speed) and allowing it to flow along gravity in downflow mode with a constant flow rate of 0.08 mL/s.

Table 5 shows a summary of the experimental design for the two objectives of this work.

Table 5. Summary of experimental design for the objectives.

	Solution pH test	Solution concentration test	Diffusion test	Functional groups loading test	Functional groups leaching test	Interference test	Column test
Objective 1	X	X	-	X	X	X	X
Objective 2	X	X	X	-	-	-	-

Chapter 4

Results and Discussion

The idea of employing sulfur-based materials as the functionalizing agents is based on HSAB (hard and soft acids and bases) theory. Based on HSAB theory, soft acids will react faster with soft bases and form strong bonds with them; on the other hand, hard acids will react faster and form stronger bonds with hard bases [131, 132]. This theory is in a good agreement with experimental studies stating that hard-hard bindings are electrostatic and soft-soft bindings are covalent. Complexes of soft cations with soft anions are present because of a favorable enthalpy change [131, 132]. As shown in Figure 3 lead is in the category of intermediate bases. Sulfur, on the other hand, is found to be in the soft acid's category. Therefore, based on HSAB theory, strong affinity toward sulfur-based materials is expected for lead. In this study, zeolite is functionalized with cystamine functional groups and ZnS nanostructure.

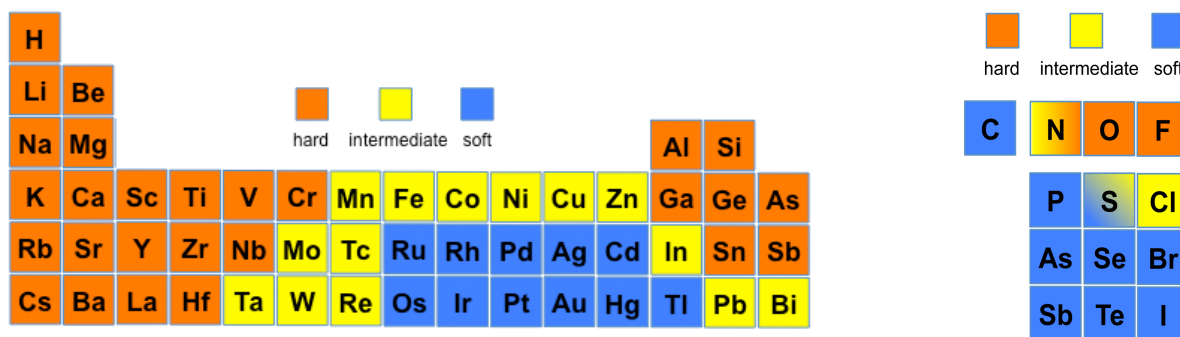


Figure 3. Acid and base categories in the periodic table.

Zeolite processing

Functionalizing zeolite with cystamine

As discussed earlier, lead shows a high affinity for sulfur. In order to increase the adsorption capacity of raw zeolite toward lead, zeolite is functionalized with cystamine dihydrochloride as a sulfur-containing functional group.

Zeolite physical properties

BET analysis was conducted to investigate the porosity properties of zeolite. The specific surface area, pore volume, and average pore radius of zeolite were measured. Results are summarized in Table 6. Pore size distribution showed that the material is 86% mesoporous and 14% macroporous.

Table 6. Porosity parameters of zeolite.

Surface area, m ² /g	Pore volume, cm ³ /g	Average pore radius, Å
15.14	0.03	10.24

The hardness of zeolite was measured to evaluate its strength while going over different steps relevant to transportation and handling of material. By using TQC hardness tester, the hardness of zeolite was evaluated as 30 N. This hardness is in a range of 6-7 Mohs hardness. Materials hardness and strength are directly related; with higher hardness, the materials more resistant against deformation.

Zeolite Functionalization with Cystamine Functional Groups

Since the functionalization process of zeolite with cystamine dihydrochloride occurs via an ion exchange process, the most favorable exchangeable cation in zeolite structure was needed to be found. Na⁺, K⁺, Mg²⁺, and Ca²⁺ are the four exchangeable cations present in zeolite structure. To determine the most exchangeable cation in the zeolite structure, zeolite was first treated with NaCl, KCl, MgCl₂, and CaCl₂ salts separately. To do this, a 2 M solution of sodium salt (NaCl) was prepared by adding 23.36 g of NaCl to 200 mL DI water. 10 g of CZ was added to the solution and refluxed at 85 °C for 48 hours. Treated zeolite was washed with DI water and dried at 100 °C for 12 hours. The process was repeated by using potassium salt (KCl), magnesium salt (MgCl₂), and calcium salt (CaCl₂).

Na, K, Mg, and Ca amounts were evaluated in zeolite by EDS before and after the treatment. Results are shown in Table 7.

Table 7. EDS analysis for CZ and salt treated zeolites.

	Na/Si, wt%/wt%	K/Si	Mg/Si	Ca/Si
CZ	0.0135 ± 0.0034	0.0303 ± 0.0018	0.0145 ± 0.0062	0.1000 ± 0.0027
Na-Z	0.0916 ± 0.0028	0.0810 ± 0.0083	0.0018 ± 0.0006	0.0247 ± 0.0004
K-Z	0.0004 ± 0.0002	0.2046 ± 0.0462	0.0003 ± 0.0003	0.0139 ± 0.0004
Mg-Z	0.0083 ± 0.0054	0.0680 ± 0.0277	0.0302 ± 0.0077	0.0626 ± 0.0097
Ca-Z	0.0008 ± 0.0002	0.0260 ± 0.0022	0.0138 ± 0.0005	0.1293 ± 0.0025

As can be seen in Table 7, sodium's content showed the most increase in zeolite structure after being treated by NaCl salt. It was concluded that Na is the most favorable exchangeable cation in zeolite structure and from that point, NaCl was selected as the pre-treatment agent for the functionalization process. The main goal of the pre-treatment step is to saturate the zeolite structure with its most favorable exchangeable cation, so that more contents of the cystamine functional group can be introduced to the zeolite structure.

It has been observed that sulfur (as a soft donor atom) which is usually formed in holodirected Pb (II) complexes, is also able to enforce a hemidirected structure [4]. Both hemidirected and holodirected environment are found for coordination numbers 6-8 [4].

As explained in chapter one sulfur (as a soft donor atom) can form complexes with lead with coordination numbers of 6-8 [4]. Considering the theoretical coordination number 6-8 the Pb : cystamine ratio falls in the range of 1 : 3 to 1 : 4. Because there are two sulfur atoms in cystamine dihydrochloride chemical formula. Table 8 shows the required number of mol of cystamine to adsorb one mole lead depending on the theoretical Pb : cystamine dihydrochloride ratio. It should be mentioned that after dissolving in water cystamine dihydrochloride ($C_{14}H_{12}N_2S_2 \cdot 2HCl$) transforms to cystamine ($C_{14}H_{12}N_2S_2$).

Table 8. Required number of sulfur atoms in lead adsorption.

Pb : cystamine ratio	mol pf Pb	mol of required cystamine
1 : 3	1	3
1 : 4		4

In order to validate the theoretical assumption and identify the actual Pb : cystamine ratio, a batch experiment was designed as follows: 200 mL of a 10 ppm lead solution was prepared and the pH level was adjusted to pH = 5. Next, 5 mL of a 0.008 M cystamine dihydrochloride solution was added to the batch (equal to 0.04 mmol cystamine dihydrochloride) as the adsorbent material. The batch was run for 24 hours at 200 rpm at room temperature. Residual lead concentration was measured in the solution by using ICP-MS. The residual concentration was measured as 0.196 ppm. Calculating the amount of lead which was adsorbed by cystamine revealed that the Pb : cystamine ratio equals 1 : 4. At this time LCMS was employed to identify: (1) the cystamine dihydrochloride from when dissolved in water and (2) the lead-cystamine complex. In the cystamine dihydrochloride solution a component with a mass of 153.05 (m/z) was observed which is attributed to cystamine. In the lead –

cystamine dihydrochloride solution, a component with a mass of 657.87 (m/z) ($3 \times 153.05 + 1 \times 207.20$) was found which shows a Pb : cystamine ratio of 1 : 3. Based on these experiments and results, adsorption capacity is expected to be improved by an amount of 1 mmol lead for every 3 mmol of cystamine dihydrochloride (or cystamine) that is loaded on the zeolite.

To functionalize the pre-treated zeolite with cystamine functional groups, a 0.05 M solution of cystamine dihydrochloride was prepared by adding 2.25 g (10 mmol) of cystamine dihydrochloride crystals to 200 mL DI water. 10 g of sodium treated zeolite (NaCl-Z) was added to the solution, and the mix was refluxed at 85 °C for 48 hours. Treated zeolite (which is mentioned as CDHZ¹ from this point on) was washed with DI water and dried at 100 °C for 12 hours. To verify if the pre-treatment process was required to introduce cystamine functional groups to the zeolite, the functionalization process was also repeated on the clean zeolite (CZ) (which is mentioned as CDHZ* from this point on).

To assure that the functionalization goals were accomplished, the chemical composition of the functionalized zeolite was analyzed by using EDS. Results are listed in Table 9.

Table 9. EDS analysis for zeolite and cystamine functionalized zeolites.

	Na/Si	K/Si	Mg/Si	Ca/Si	S/Si
CZ	0.0135 ± 0.0034	0.0303 ± 0.0186	0.0145 ± 0.0062	0.1000 ± 0.0027	0.0078 ± 0.0011
CDHZ*	0.0132 ± 0.0098	0.0477 ± 0.0193	0.0145 ± 0.0039	0.0860 ± 0.0136	0.0230 ± 0.0096
CDHZ ¹	0.0694 ± 0.0115	0.0298 ± 0.0140	0.0100 ± 0.0093	0.0231 ± 0.0024	0.0572 ± 0.0041

As can be seen in Table 9, the sulfur amount (sulfur was considered as an element to identify cystamine functional group) in CDHZ¹ is greater than that of CDHZ*. This confirmed that pre-treating zeolite with NaCl successfully allowed introduction of more cystamine functional groups to zeolite structure. Greater amounts of Na⁺, as the most favorable exchangeable cation in the zeolite structure, can address this observation. Another point that should be mentioned here is the Na content in NaCl-Z and CDHZ¹. The Na/Si value was decreased from 0.0916 in NaCl-Z to 0.0694 in CDHZ¹. This verifies that cystamine groups have been introduced to the zeolite structure via an ion exchange with Na⁺ ions. Also, as shown in Figure 4, the functionalization does not lead to any observable surface changes as the functionalization is only a surface treatment technology. Figure 5 shows the sulfur distribution in functionalized zeolites structure.

To quantify the amount of cystamine functional groups that are introduced to zeolite, the concentration of sulfur in the cystamine dihydrochloride solution was measured before and after the functionalization process by using ICP-MS. Calculations based

on the measured concentrations revealed that 57.21% of the cystamine groups have been successfully introduced to zeolite during the fabrication process. By considering the actual amount of loaded cystamine on zeolite, the adsorption capacity of the treated zeolite is expected to be improved as shown in Table 10.

Table 10. Expected improvement in the zeolite's adsorption capacity.

mmol Cystamine	mmol Pb	mg Pb
3	1	207.20
0.57	0.19	39.37

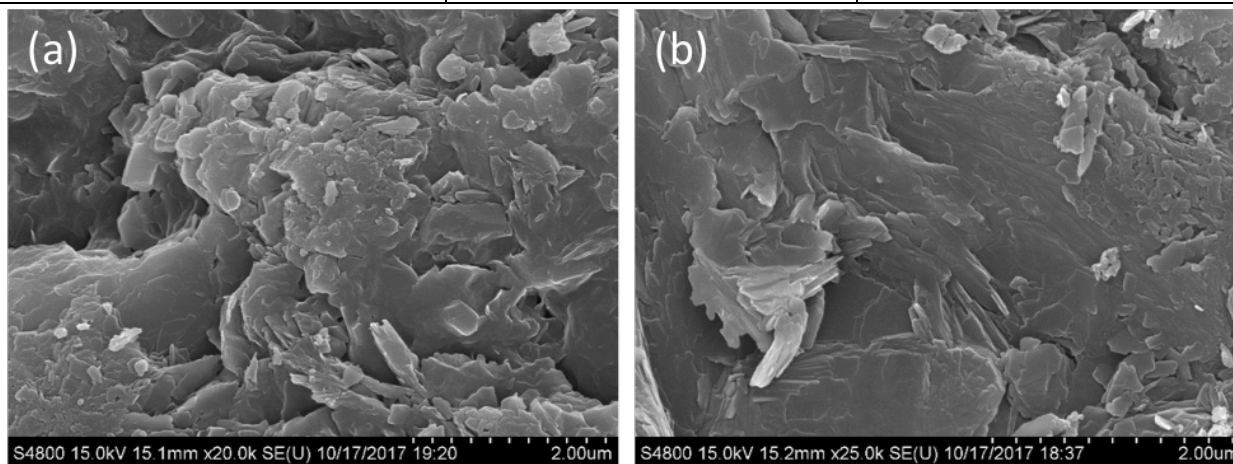


Figure 4. SEM images for: (a) CZ and (b) CDHZ¹: no significant change in structure is seen after functionalization process.

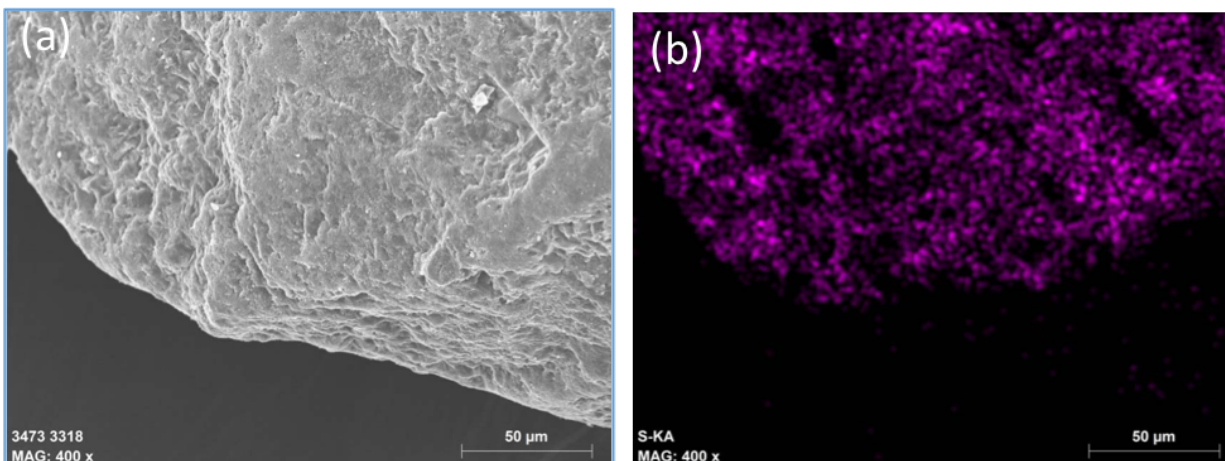


Figure 5. Sulfur distribution on CDHZ¹: sulfur distribution on CDHZ¹.

FTIR spectroscopy was used for cystamine functional group analysis of the CDHZ¹.

FTIR spectra were recorded in the range of 4000 to 400 cm⁻¹.

The FTIR spectra of CDHZ¹ is shown in Figure 6. Clear Si-O-Si bands are found at 1450 and 1000 cm⁻¹. The peak at 780 cm⁻¹ corresponds to Al-O-Si stretching vibrations. The peak at 2360 cm⁻¹ and the broad peak at 1660 cm⁻¹ are attributed to the O-H stretching and bending vibration of water molecules, indicating an entrapped water in the zeolite structure.

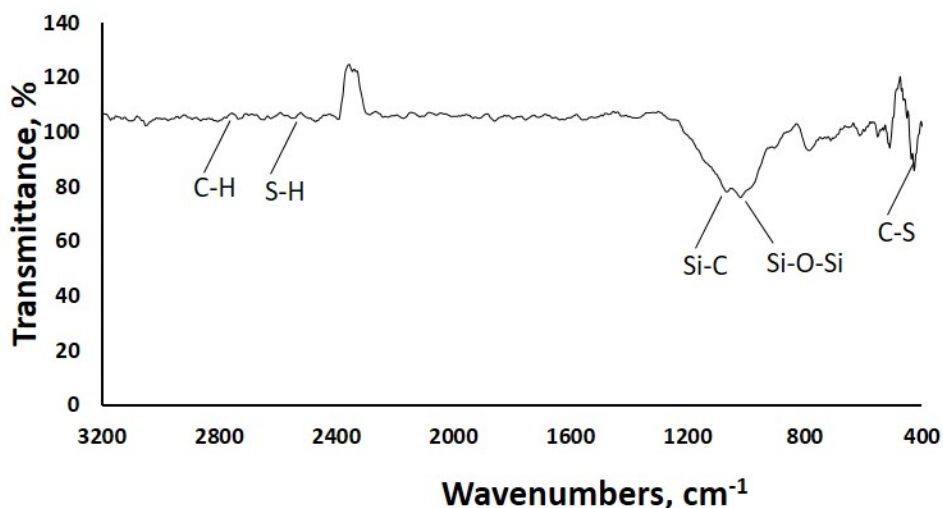


Figure 6. FTIR spectra of CDHZ¹.

As shown in Figure 6, the presence of cystamine ions is confirmed by the observation of bands assigned to C-H vibrations at 2850-2930 cm^{-1} , and of stretching bands attributed to the S-H and C-S vibrations at 2555 and 686 cm^{-1} [120], respectively. Si-C and Si-O-Si bands were also observed at 1100 and 1024 cm^{-1} , respectively.

The thermogravimetric analysis, Figure 7, shows a water loss of (CZ = 3.31%, CDHZ¹ = 2.83%) in the 60-150 °C. This water loss is due to the weakly bounded water. The TGA thermograms show another weight loss of (CZ = 2.18%, CDHZ = 2.05%) in the temperature 150-250 °C, due to the water located in zeolite cavities, and bound to the non-framework cations. There is a third water of (CZ = 0.27%, CDHZ = 0.52%) in 450-500 °C corresponding to structural water [133]. An important weight loss of cystamine dihydrochloride in 200-300 °C is reported [134].

CZ and CDHZ¹ showed 3.1% and 5.76% weight loss respectively in 200-800 °C, so the difference is attributed to the decomposition of cystamine functional groups on CDHZ¹.

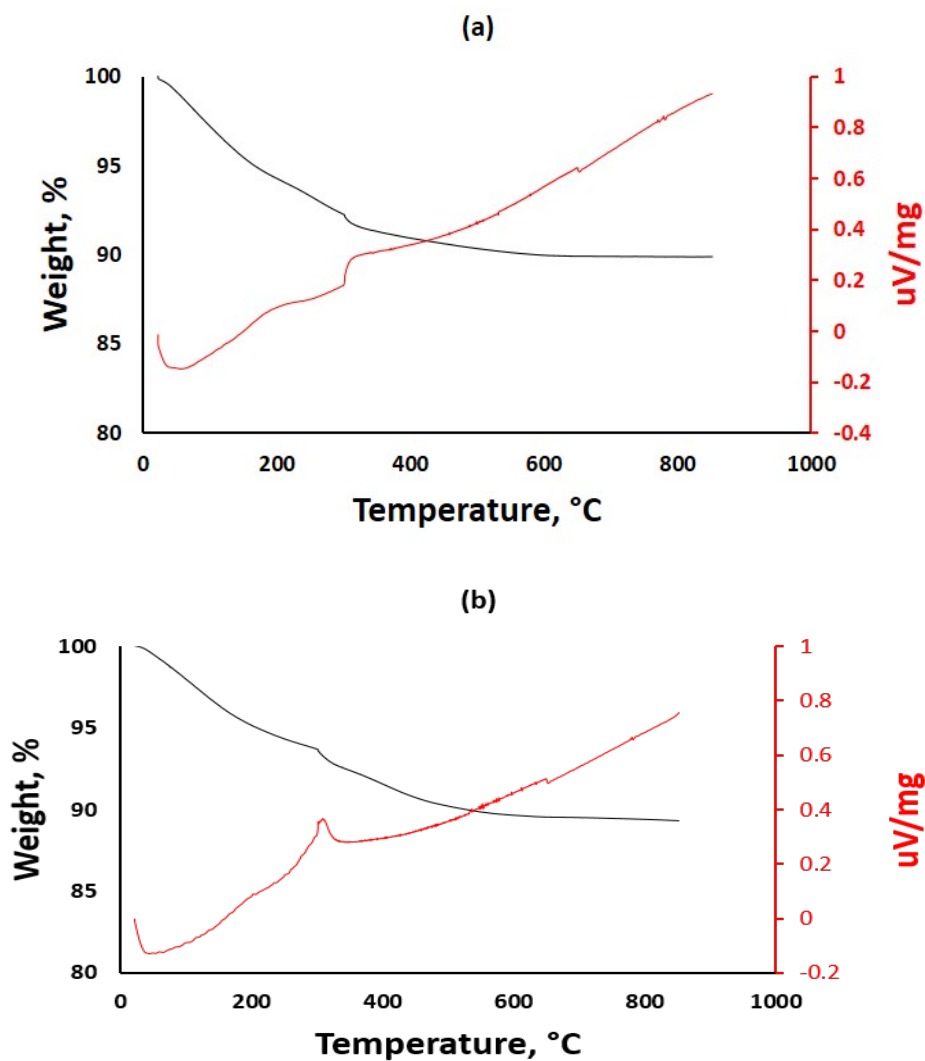


Figure 7. TGA plot of: (a) CZ and (b) CDHZ¹.

Equilibrium Adsorption Experiments for Lead

Table 11 shows the list of experimental factors, and the range of each factor.

Table 11. Experimental factors.

	Factors		Range
Zeolite	Particle size	Fixed	0.7 – 1.0 mm
	Structure/type	Fixed	Clinoptilolite
	dosage	Fixed	0.20 g – 0.50 g
Functional groups	Functional groups/zeolite ratio	Variable	1 mmol /g 2 mmol/g
Performance	Initial concentration	Variable	0.5 – 500 ppm
	Solution pH	Variable	4 - 10
	Temperature	Fixed	RT
	Contact time	Variable	0.1 - 24 h

Adsorption experiments were performed in ppb scale to investigate the initial solution pH on adsorption behavior of CDHZ¹. The pH values of 560 ppb solutions were adjusted to 4,7, and 10 (by using HNO₃ and NaOH solutions) to study the effect of initial solution pH on adsorbents' removal efficiency. To do this, 0.50 g of CDHZ¹ was added to 100 mL of the solution while on the shaking table at 200 rpm for 4 hours. Solutions at different pHs with CDHZ¹ were sampled at minutes 3, 10, 30, 90, 180, and 240. The residual concentration of lead was determined by ICP-MS.

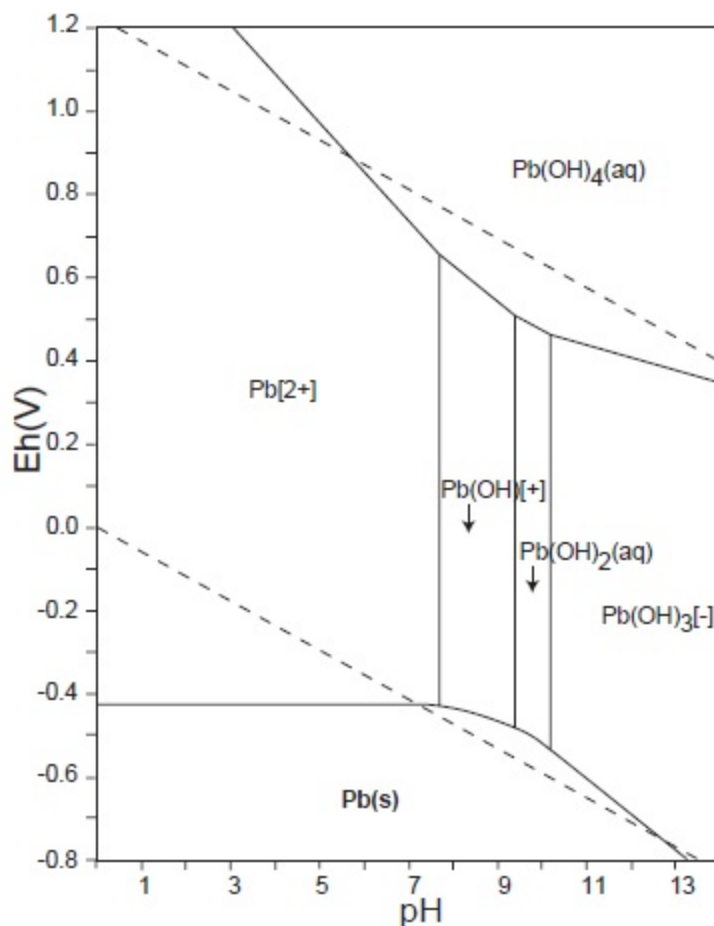
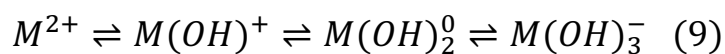


Figure 8. Pourbaix diagram for Pb.

The general reaction scheme for hydroxide formation of divalent metal cations, M^{2+} , is described in Equation (9):



As shown in Figure 8, Pb^{2+} is the predominant specie in the solution at $pH < 8$; at $pH \geq 8$ $Pb(OH)^+$ cations begin to form and are the dominant species in this range.

Lead starts to precipitate as $Pb(OH)_2$ at $pH \geq 9.5$.

The effect of solution pH on the adsorption reaction can be interpreted in terms of (a) electrostatic interactions between charged adsorbent particles and the heavy metals ions and (b) Pb species at tested pH ranges.

In order to investigate the electrostatic interactions between the surface of the adsorbent and Pb at different pH ranges, the zeta potential of the adsorbent surface was measured at pH = 4, pH = 7, and pH = 10. As can be seen in Figure 9, the zeta potential at CDHZ¹ surface is a negative value at all the studied pH ranges and was decreased from -43.80 mV to -44.70 mV by increasing the solution pH from 4 to 10. The negative charge of CDHZ¹ surface can be addressed by Si:Al ratio in the zeolite's structure. The negative charge of zeolite is resulted from the isomorphous substitution of Si by Al.

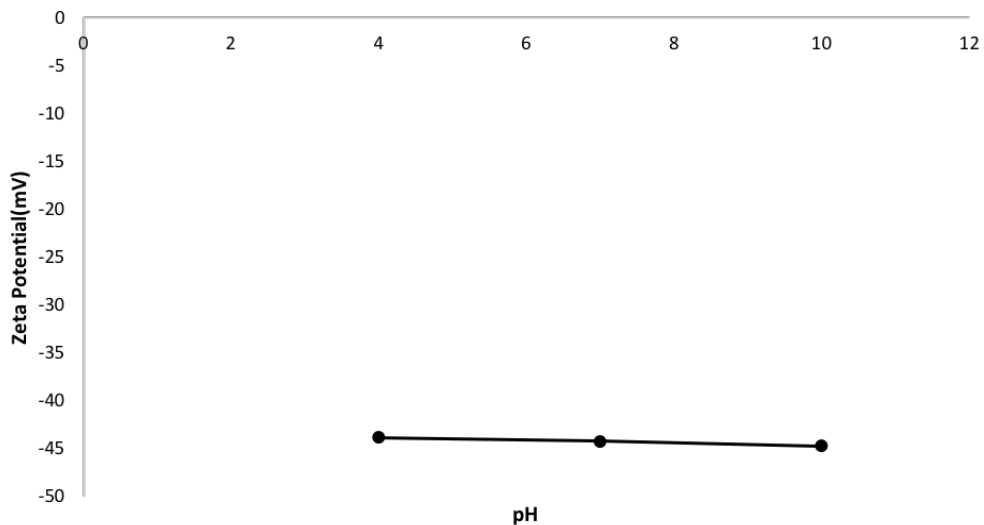


Figure 9. Zeta potential of CDHZ¹ at different pH values.

Under all investigated conditions (pH = 3, 7, 10), the adsorbent is negatively charged which caused Pb^{2+} (at pH = 4) and $Pb(OH)^+$ (at pH = 7) to electrostatically adsorb onto the adsorbent. This is not valid at pH = 10 because $Pb(OH)_2$ is electrically neutral.

As seen in Figure 10 fabricated materials in this research can effectively remove Pb^{2+} from contaminated waters in pH range of 4-7.

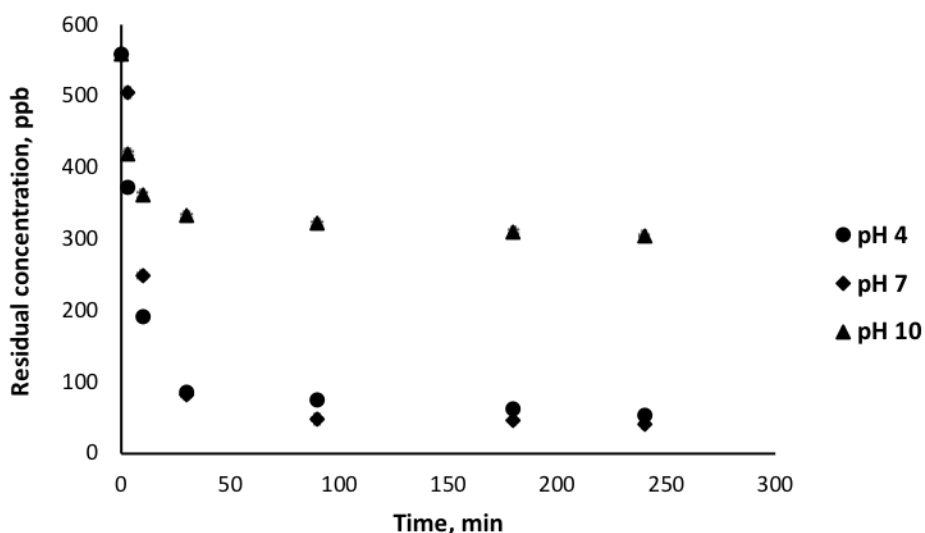


Figure 10. pH effect on residual concentration of lead for CDHZ¹.

Increasing solution pH from 7 to 10 resulted in a decrease in the performance of CDHZ¹. This can be attributed to the $Pb(OH)_2$ precipitates formed in this pH range, shown in Figure 9. These precipitates limited the accessibility of the Pb^{2+} ions to the cystamine functional groups in CDHZ¹ structure. Although the concentration of cystamine functional groups is a factor affecting the immobilization of Pb^{2+} ions, the

accessibility of metal ions to these binding sites is also a controlling factor in the process [120].

Adsorption Isotherms

As explained earlier, the adsorption isotherm is used to address the interactive behavior between solutes, and adsorbent materials [135]. The fit of an isotherm with using the Langmuir equation, Equation 10, assumes that adsorption occurs at specific homogeneous sites within the adsorbent. A linear expression for Langmuir isotherm is:

$$\frac{1}{q_e} = \frac{1}{q_{max}K_L C_e} + \frac{1}{q_{max}} \quad (10)$$

where q_e is the equilibrium concentration of lead on adsorbent ($\mu\text{g/g}$), C_e is the equilibrium concentration of lead in solution ($\mu\text{g/L}$), and q_{max} is the adsorption capacity of the adsorbent. K_L is the Langmuir constant that evaluates the affinity between adsorbate and adsorbent [136]. Freundlich isotherm is one of the most common model in explaining the non-ideal and reversible adsorption process [137]. This model is not limited to the formation of a monolayer on the adsorbent surface, which means it can also be applied to multilayer adsorptions as well. With considering multilayer adsorption, the total adsorbed amount is the summation of adsorption on all sites, where stronger binding sites are occupied first until the adsorption energy is decreasing up to the completion of the adsorption process [138].

Freundlich model is based on the relation between the adsorbed quantity (q_e) and the remained solute concentration (C_e), equation (11):

$$q_e = K_F C_e^{\frac{1}{n}} \quad (11)$$

where K_F is the constant of Freundlich isotherm ($L^{1/n}mg^{(1-1/n)}/g$), and $1/n$ is the Freundlich exponent [139, 140]. Equation (11) can be written in linear form as shown in Equation (12):

$$\log q_e = \frac{1}{n} \log C_e + \log K_F \quad (12)$$

A lead solution with initial concentrations of 10, 25, 50, 100, 250 and 500 ppm at a pH level of 5 have been employed for the batch tests. Lead removal tests were conducted by using 0.20 g of CZ and CDHZ¹ over 24 hours to evaluate equilibrium residual concentration. Figure 11 shows the isotherm plot for CZ and CDHZ.

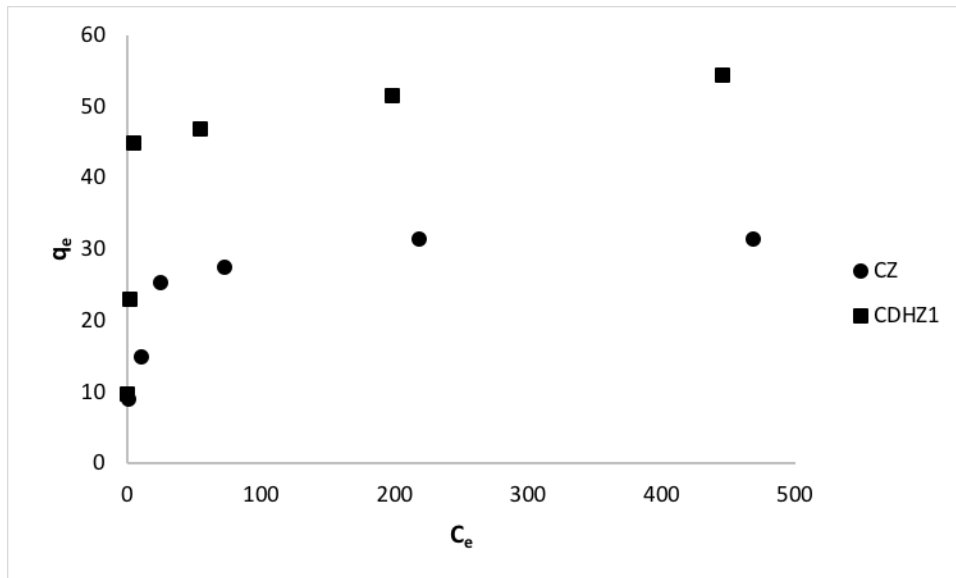


Figure 11. Isotherm plot of CZ and CDHZ¹.

In 1974 Giles and colleagues [141] proposed a general model for isotherms' sorption. In their model, they categorized the isotherms in 4 cases which are now used as the 4 main shapes of isotherms. Figure 12 schematically shows the shape of these 4 isotherms.

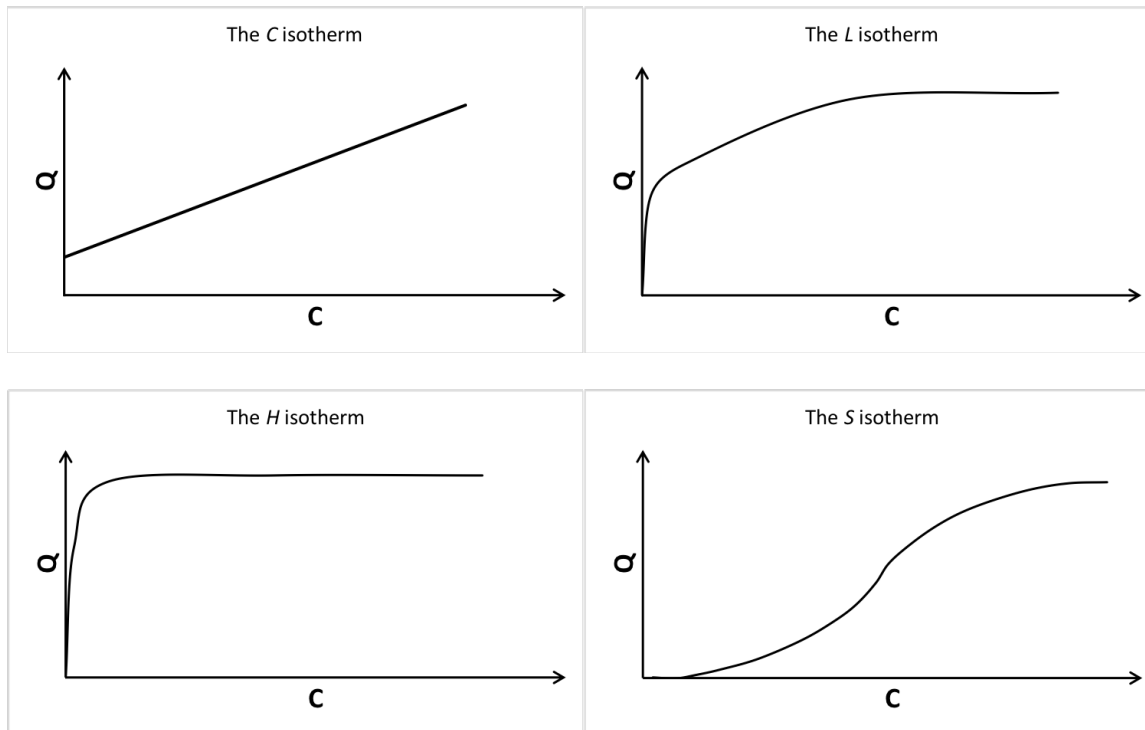


Figure 12. The four main shapes of isotherms [142].

By comparing the results shown in Figure 11 with the four main types of isotherms, shown in Figure 12, it seemed that CZ and CDHZ¹ fit within the H isotherm. H isotherm is considered as a case of the L isotherm, with the only difference that in isotherm H the initial slope is very high. In L and H models, the ratio between the residual concentration of the solute in the solution and adsorbed on the adsorbent decreases when the initial concentration of the solute increases. This suggests a progressive saturation of the adsorbent material [142].

Figure 13 shows Langmuir and Freundlich models for CZ and CDHZ¹.

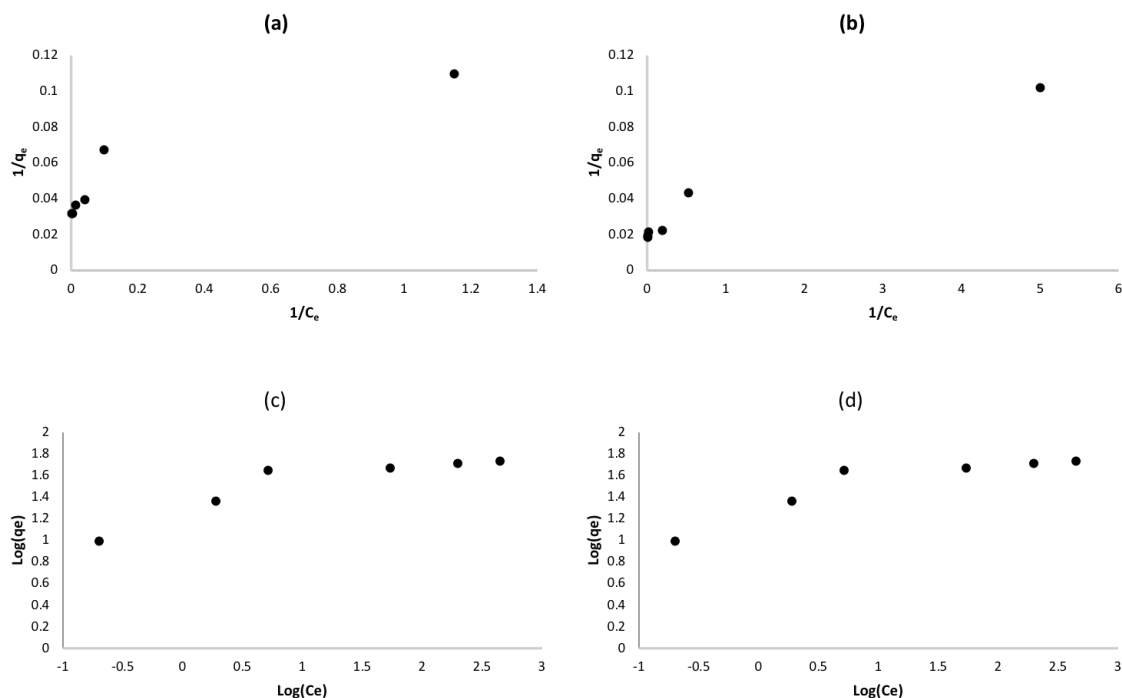


Figure 13. Isotherm models: (a) and (b) show Langmuir model for CZ and CDHZ¹, respectively. (c) and (d) show Freundlich model for CZ and CDHZ¹, respectively.

The adsorption equilibrium between the adsorbate and a surface is a measure of their interactions. The driving force for adsorption results from the specific affinity of the solute for the solid. This kind of attraction can be predominantly one of electrical, van der Waals (physisorption), or of a chemical nature (chemisorption). The isotherm constants and correlation coefficients were calculated for the mentioned isotherm models and listed in Table 12.

Table 12. Isotherm constants for CZ and CDHZ¹.

	Parameters	CZ	CDHZ ¹
Langmuir	R ²	0.872	0.964
	K _L , L/mg	0.617	1.376
	q _{max} , mg/g	25.707	44.843
Freundlich	R ²	0.752	0.813
	K _F , L ^{1/n} mg ^(1-1/n) /g	10.179	19.218
	1/n	0.209	0.204

As explained earlier in this section, adsorption capacity was expected to be improved by an amount of 39.37 mg after functionalizing zeolite with the cystamine functional groups that are loaded on the zeolite. Experimental values in Figure 11 showed an increase of 23.04 mg/g for the cystamine dihydrochloride zeolite, CDHZ¹. This difference in calculated improvement in maximum adsorption capacity of CDHZ¹ (39.37 mg/g), and actual improvement in maximum adsorption capacity of CDHZ¹ (23.04 mg/g) was attributed to the accessibility of the functional groups for the Pb²⁺ cations. When CDHZ¹ is added to a solution containing Pb²⁺ cations while stirring, the adsorbent comes in contact with the bulk of the solution, Figure 14. At first, Pb²⁺ ions react with the cystamine functional groups located at the edge of the pores of the microporous adsorbent. Adsorption of more Pb²⁺ on the adsorbent during the contact time can create a partial block against the entry of additional aqueous solution. As the number of inserted ions increases the blocking increases, resulting in harder access to the binding sites for more metal ions. This mechanism allows explaining the adsorption behavior of CDHZ¹ and the differences found between the theoretical and actual maximum adsorption capacities by using the concentration of cystamine functional groups combined with their accessibility. Based on the explained mechanism, not all the binding sites can be expected to be accessible for Pb²⁺ cations. Comparing the theoretical adsorption capacity of CDHZ¹ (69.97 mg/g CDHZ¹) with that of the experimental value (54.50 mg/g CDHZ¹), it was concluded

that 77.89% of the functional groups were accessible to Pb^{2+} cations. Also, functionalizing zeolite improved its adsorption capacity for lead by 173.24% compared with the adsorption capacity of zeolite.

It needs to be motioned that although there is a theoretical cation exchange capacity of the zeolite, this number cannot be considered as the exchange capacity for lead ions. It reports the total amount of cations that can be exchanged. Experiments were performed to evaluate the actual amount of lead that zeolite is able to exchange with its exchangeable cations.

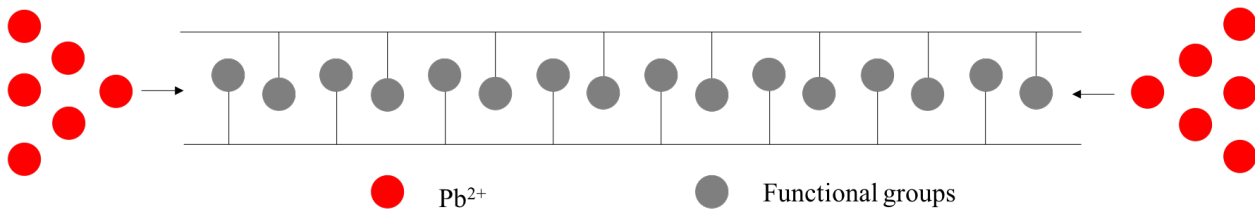


Figure 14. Pb adsorption schematics on CDHZ¹.

Mechanism and Kinetics: Pseudo Model and Diffusion Studies

To study the kinetics of metal ion uptake by CDHZ¹ and investigate the contact time effect to find the equilibrium state, Pseudo model, first and second order was employed. As discussed in chapter 1, the Pseudo first-order and Pseudo second-order models can be formulated in Equations (13) and (14), respectively:

$$\ln(q_e - q_t) = \ln q_e - K_{P1}t \quad (13)$$

$$\frac{t}{q_t} = \frac{1}{(K_{P2}q_e^2)} + \left(\frac{1}{q_e}\right)t \quad (14)$$

where q_t is adsorption capacity at time t , K_{p1} and K_{p2} are the Pseudo first-order and Pseudo second-order adsorption rate constant (min^{-1}), respectively. 1000 mL Lead solution with a concentration of 12 ppm at pH the level of 5 was used for a batch test. Lead removal tests conducted using 0.20 g of CDHZ¹ and solution was sampled at hours: 0.5, 1.5, 3, 6, 12, 24, 48 and 72. Figure 15 shows the Pseudo plots for CZ and CDHZ¹. Calculated parameters are listed in Table 13.

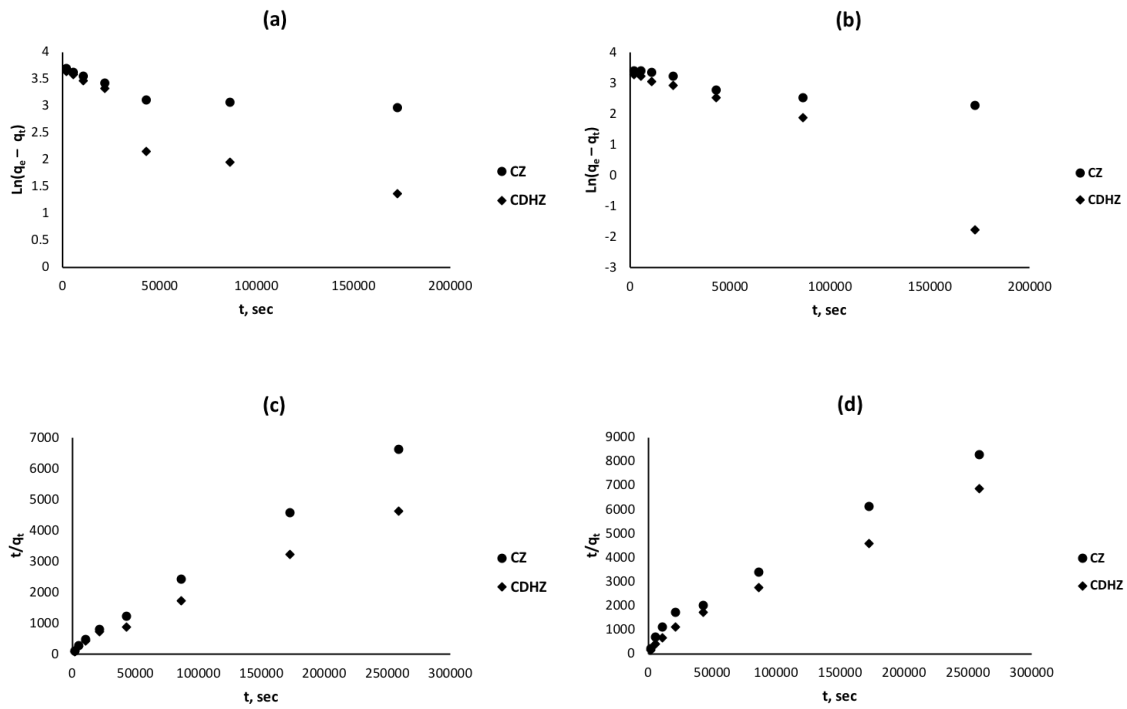


Figure 15. Pseudo isotherm models: (a)-(b) Pseudo first order model before and after the interruption, (c)-(d) Pseudo second order model before and after the interruption, respectively.

Table 13. Pseudo model parameters.

		CZ	CDHZ ¹
Pseudo first order Before interruption	R^2	0.734	0.841
Pseudo second order	R^2	0.995	0.997

The rate-determining step of the adsorption process is established to be a diffusion of the counter ions, rather than an actual chemical exchange reaction at the fixed ionic groups [143]. In a sorption experiment, there are two potential rate determining steps: interdiffusion of ions in the adsorbent (particle diffusion), and interdiffusion of ions in the liquid film (film diffusion) [144]. There are two other rate-determining steps that have been investigated: counter ion exchange across the interface between ion exchanger and solution, and actual chemical exchange reaction. The first one is very unlikely due to theoretical reasons and is not supported by experiments. The second one has been ruled out for the ordinary ion exchange process [144]. Figure 16 schematically shows particle diffusion and film diffusion in an adsorption process.

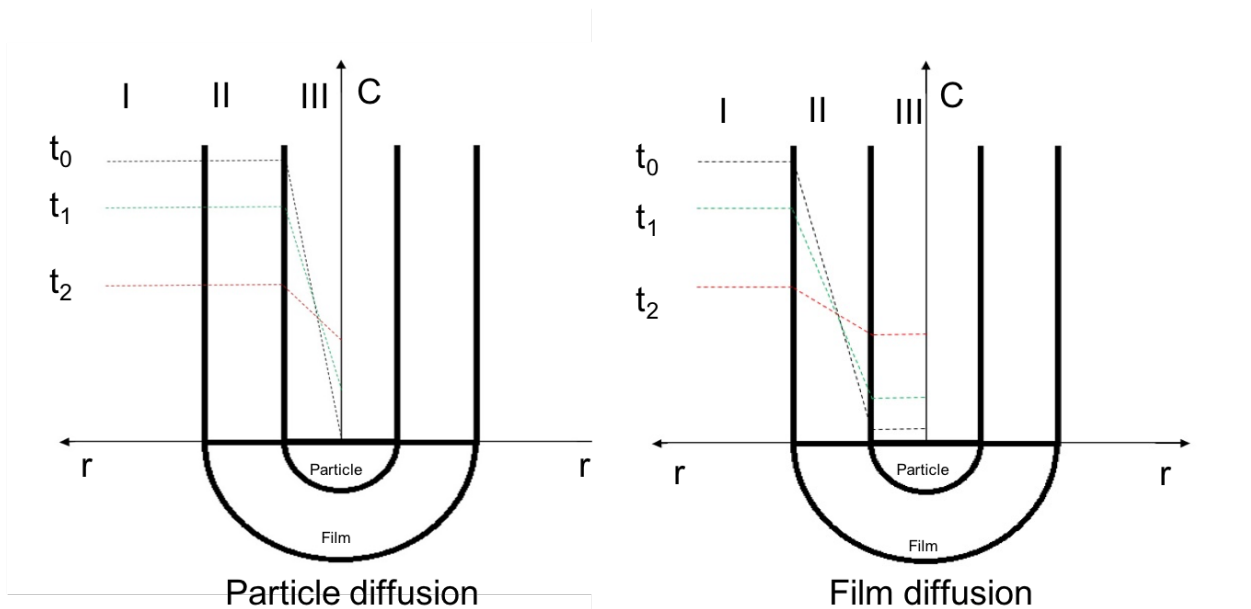


Figure 16. Diffusion model schematics.

Using Fick's first law in diffusion, Equation (15):

$$J = D \frac{dC}{dX} \quad (15)$$

Where J is diffusion flux ($\text{mol m}^{-2} \text{ s}^{-1}$), D is the diffusion coefficient ($\text{m}^2 \text{ s}^{-1}$), C is concentration (mol m^3), and X is position (m) [145]. Faster mixing speeds in batch tests increase the concentration gradient between solution and particle; this causes an increase in diffusion's flux. Faster mixing speed also makes the film thinner; this, again causes an increase in diffusion's flux. Faster mixing speeds shorten the required time to the equilibrium state by increasing the diffusion's flux. In other words, mixing speed does not affect the adsorption capacity, it affects the required time to reach the equilibrium state.

Following discussion explains the specifications of particle diffusion control process and film diffusion control process:

In particle diffusion: (1) the film diffusion is much faster than particle diffusion, (2) concentration gradients exist only in the beads, (3) exchange flux is proportional to the concentration of fixed charges, interdiffusion coefficient in the beads, and inversely proportional to the radius of the beads. In film diffusion: (1) particle diffusion is much faster than film diffusion, (2) concentration gradients exist only in the film, (3) exchange flux is proportional to solution concentration, interdiffusion

coefficient in the film, and inversely proportional to the film thickness [143]. To distinguish between particle diffusion and film diffusion in the adsorption process, interruption test [143] was employed as an experimental method. To do this, after letting the batch (with same experimental design as explained earlier for the kinetics study) run for 72 hours, the particles were removed from the solution for a brief period of time (without any actions on the particles) and then re-immersed the particles in a fresh lead solution (1,000 mL of 12 ppm concentration at a pH level of 5). The batch was run for another 72 hours while the solution was sampled at hours: 0.5, 1.5, 3, 6, 12, 24, 48 and 72. The short time between the two batches gives enough time for the concentration gradient in the particles to disappear, so: (1) with particle diffusion control, the adsorption rate immediately after re-immersion is greater than that prior to the interruption, (2) with film diffusion control, no concentration gradients in the particles exist, and the rate depends on the concentration difference across the film. Figure 17 shows the interruption test results for CZ and CDHZ¹.

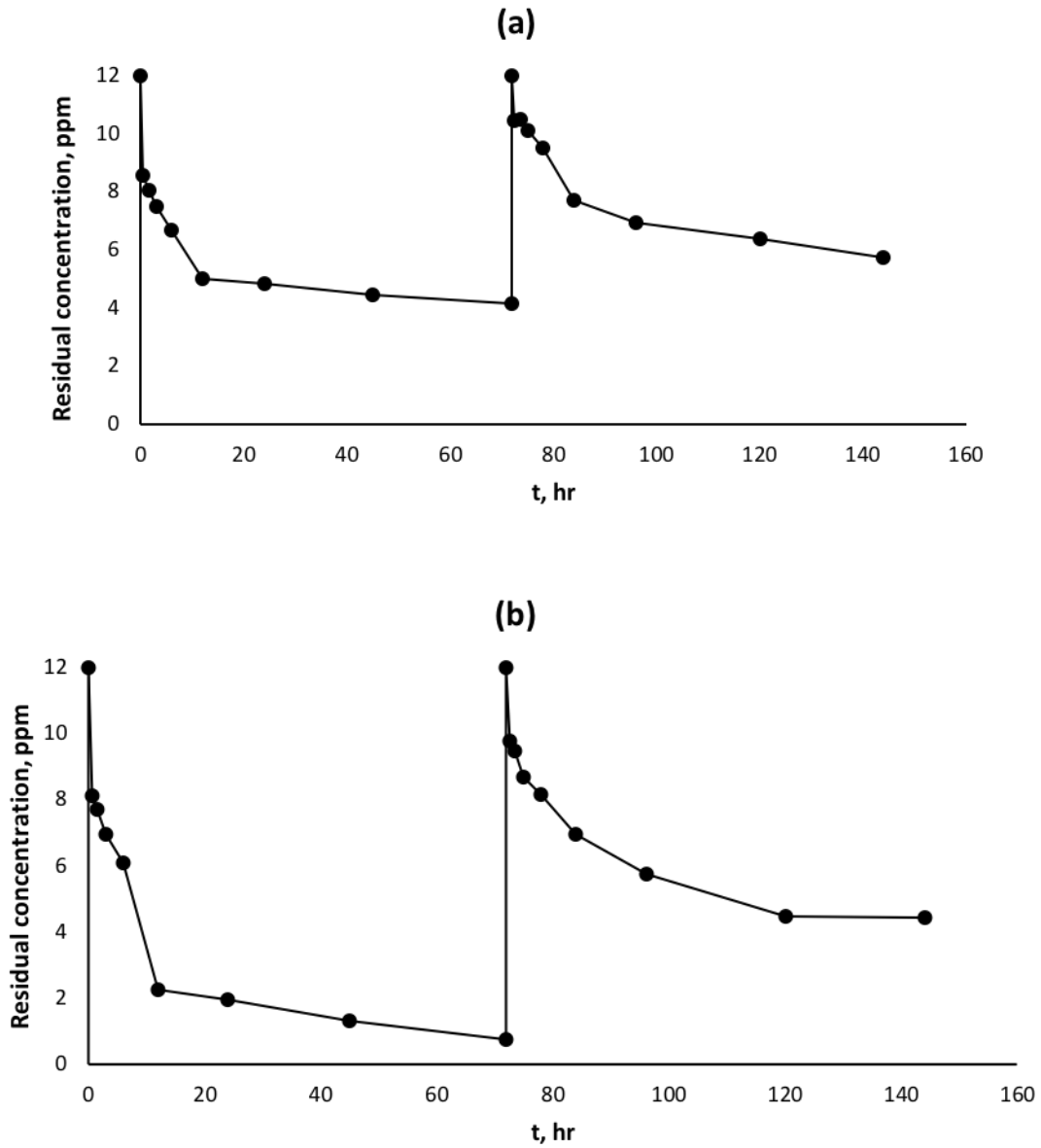


Figure 17. Interruption test results for: (a) CZ, (b) CDGHZ¹.

As can be seen in Figure 17, the ion exchange rate was found to be greater than prior to the interruption immediately after reimmersion, which confirms the ion exchange process to be as a particle diffusion-controlled process. With the obtained evidence

of a particle diffusion control process, analysis of the experimentally gathered data was performed using the following particle diffusion Equation (16) [27, 144, 146]:

$$\frac{q_t}{q_e} = \frac{6}{r} \sqrt{\frac{Dt}{\pi}} + C \quad (16)$$

where t is contact time (s), r is the radius of the adsorbent particle (equal to 0.5 mm in this work), and D is apparent diffusion coefficient. q_t/q_e was plotted versus $t^{1/2}$ and shown in Figure 18. The plots show a linear trend with an intercept close to zero for CZ and CDHZ, thus this model is likely to be the dominant rate controlling step.

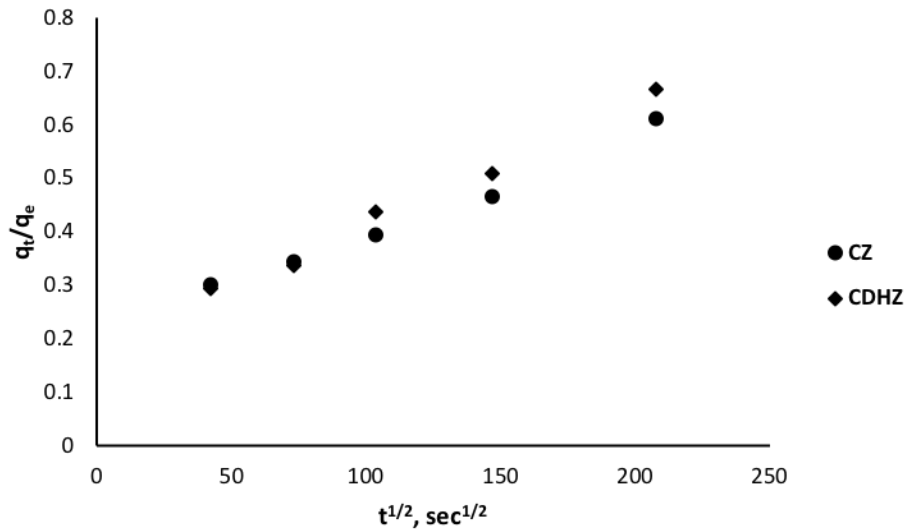


Figure 18. Particle diffusion model plot.

Calculation results of the kinetic models mentioned above showed that the Pseudo second-order had the best linearity for Pb adsorption, and according to the R^2 values, is the kinetic mechanism for lead adsorption.

Diffusion of Pb^{2+} into CDHZ¹ was faster than CZ (due to greater diffusion coefficient value), as can be seen in Table 14. This can be addressed by considering the presence of other components in CZ (impurities of the natural zeolite) that can affect the pass of Pb^{2+} through the CZ structure, since this adsorbent material was not pretreated before the adsorption test, or it was more difficult for Pb^{2+} ions to be exchanged with exchangeable cations in the natural zeolite structure.

Table 14. Particle diffusion parameters.

	CZ	CDHZ
R ²	0.986	0.991
C	0.210	0.188
D (cm ² s ⁻¹)	7.01*10 ⁻⁹	9.37*10 ⁻⁹

Effect of Cystamine Loadings on Removal Efficiency

As shown in the previous section, the adsorption capacity of CZ was increased from 31.46 to 54.50 mg/g for CDHZ¹. At this point, cystamine functional group's concentration is assumed to be in a direct relationship with the adsorption capacity of the functionalized zeolite. In order to investigate this assumption, zeolite was functionalized in a way that greater amounts of cystamine groups were introduced to the zeolite's structure. To functionalize the pre-treated zeolite (NaCl-Z) with cystamine functional groups, a 10 mM solution of cystamine dihydrochloride was

prepared by adding 4.50 g (20 mmol) of cystamine dihydrochloride crystals to 200 mL DI water. 10 g of sodium treated zeolite (NaCl-Z) was added to the solution and refluxed at 85 °C for 48 hours. Treated zeolite was washed with DI water and dried at 100 °C for 12 hours. This material is called as CDHZ². EDS analysis was employed to investigate the chemical composition of CDHZ² adsorbent.

Table 15. EDS analysis for CDHZ¹ and CDHZ².

	Na/Si	K/Si	Mg/Si	Ca/Si	S/Si
CZ	0.0135 ± 0.0034	0.0303 ± 0.0186	0.0145 ± 0.0062	0.1000 ± 0.0027	0.0078 ± 0.0011
CDHZ ¹	0.0694 ± 0.0115	0.0298 ± 0.0140	0.0100 ± 0.0093	0.0231 ± 0.0024	0.0572 ± 0.0041
CDHZ ²	0.0499 ± 0.0350	0.0448 ± 0.0350	0.0059 ± 0.0038	0.0353 ± 0.0072	0.0762 ± 0.0045

As can be seen in Table 15 the sulfur amount (as an element to quantify the amount of cystamine functional group) in CDHZ² is greater than that of CDHZ¹. This proves that functionalizing zeolite with a more concentrated cystamine dihydrochloride was successfully able to increase the amount of cystamine functional groups on the zeolite.

To evaluate the effectiveness of increased loadings of cystamine dihydrochloride on zeolite (from 1 mmol to 2 mmol), a batch test with the following specifications was designed: 200 mL of a 100 ppm lead solution was prepared, and the pH level was adjusted to pH = 5. Next, 0.20 g of CDHZ² was added to the batch as the adsorbent material. The batch was mixed for 24 hours at 200 rpm at room temperature. Residual lead concentration was measured in the solution by using ICP-MS. The

residual concentration was measured to be 51.26 ppm. No significant improvement in adsorption capacity can be found when comparing the results with the same batch by using CDHZ¹ (54.09 ppm residual concentration of lead). As explained earlier, it was assumed that the concentration of cystamine groups on zeolite structure can play a critical role in improving the adsorption capacity of the adsorbent. What the observed results suggest is that although the concentration of the cystamine groups on zeolite was increased, only a small number of Pb²⁺ ions were able to access the binding sites. In other words, the results demonstrated that the concentration of the cystamine groups is not the only parameter that affects the Pb²⁺ adsorption capacity of cystamine functionalized zeolite. And the adsorption of the Pb²⁺ is also affected and controlled by their accessibility to the active sites [120, 128].

Leaching of Cystamine Groups from Functionalized Zeolites

In this section, the leaching of cystamine groups from CDHZs is investigated. There are two possible reasons that cystamine groups might be leached off from the CDHZs: (1) leaching of cystamines from CDHZs because of a loose connection, and (2) leaching of cystamines from CDHZs during the Pb²⁺ adsorption tests. To quantify the amount of lost cystamines because of any of the mentioned reasons, first the amount of sulfur that is present in CDHZs structure (because of cystamine groups) was calculated as shown below and summarized in Table 16.

Cystamine dihydrochloride formula = C₄ H₄ Cl₂ N₂ S₂, molar weight = 225.20 g/mol.

There are two sulfurs in one structure unit, which is 2*32.06 g sulfur in 1 mole cystamine dihydrochloride.

Table 16. Cystamine dihydrochloride and sulfur loadings on zeolite.

	Cystamine dihydrochloride loading on adsorbent	S loading on adsorbent, mg/g zeolite
CDHZ ¹	1 mmol	64.14
CDHZ ²	2 mmol	128.26

To examine the first possibility of leaching cystamines, 0.20 g of CDHZ¹ added to 200 mL of Ultra-high purity water for 24 hours at 200 rpm. The amount of sulfur in the batch was measured by using ICP-MS. Results are listed in Table 17.

Sulfur concentration in the batch was converted to sulfur loss as μg Sulfur/g Zeolite, by using Equation (17):

$$Sulfur\ loss\left(\frac{\mu g\ S}{g\ Z}\right) = sulfur\ concentration\ in\ batch\ \left(\frac{\mu g}{L}\right) * Batch\ Volume\ (L) * \frac{1}{CDHZ\ mass\ (g)} \quad (17)$$

Since the batch volume of 0.20 L, and adsorbent mass in the batch equals to 0.20 g, these two cancel out and the value of sulfur loss (μg S/g Z) equals to the concentration of sulfur in the batch.

Sulfur loss percent was also calculated by using Equation (18):

$$Sulfur\ loss\ percent = \frac{sulfur\ loss}{initial\ sulfur} * 100 \quad (18)$$

Table 17. Sulfur concentration in Ultra-high purity water batch.

	Initial sulfur in adsorbent, mg /g	Sulfur loss, mg/g	Sulfur loss, %
CDHZ ¹	64.14	75.16 * 10 ⁻³	0.12

To calculate the number of mol of cystamine groups that was lost, Equation (19) was used:

$$\text{mol of thiol loss} = \frac{\text{sulfur loss}}{2 * \text{molar mass of sulfur}} \quad (19)$$

$$\text{thiol loss percent} = \frac{\text{mol thiol of loss}}{\text{initial thiol mol}} * 100 \quad (20)$$

Table 18 shows the cystamine groups loss in Ultra-high purity water batch.

Table 18. Cystamine groups loss in Ultra-high purity water batch.

	Initial cystamine in adsorbent, mol	Mol of cystamine loss	Cystamine loss, %
CDHZ ¹	1*10 ⁻³	1.17 *10 ⁻⁶	0.12

To quantify the amount of cystamine loss in an adsorption batch, this time 0.20 g of CDHZ¹ was added to 200 mL of a 10 ppm lead solution at pH =7, and mixed for 24 hours at 200 rpm at room temperature. The amount of sulfur in the batch was measured by using ICP-MS. Results are listed in Table 19.

Table 19. Sulfur concentration in lead removal batch.

	Initial sulfur in adsorbent, mg /g	Sulfur loss, mg/g	Sulfur loss, %
CDHZ ¹	64.14	$89.75 * 10^{-3}$	0.14

Percent loss of cystamine in lead removal batch is shown in Table 20.

Table 20. Cystamine groups loss in lead removal batch.

	Initial cystamine in adsorbent, mol	Mol of cystamine loss	Cystamine loss, %
CDHZ ¹	$1 * 10^{-3}$	$1.40 * 10^{-6}$	0.14

As shown earlier, 0.12% of the cystamine loss is due to the loose connection between cystamine groups and zeolite structure, which means only 0.02% of cystamine functional groups are lost in the lead adsorption batch.

ZnS-Z Fabrication

Nowadays, sonochemical methods have been proven as a useful technique for generating novel materials [147]. Ultrasound has its chemical effects from acoustics cavitation, which is basically formation, growth and impulsive collapse of bubbles in the liquid. Localized hot spots are formed as a result of the implosive collapse of the bubbles, through an adiabatic compression within the gas phase of the collapsing bubble. The extreme conditions resulted from bubble collapse have made the opportunity to prepare amorphous metals, carbides, oxides, sulfides, and composite

nanoparticles [148-155]. Zinc sulfide nanoparticles were grown on zeolite microstructure by using sonochemical methods in an aqueous batch containing zinc source and sulfur source.

Zn^{2+} was introduced to the silica structure via sonochemical process [148] in two possible ways: (1) the reactivity of surface -OH groups and solute radical groups, and (2) the chemical reactivity of Si-O⁻ nucleation sites which are formed due to ultrasonic breakage of the strained siloxane link toward the solute radicals. Since the zeolite used in this study includes 67 wt% of silica in its structure, similar reactions were expected to occur as shown in Figure 19.

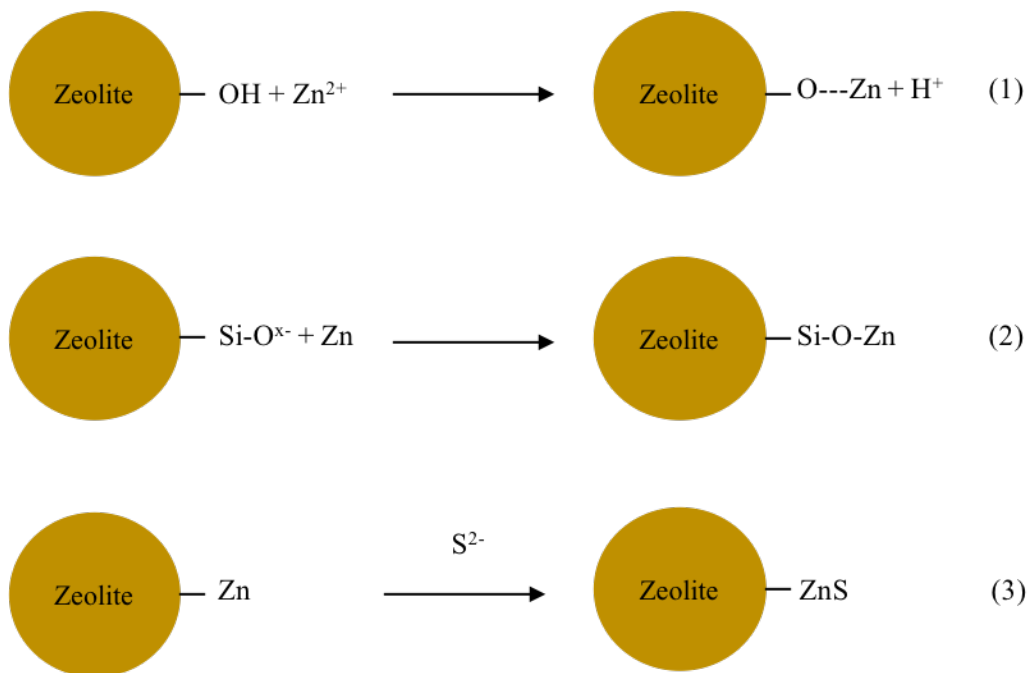


Figure 19. ZnS-Z fabrication schematic.

Zeolite Functionalization with Sulfide Nanostructures

A stoichiometrically equal ratio of zeolite, zinc acetate dihydrate and thioacetamide was mixed in a 4L round-bottom flask and sonicated in an aqueous medium. Ultrasonic irradiation was carried out with a high intensity (20 KHz) ultrasonic probe (QSONICA). The reaction vessel was kept in a water bath to maintain the temperature of the batch below 80°C. The reactant quantities and experimental parameters for the sonochemical preparation of ZnS functionalized zeolite (ZnS-Z) are summarized in Table 21.

Table 21. Reactant amounts and experimental parameters for sonochemical preparation of ZnS-Z.

reactant quantities, g				Sonication time, h	Batch temperature
Zeolite	Zinc acetate dihydrate	thioacetamide	DI-water		
4.50	21.53	7.51	3000	3	< 80 °C

In order to make sure that the functionalization process was successful, SEM imaging and EDS analysis were performed. As shown in Figure 20, the sonochemical treatment was able to form ZnS nanoparticles on the zeolite. The EDS pattern of ZnS-Z, Figure 21, shows the presence of Zn and S peaks. The measured amounts of Si, Zn, and S by using the EDS are summarized in Table 22. The variation of Zn:S ratio from 1:1 was related to the presence of Z in zeolite structure prior to the sonochemical process.

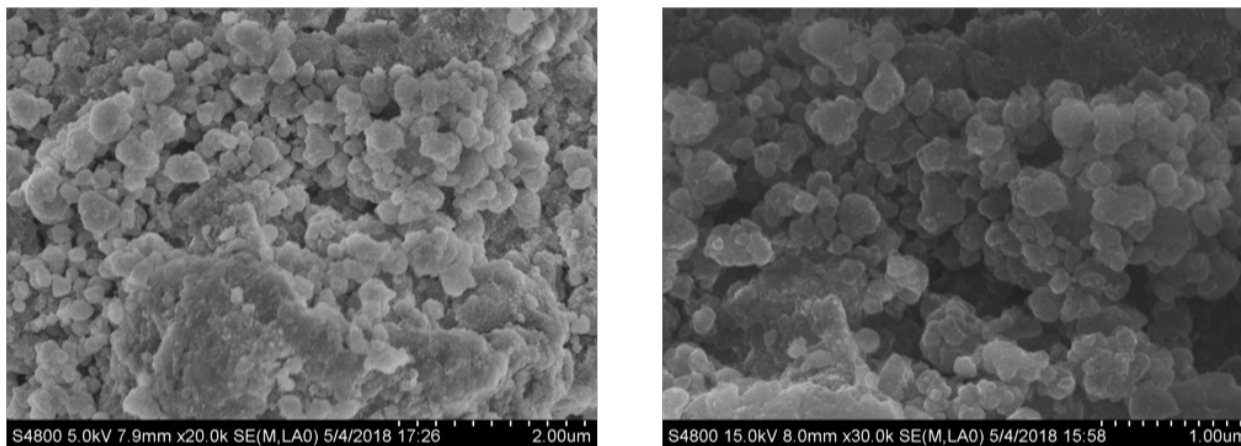


Figure 20. SEM images of ZnS-Z: ZnS nano particles.

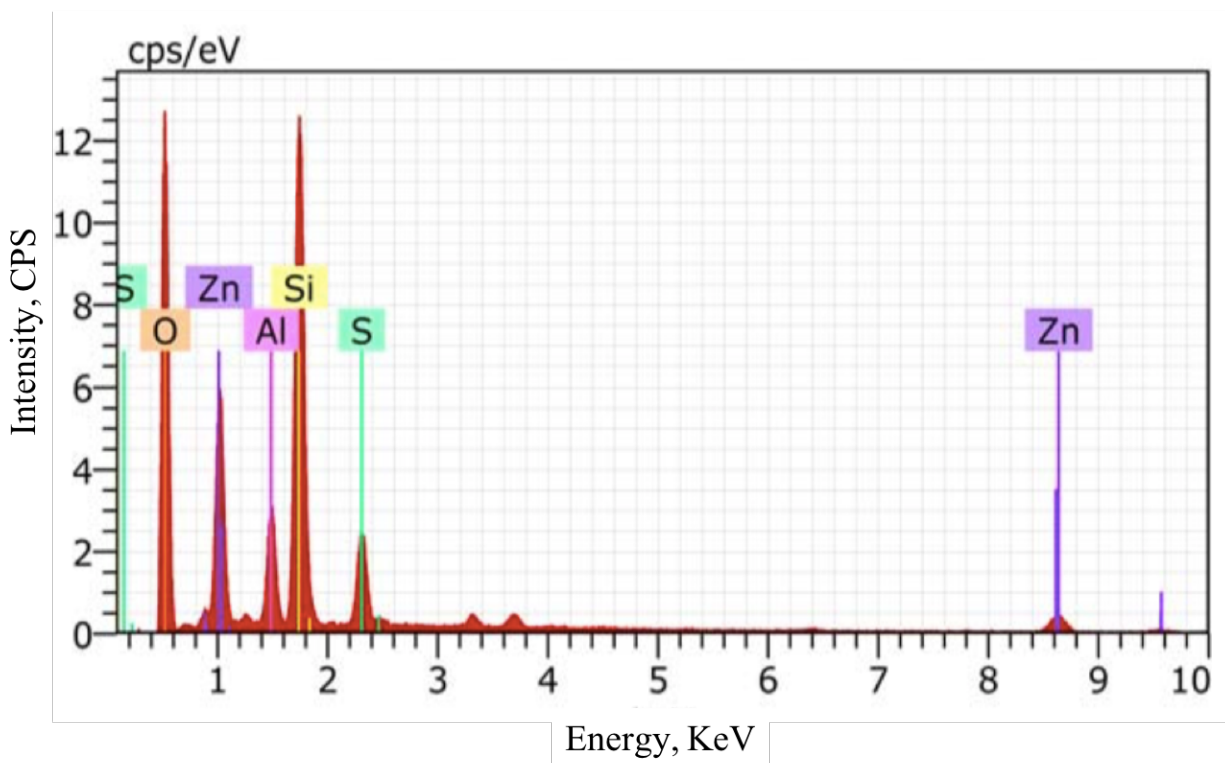


Figure 21. EDS plot for ZnS-Z: zinc and sulfur in ZnS-Z.

Table 22. Atomic percent of O, Si, Zn, and S in CZ and ZnS-Z.

Element	C, wt.%	
	CZ	ZnS-Z
O	52.26	49.12
Si	30.81	27.33
Zn	3.85	6.59
S	0.23	5.26

Effect of Competing Ions on ZnS-S' Removal Efficiency

The sorption of Pb, Hg, and Ni onto ZnS-Z was investigated as a function of their initial concentration in a mixed system by varying the metal concentrations from 1 to 25 ppm at room temperature while keeping all other parameters constant. Results are shown in Table 23. Distribution coefficient (K_d) is defined as the ratio of the metal concentration on the adsorbent (solid phase) to that in the solution at the equilibrium state [54, 156, 157]. Such coefficient is a useful index for comparing adsorption capacities of ZnS-Z for a particular ion under the same experimental condition.

Higher K_d values indicate high metal retention by the adsorbent (solid phase) through chemical reactions [156-161]. The distribution coefficient (K_d) was calculated over the whole range of the initial concentrations of Pb, Hg, and Ni. Also, an average K_d was calculated to obtain a comparable value for each metal, so that the selectivity sequence of the metal ions has been established.

K_d is illustrated as a function of metal ions concentration in Table 23. Data in this table shows that with the increase in initial concentration the removal percentage of the metal ions is decreased. This shows that changes occur in the nature of adsorption sites involved in the sorption process, based on the metal ions concentration level [162]. The higher K_d values resulted in the experiments with lower metals concentrations associated with the adsorption sites of high selectivity, with relatively strong bonding energies. Otherwise, adsorption becomes unspecific at higher metal concentrations, when bonding sites become progressively occupied, and this results in lower K_d values [162-164]. Increasing the metal concentrations may also result in saturation of adsorption sites and decreasing the adsorption capacity.

According to the distribution coefficient values, the selectivity sequence of Pb, Hg, and Ni by ZnS-Z was obtained as $Hg > Pb > Ni$. Mercury showed the highest K_d values followed by lead and nickel, Table 23. This behavior is attributed to differences in metal characteristics and affinity for adsorption sites [165]. Hg has a greater affinity to ZnS-Z functional groups since it is a soft Lewis acid; compared with Ni^{2+} and Pb^{2+} which are borderline Lewis acids. The sorption preference found by ZnS-Z for Pb over Ni is explained by: (a) the greater hydrolysis constant, (b) the higher atomic weight, and (c) the higher ionic radius (smaller hydrated radius).

Table 23. Removal efficiency and distribution coefficient at equilibrium time.

	Pb		Hg		Ni	
	Removal efficiency, %	K_d	Removal efficiency, %	K_d	Removal efficiency, %	K_d
1	74.00	2.85	87.00	6.69	14.00	0.16
5	52.00	1.08	80.40	4.10	13.60	0.15
10	21.00	0.26	69.80	2.31	7.40	0.08
25	2.08	0.02	26.80	0.37	6.00	0.06
K_d , average		1.05		3.37		0.11

ZnS-Z Particles Regeneration

In this section, four adsorption/desorption cycles were conducted for Pb, to investigate the adsorption/desorption behavior of ZnS-Z once it has been regenerated three times. Column test was employed to saturate the adsorbents particles with Pb. A column with a height of 200 mm and an internal diameter of 10 mm was used. The column was packed with 4.00 g of ZnS-Z to make a height of 50 mm. the column was then operated in such a manner that 1000 mL of 100 ppm lead solution was constantly added to it by using a peristaltic pump and allowing it to flow along gravity in down-flow mode with a constant flow rate of 0.08 mL/s. The rate of flow was monitored by measuring the amount of lead solution in mL flowing per minute at regular time intervals. Once the column was started, samples were collected at different time intervals. The process was continued until the whole 1000 mL lead solution is passed the column. Samples were taken to ICP-MS to measure the lead concentration in the samples. Figure 22 shows schematics of the column test set up.

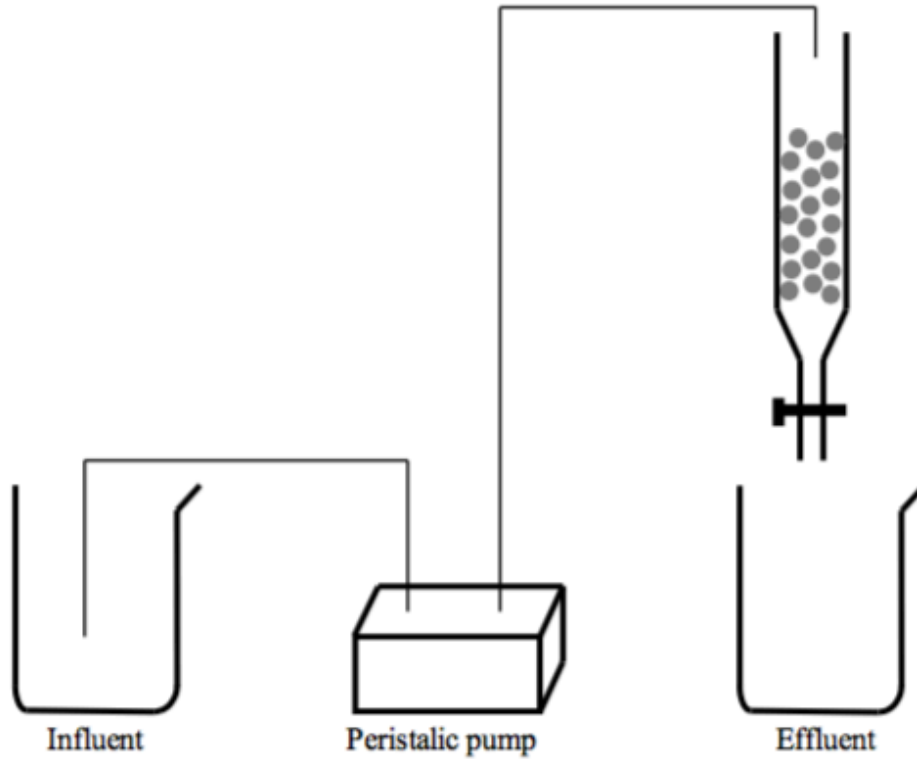


Figure 22. Column test schematic.

The main design parameters of this system are the contact time, and linear velocity which are shown in Equations (21-23):

$$\text{contact time} = \frac{\text{Bed volume (m}^3\text{)} * 60 \left(\frac{\text{min}}{\text{h}}\right)}{\text{Flow rate (}\frac{\text{m}^3}{\text{h}}\text{)}} = 0.82 \text{ min} \quad (21)$$

$$\text{linear velocity} = \frac{\text{Flow rate (}\frac{\text{m}^3}{\text{h}}\text{)} * \frac{\text{h}}{60 \text{ min}}}{\text{Surface area (m}^2\text{)}} = 0.06 \text{ m/min} \quad (22)$$

$$\text{space velocity} = \frac{\text{Flow rate (}\frac{\text{m}^3}{\text{h}}\text{)}}{\text{Bed volume (m}^3\text{)}} = 73.38 \text{ hr}^{-1} \quad (23)$$

In Table 24 all the parameters of the column test are listed.

Table 24. Column test parameters.

Parameter	Value
Particles diameter, mm	0.70 – 1.00
Column height, mm	200
Bed height, mm	50
Bed diameter, mm	10
Flow rate, mL/sec	0.08
Contact time, min	0.82
Linear velocity, m/min	0.06
Space velocity, hr ⁻¹	73.38
Influent concentration, ppm	100

The desorption was completed by using a 10% HNO₃ solution [166]. After the desorption step, particles were re-functionalized according to the sonochemical process explained earlier in this paper. Figure 23 shows C_t/C_0 (C_t is Pb concentration in effluent at time t , C_0 is the effluent initial concentration) plots against time.

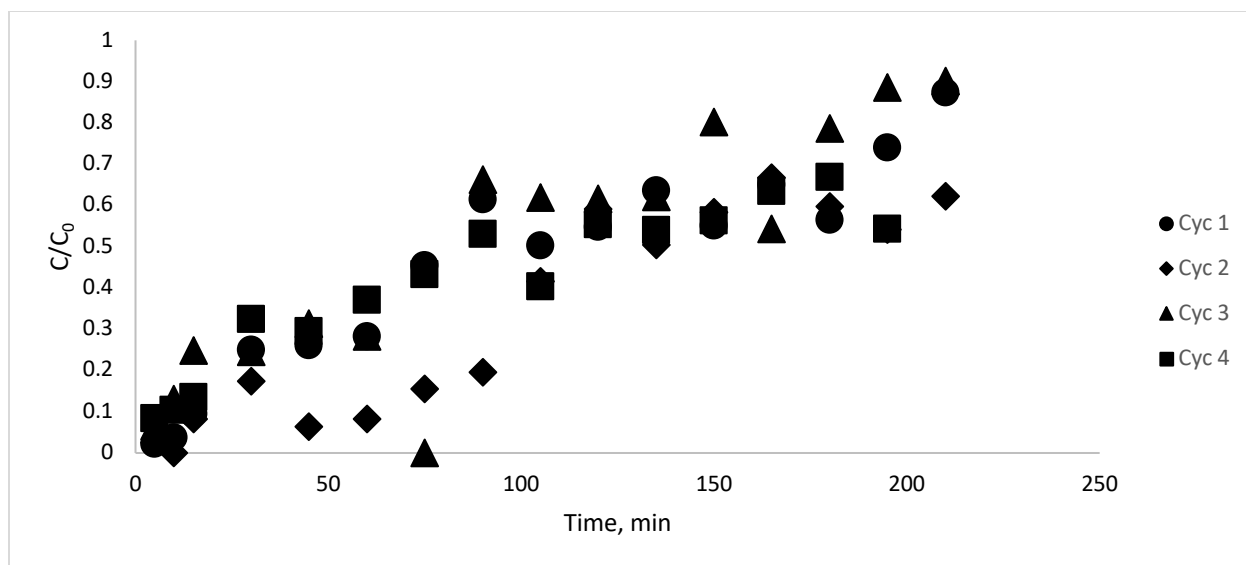


Figure 23. Regeneration cycles for Pb removal by using ZnS-Z.

As seen in Table 25 during the first four cycles of adsorption/desorption, the regenerated ZnS-Z retained its removal efficiency. One main reason that accounts for this behavior is the fact that re-functionalization step can modify ZnS-Z structure by introducing functional groups to the particles. During the adsorption and/or desorption process, ZnS-Z can possibly lose some of its functional groups, so the re-functionalization step helps the particles to regain their functional groups. No reduced regeneration efficiency was found up to four cycles.

Table 25. Removal efficiency for regenerated ZnS-Z particles.

	Cycle 1	Cycle 2	Cycle 3	Cycle 4
Removal efficiency, %	63	61	61	59

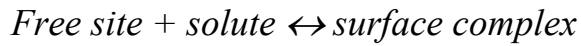
Chapter 5

Application of Isotherm Models to Predict: Equilibrium Concentration, Removal Efficiency, Adsorption Capacity, and Required Amount of Adsorbent

In this chapter, equations are developed to predict the equilibrium concentration (C_e), the removal efficiency (R%), the adsorption capacity (q_e), and the required amount of adsorption (M). Isotherm models used as explained in this chapter.

Langmuir Isotherm

In Langmuir model, the solid is assumed to have an adsorption capacity as q_{max} . In this model: (a) all adsorption sites are assumed to be identical, (b) each site adsorbs one molecule of the adsorbate material, and (c) all sites are independent energetically [142]. Holding these assumptions true, the following reaction can be considered as shown in Equation (24):



And Langmuir isotherm is equation (25):

$$\frac{1}{q_e} = \left(\frac{1}{K_L q_{max}} \right) \frac{1}{C_e} + \frac{1}{q_{max}} \quad (25)$$

Where q_e is adsorbate mass adsorbed per unit adsorbent mass at equilibrium (mg/g), K_L is Langmuir isotherm constant (L/mg), C_e is adsorbate concentration at equilibrium (mg/L), and q_{max} is the maximum adsorption capacity (mg/g). Maximum

adsorption capacity, q_{\max} can also be expressed as N_t , which is a measure of the total number of functional groups available per gram of adsorbent.

Lead solution with initial concentrations of 10, 25, 50, 100, 250 and 500 ppm at a pH level of 5 were employed for the batch tests. Lead removal tests were conducted by using 0.20 g of ZnS-Z in 200 mL of the solution. The solution was mixing over 24 hours at 200 rpm at room temperature to reach the equilibrium state. Figure 24 shows the isotherm plot for lead removal experiments.

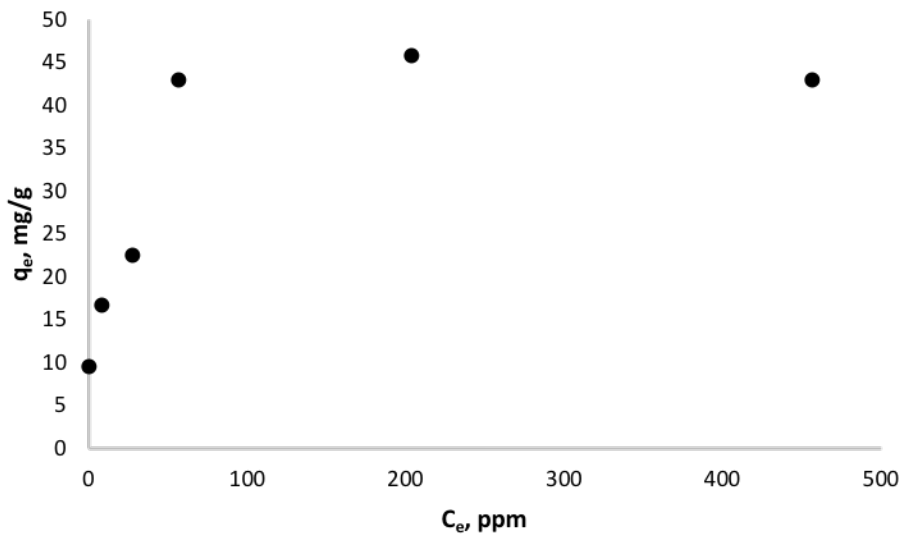


Figure 24. Isotherm plot for lead removal tests by using ZnS-Z at pH = 5.

In Equation (25), $1/q_e$ can be plotted as a function of $1/C_e$. When the data shows a good linearity, the adsorption process is considered to follow Langmuir isotherm.

K_L and q_{\max} can be calculated by using slope and intercept, respectively.

Figure 25 shows the Langmuir model plot for removal batch tests at pH = 5. Calculated parameters are listed in Table 26.

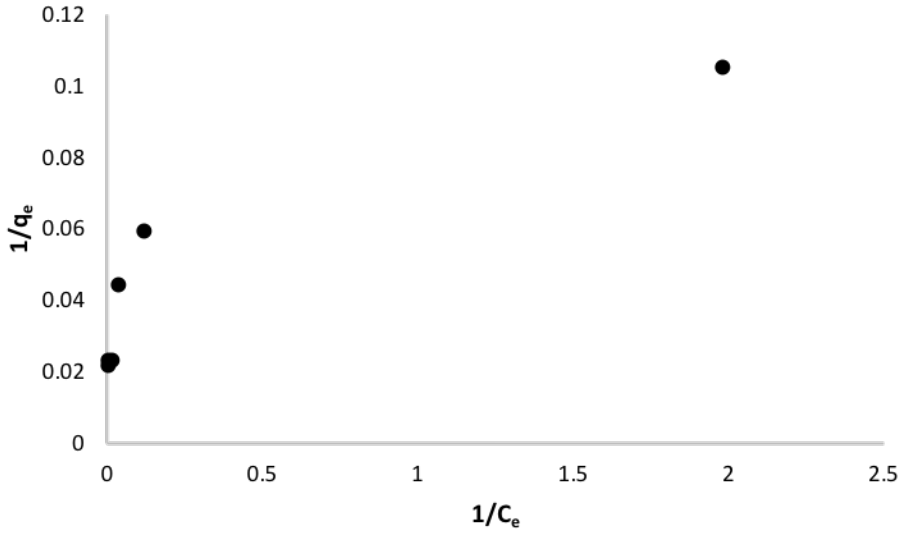


Figure 25. Langmuir plot for lead removal tests by using ZnS-Z at pH = 5.

Table 26. Langmuir model parameters for lead removal tests by using ZnS-Z at pH = 5.

Parameter	Value
R ²	0.826
q _{max} , mg/g	30.487
K _L , L/mg	0.879

In this study, the mass balance in the batch was also used as shown in Equation (26)

[140]:

$$V.C_0 = V.C_e + V.C_e^s \quad (26)$$

Where C_0 is the initial concentration of the solute, C_e^S is the concentration of the solute on adsorbent at the equilibrium. Equilibrium adsorption capacity q_e can be expressed in terms of solution volume, V , and adsorbent mass, M , as Equation (27):

$$q_e = \frac{V \cdot C_e^S}{M} = \frac{V(C_0 - C_e)}{M} \quad (27)$$

Substituting Equation (27) in Equation (25), gives the following second-order function in which C_e is one argument variable, Equation (28):

$$K_L C_e^2 + \left(1 + \frac{K_L \cdot q_{max} \cdot M}{V} - K_L \cdot C_0\right) \cdot C_e - C_0 = 0 \quad (28)$$

All variables other than C_e were considered as constants, and C_e can explicitly be solved [167, 168]:

$$K_L = a \quad (28.1)$$

$$\left(1 + \frac{K_L \cdot q_{max}}{V} - K_L \cdot C_0\right) = b \quad (28.2)$$

$$C_0 = c \quad (28.3)$$

$$C_e = \frac{-b \pm \sqrt{b^2 - 4ac}}{2a} \quad (28.4)$$

The calculated C_e is a function of C_0 and M for a specific V with parameters K_L and q_{max} . Once K_L and q_{max} were obtained from the conducted set of adsorption experiments (Table 26), equilibrium solute concentrations were calculated for the

given initial solute concentration and adsorbent mass in a fixed volume. Calculated values were plotted versus the experimental values of equilibrium concentration (C_e), and is shown in Figure 26.

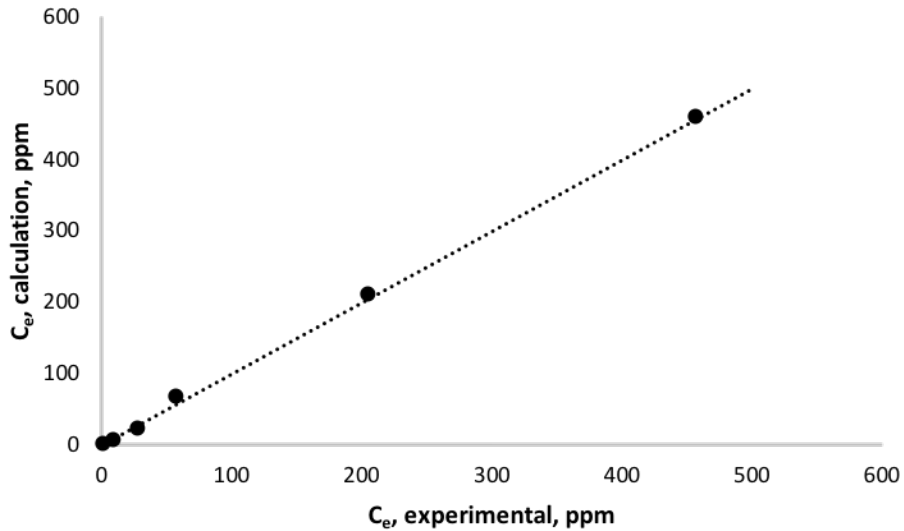


Figure 26. Calculated versus experimental values of C_e , by using Langmuir model.

As shown in Figure 26, calculated values for equilibrium concentrations, C_e , are in agreement with the experimental values.

After finding C_e , removal efficiency, R , can also be calculated as a function of C_0 and M by using Equation (29).

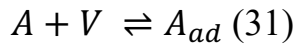
$$R = \frac{C_0 - C_e}{C_0} \quad (29)$$

Also, for a given C_0 and target removal efficiency, the model equation to predict the required mass of adsorbent can be obtained by using Equation (30):

$$M = \frac{V \cdot R}{K_L \cdot q_{max} \cdot (1 - R)} + \frac{V \cdot R}{q_{max}} \cdot C_0 \quad (30)$$

Modified Langmuir Equation

If one investigates the Langmuir model in generate detail, and considers its theoretical background that can be explained as a reversible adsorption and desorption process for A species, the equation will be expressed as Equation (31):



Where V and A_{ad} are the vacant and occupied sites, respectively. The respective rates for adsorption and desorption can be expressed by Equations (32-33):

$$r_a = k_a C(1 - \theta) \quad (32)$$

$$r_d = k_d \theta \quad (33)$$

Where C is solute concentration and θ is surface coverage. This coverage θ also can be defined as q/q_{max} , where q is the adsorption capacity and q_m is maximum adsorption capacity, respectively.

When in equilibrium, $r_a = r_d$, yielding the Langmuir isotherm, modelled in Equations (34-35):

$$\theta_e = \frac{K_L C_e}{1 + K_L C_e} \quad (34)$$

Or

$$q_e = \frac{q_m K_L C_e}{1 + K_L C_e} \quad (35)$$

Where $K_L = K_a / K_d$ is the Langmuir equilibrium constant.

Equation (32) shows that the rate of adsorption depends on the fraction of available vacant sites, and the concentration of the solute. This means that the forward adsorption rate approaches zero when the available vacant sites are being occupied by the adsorbate, or in other words, when the adsorbent is saturated by solute, $\theta = 1$.

In equation (32) the term $(1-\theta)$ is the limiting factor for the adsorption rate. On the other hand, in equation (33), it shows that the desorption rate only depends on the surface coverage, θ , without the concentration of the solute being considered as a factor. Following the statistical rate theory [169, 170] differences in chemical potential ($\mu_s - \mu_b$) of solute in adsorbent phase (μ_s) and solution phase (μ_b) is the

driving force of the desorption reaction. Therefore, solute concentration is a parameter affecting the desorption process. For example, if we consider two systems with adsorbents that have similar surface coverage and are in contact with solutions of differing solute concentrations, $C_1 < C_2$. According to the Langmuir model the desorption rate in these two systems should be similar since the rate of desorption only depends on surface coverage, θ . However, the solute chemical potential in solution μ_b is not identical between the two systems. The tendency of the solute to be desorbed from the adsorbent's surface is greater in the system with a lower solute concentration in the solution, system 1. Thus, it can be concluded that desorption is affected by the solution's solute concentration. As soon as the bulk solution is saturated by the solute (C_s), there will be no further unidirectional desorption occurring, so it can be said that desorption is possible in an unsaturated solution, with its highest rate of desorption at $C = 0$. The lowest rate, on the other hand, is when $C \rightarrow C_s$. This leads to the conclusion that the rate of desorption is proportional to $C_s - C$, as shown in Equation (36):

$$r_d = k_d(C_s - C)\theta \quad (36)$$

Equating Equations (32) and (36) at equilibrium yields Equations (37) and (38):

$$\theta_e = \frac{K_{ML}C_e}{(C_s - C_e) + K_L P_e} \quad (37)$$

Or,

$$q_e = \frac{q_m K_{ML} C_e}{(C_s - C_e) + K_{ML} C_e} \quad (38)$$

Where K_{ML} is the modified Langmuir equilibrium constant, and C_s is solute solubility in water. It is important to note that K_{ML} is a dimensionless constant.

Finally, the linear form of this equation can be written as Equation (39):

$$\frac{1}{q_e} = \frac{C_s}{K_{ML} q_m C_e} + \frac{(K_{ML} - 1)}{K_{ML} q_m} \quad (39)$$

Plotting $1 / q_e$ versus $1 / C_e$ yields a straight line with a slope of $C_s / K_{ML} q_m$ and an intercept value of $(K_{ML} - 1) / K_{ML} q_m$. The shape of this plot will be identical to the Langmuir model plot, because the q_e and C_e values are determined experimentally and regardless of the model which is used to fit the data. C_s values are available in [171]. Since in this study lead solutions were prepared by using lead nitrate, $Pb(NO)_3$, the solubility of lead nitrate in water at room temperature was used to calculate the C_s value for lead. Lead nitrate solubility in water at room temperature

equals 597 g/L [171], and this equals 373.485 g/L lead ions. Calculated values of the modified Langmuir model are listed in Table 27.

Table 27. Calculated values of the modified Langmuir model for ZnS-Z at pH = 5.

Parameter	Value
R ²	0.826
C _s , mg/L	373.485 * 10 ³
q _m , mg/g	30.497
K _{ML}	3.287 * 10 ⁵

As can be seen in Tables 23-24, calculated values of q_m are very close: 30.497 versus 30.497 for Langmuir and modified Langmuir models, respectively. This can be addressed by considering the range of solute concentration at which the experiments were carried out. The most concentrated solution had a concentration level of 500 ppm (500 mg/L), while the solubility of the solute was 373.485 * 10³ mg/L. Which means the solubility of the solute is about 747 times and 830 times larger than initial and equilibrium concentrations of the solute respectively. It can be concluded that the tendency of the solute to be desorbed from the adsorbent's surface is high in the

system where the equilibrium concentration is negligible compared to the saturation concentration of the solute.

Freundlich Isotherm

Freundlich isotherm is the most commonly used model that explains the non-ideal and reversible adsorptions [137]. This model is not limited to the formation of a monolayer on the adsorbent surface, so it can be applied to multilayer adsorption systems. Considering multilayer adsorption, the total quantity adsorbed is the summation of adsorption on all sites, where sites possessing greater binding activity are occupied first until the adsorption energy has decreased to the point of adsorption process completion [138]. The Freundlich model is based on the relation between the adsorbed quantity (q_e) and the concentration of remaining solute (C_e) [172], equation (40):

$$q_e = K_F \cdot C_e^{1/n} \quad (40)$$

Where K_F is the constant of the Freundlich isotherm constant ($L^{1/n}mg^{(1-\frac{1}{n})}/g$), and $1/n$ is the Freundlich exponent ($n =$ the index of heterogeneity). Equation (40) can be written in linear form as shown in equation (41):

$$\log q_e = \frac{1}{n} \log C_e + \log K_F \quad (41)$$

Like the Langmuir adsorption isotherm, Equation (41) was used to evaluate whether or not the adsorption process satisfies the Freundlich isotherm. To do this, the data from the batch experiments were employed. Figure 27 shows the Freundlich isotherm plot for lead removal experiments.

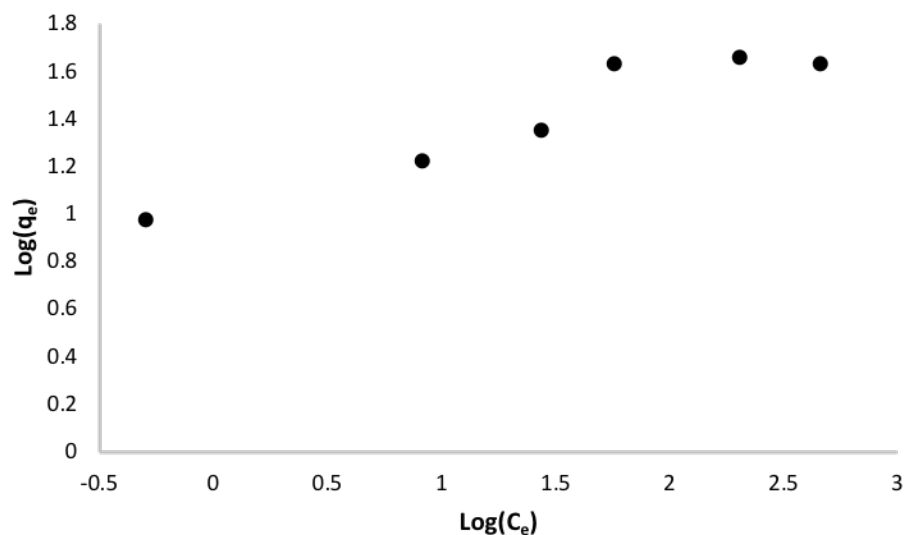


Figure 27. Freundlich plot for lead removal tests by using ZnS-Z at pH = 5.

Calculated parameters for the Freundlich isotherm are listed in Table 28. As can be seen in Figure 27 and Table 28 the experimental results showed appreciable linearity, $R^2 = 0.910$, meaning that the adsorption process was considered to follow Freundlich isotherm.

Table 28. Freundlich isotherm constants for ZnS-Z at pH = 5.

Parameter	Value
R ²	0.910
1/n	0.251
K _F	11.145

Reformulating the Freundlich isotherm with mass balance in the system can be expressed as Equation (42):

$$\frac{K_F M}{V} \cdot C_e^{1/n} + C_e - C_0 = 0 \quad (42)$$

In which, C_e is the argument variable. Again, C_e is a function of C_0 and M for a specific V with parameters K_F and $1/n$.

Once K_F and $1/n$ were obtained from the conducted set of adsorption experiments (Table 28), equilibrium solute concentrations were calculated for the given initial solute concentration and adsorbent mass in a fixed volume. Calculated values were plotted versus the experimental values of equilibrium concentration (C_e), and is shown in Figure 28.

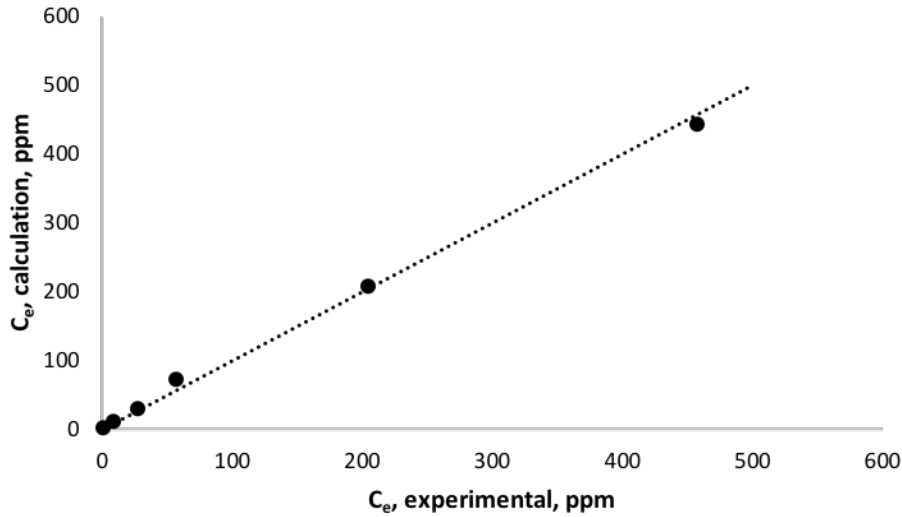


Figure 28. Calculated versus experimental values of C_e , by using Freundlich model.

As shown in Figure 28, calculated values for equilibrium concentrations, C_e , are in agreement with the experimental values.

The required mass of the adsorbent for the desired removal efficiency can also be derived as equation (43):

$$M = \frac{V}{K_F} \frac{R}{(1 - R)^{1/n}} C_0^{(1-1/n)} \quad (43)$$

pH-dependent Model

As described in the following section, all experiments were carried out at a constant pH level. Therefore, all the derived equations are only valid for the pH level at which the experiments are conducted. In order to develop a model with the ability to predict the equilibrium residual concentration at different pH levels, experiments were

conducted to generate adsorption isotherm data across multiple pH values. All the data sets were able to be fitted to the Langmuir model, and K_L values were calculated across the experimental range of pH values. Considering the K_L value as a criterion for the affinity between adsorbent and adsorbate, it was assumed that the value of K_L could vary with the change of solution pH. To obtain the relationship between K_a and pH: $\log(K_a)$ values were plotted against pH. The linear relationship is described using Equation (44):

$$\text{Log}K_a = m * \text{pH} + d \quad (44)$$

Where m and d are line fitting parameters.

Substituting Equation (44) in Equation (28) will give:

$$\begin{aligned} (10^{m*\text{pH}+d})C_e^2 + \left(1 + \frac{(10^{m*\text{pH}+d}) \cdot q_{max}}{V} - (10^{m*\text{pH}+d}) \cdot C_0\right) \cdot C_e - C_0 \\ = 0 \quad (45) \end{aligned}$$

This analytical equation can be used to describe variation in adsorption at differing pH values using a consistent set of isotherm parameters.

To verify the hypothesis, the data set were generated by performing lead adsorption tests on ZnS-Z at pH levels of 3 and 4. The data were fitted with the Langmuir model and are shown in Figure 29. The estimated values of K_L are summarized in Table 29.

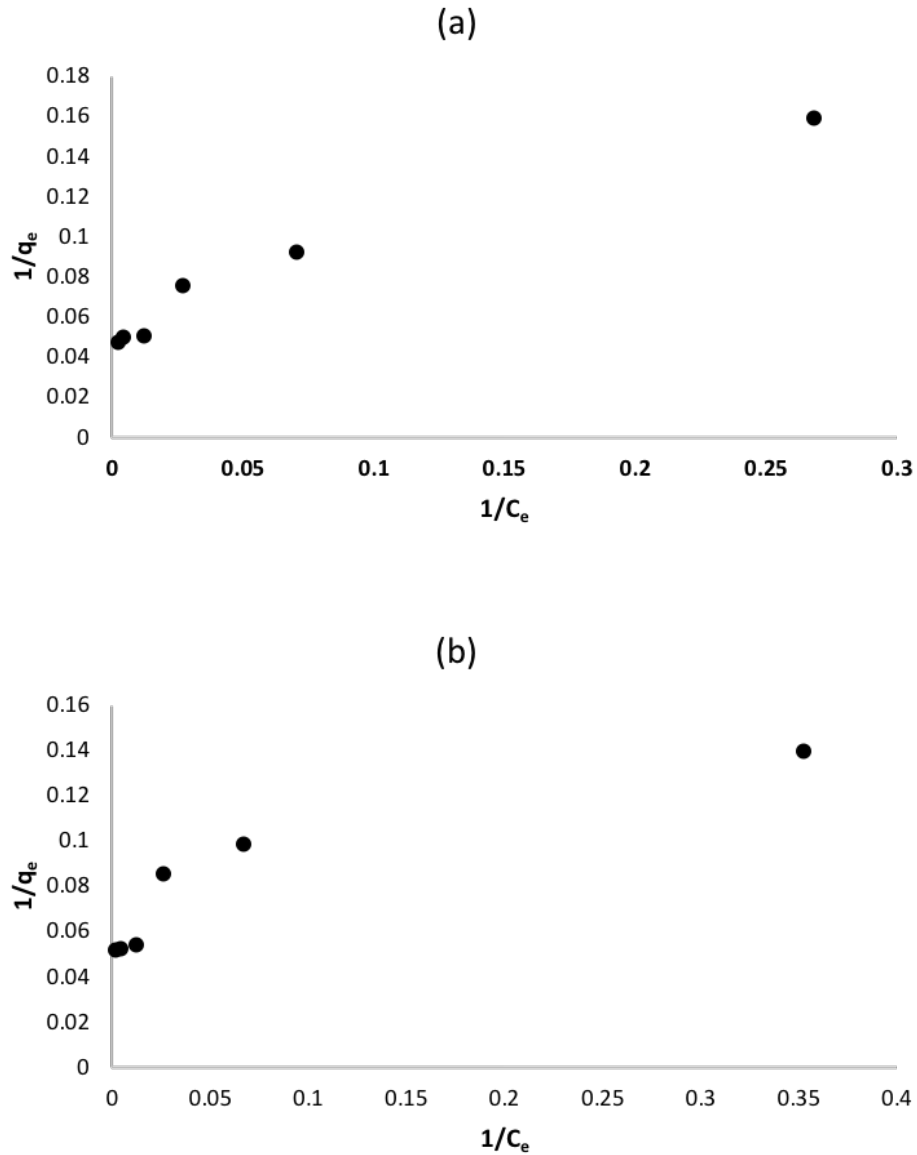


Figure 29. Langmuir plots for lead removal tests by using ZnS-Z: (a) pH = 3, (b) pH = 4.

Table 29. Langmuir isotherm parameters for lead adsorption on ZnS-Z at pH = 3 and pH = 4.

		pH = 3	pH = 4
Langmuir isotherm	R^2	0.961	0.820
	q_{\max} , mg/g	18.780	19.223
	K_L , L/mg	0.130	0.270

To establish a relationship between K_L and pH, $\text{Log}(K_L)$ values were plotted against pH values as shown in Figure 30.

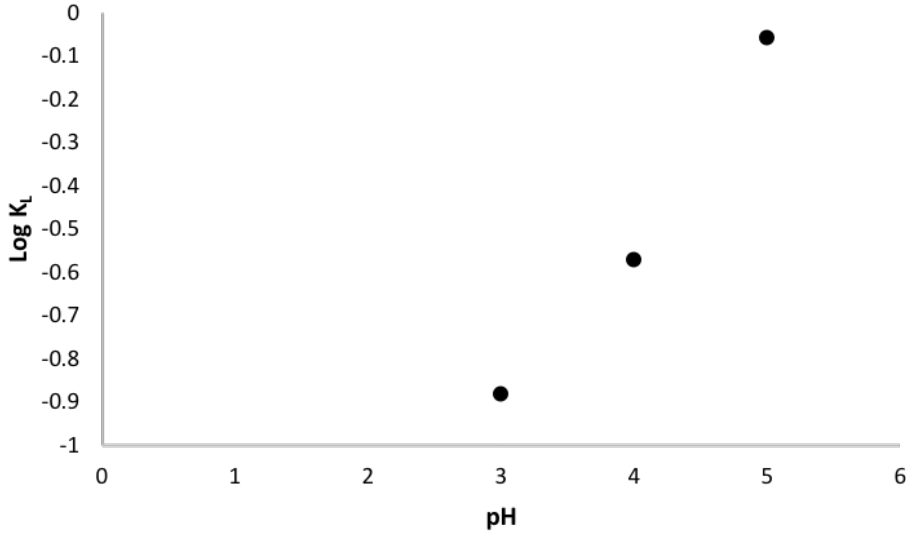


Figure 30. Langmuir constant (K_L) vs. pH for lead adsorption on ZnS-Z.

The R^2 value for the linear fit was 0.98 and the linear equation is shown in Equation (46):

$$\text{Log}(K_L) = 0.41\text{pH} - 2.14 \quad (46)$$

Substituting Equation (46) in Equation (45):

$$(10^{0.41 \cdot \text{pH} - 2.14}) C_e^2 + \left(1 + \frac{(10^{0.41 \cdot \text{pH} - 2.14}) \cdot q_{\text{max}} \cdot M}{V} - (10^{0.41 \cdot \text{pH} - 2.14}) \cdot C_0\right) \cdot C_e - C_0 = 0 \quad (47)$$

To validate the ability of Equation (47) to predict the equilibrium residual concentration, predictions for experimental adsorption data was carried out. These predictions were compared with the experimental data of lead adsorption on ZnS-Z

at multiple pH values of 3, 4, and 5; the results are summarized in Figure 31. This figure shows that Equation (47), as a prediction model, was able to predict experimental data at different pH levels. Predictions were conducted for 6 different initial concentrations and showed an excellent match with experimental data.

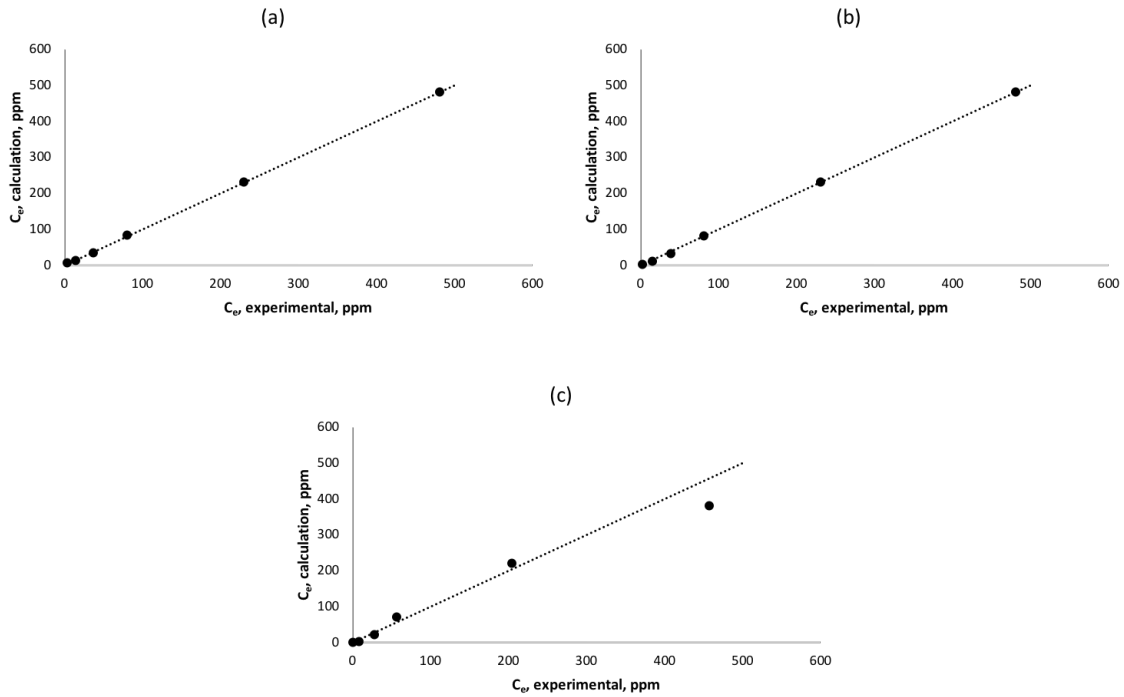


Figure 31. Predicted versus experimental values of C_e : (a) pH = 3, (b) pH = 4, (c) pH = 5.

Chapter 6

Conclusions

Zeolite was functionalized by sulfide-based materials (as functional groups) to remove lead from aqueous solutions. The effect of multiple factors such as solution's initial concentration, solution pH, contact time, and functional groups content on the structure, properties, and performance of the functionalized zeolites were investigated. ICP-MS was used to determine the lead residual concentration. The research led to the following conclusions:

1. Treating zeolite with different salts confirmed that sodium ion is the most exchangeable cation in the zeolite's structure. Zeolite is successfully functionalized by cystamine dihydrochloride with a loading amount of 0.57 mmol cystamine per g zeolite.
2. Functionalizing zeolite improved its adsorption capacity for lead by 173.24% compared with the adsorption capacity of zeolite. The analysis of cystamine functional group's concentration on the adsorption capacity of CDHZ show that the concentration of the cystamine groups is not the only parameter that affects the Pb^{2+} adsorption capacity of cystamine functionalized zeolite. The adsorption of the Pb^{2+} is also affected and controlled by their accessibility to the active sites.
3. By using adsorption isotherms and mass balance in the adsorption process, the equilibrium residual concentration for lead adsorption is successfully predicted for a known adsorption test.

4. The relationship between the Langmuir constant (K_L) and the solution pH is determined, so an isotherm based analytical model is proposed to predict the equilibrium residual concentration and removal efficiency at multiple pH values.

Future work

The knowledge that is gained from this work can be applied to improve the heavy metal removal capacity of the functionalized zeolite toward a vast range of heavy metal ions. One or a combination of the following methods can be helpful to reach this goal:

1. Introducing different functional groups to zeolite which are capable of binding to a vast range of heavy metal ions.
2. Introducing suitable functional groups to the existing functionalized zeolites to improve their adsorption capacity toward other heavy metals such Hg, Ni, Cd, etc.

References

1. Fu, F. and Q. Wang, *Removal of heavy metal ions from wastewaters: a review*. Journal of environmental management, 2011. **92**(3): p. 407-418.
2. Barakat, M., *New trends in removing heavy metals from industrial wastewater*. Arabian Journal of Chemistry, 2011. **4**(4): p. 361-377.
3. Srivastava, N. and C. Majumder, *Novel biofiltration methods for the treatment of heavy metals from industrial wastewater*. Journal of hazardous materials, 2008. **151**(1): p. 1-8.
4. Sharma, R.K. and M. Agrawal, *Biological effects of heavy metals: an overview*. Journal of environmental Biology, 2005. **26**(2): p. 301-313.
5. <http://2015.igem.org/Team:Bielefeld-CeBiTec/Project/HeavyMetals>.
6. <https://www.epa.gov/dwreginfo/drinking-water-regulatory-information>.
7. <https://www.epa.gov/dwregdev/drinking-water-treatment-technology-unit-cost-models-and-overview-technologies>.
8. Muhammad Mahmood Ibrahim, A.S.S., *Application of natural and modified Zeolites in removing heavy metal Cations from aqueous media: an overview of including parameters affecting the process*. International Journal of Geology, Agriculture and Environmental Sciences 2015. **3**(2).

9. Margeta, K., et al., *Natural zeolites in water treatment-how effective is their use*. 2013: INTECH Open Access Publisher.
10. <http://www.explainthatstuff.com/zeolites.html>., et al.
11. INGLEZAKIS, V.J. and A. Zorpas, *NATURAL ZEOLITES: INDUSTRIAL AND ENVIRONMENTAL APPLICATIONS*. Modelling and Optimization in the Machines Building Field, 2007. **2**.
12. Ordonez, S. and D. Eva, *Basic Zeolites: Structure, preparation and environmental applications*. Handbook of Zeolites: structure, properties and applications, Nova Science Publishers, Inc., New York, USA, 2009: p. 51-66.
13. Figueiredo, H. and C. Quintelas, *Tailored zeolites for the removal of metal oxyanions: Overcoming intrinsic limitations of zeolites*. Journal of hazardous materials, 2014. **274**: p. 287-299.
14. Misaelides, P., *Application of natural zeolites in environmental remediation: A short review*. Microporous and Mesoporous Materials, 2011. **144**(1): p. 15-18.
15. Dyer, A., *An introduction to zeolite molecular sieves*. 1988.
16. Motsi, T., N. Rowson, and M. Simmons, *Adsorption of heavy metals from acid mine drainage by natural zeolite*. International Journal of Mineral Processing, 2009. **92**(1): p. 42-48.

17. Colella, C., *Environmental applications of natural zeolitic materials based on their ion exchange properties*. Natural Microporous Materials in Environmental Technology, 1999: p. 207-224.
18. Berber-Mendoza, M., et al., *Comparison of isotherms for the ion exchange of Pb (II) from aqueous solution onto homoionic clinoptilolite*. Journal of colloid and interface science, 2006. **301**(1): p. 40-45.
19. Neuhoff, P.S., *NATURAL ZEOLITES: OCCURRENCE, PROPERTIES, APPLICATIONS*. 2002, Mineral Soc America.
20. Adinehvand, J., A.S. Rad, and A. Tehrani, *Acid-treated zeolite (clinoptilolite) and its potential to zinc removal from water sample*. International Journal of Environmental Science and Technology, 2016. **13**(11): p. 2705-2712.
21. Sprynskyy, M., et al., *Study of the selection mechanism of heavy metal (Pb²⁺, Cu²⁺, Ni²⁺, and Cd²⁺) adsorption on clinoptilolite*. Journal of colloid and interface science, 2006. **304**(1): p. 21-28.
22. Inglezakis, V.J., M.D. Loizidou, and H.P. Grigoropoulou, *Ion exchange of Pb²⁺, Cu²⁺, Fe³⁺, and Cr³⁺ on natural clinoptilolite: selectivity determination and influence of acidity on metal uptake*. Journal of Colloid and Interface Science, 2003. **261**(1): p. 49-54.
23. Amarasinghe, B. and R. Williams, *Tea waste as a low cost adsorbent for the removal of Cu and Pb from wastewater*. Chemical Engineering Journal, 2007. **132**(1): p. 299-309.

24. Wingenfelder, U., et al., *Removal of heavy metals from mine waters by natural zeolites*. Environmental Science & Technology, 2005. **39**(12): p. 4606-4613.
25. Colella, C., *Ion exchange equilibria in zeolite minerals*. Mineralium Deposita, 1996. **31**(6): p. 554-562.
26. Li, Z., et al., *Sorption of arsenic by surfactant-modified zeolite and kaolinite*. Microporous and Mesoporous Materials, 2007. **105**(3): p. 291-297.
27. Gebremedhin-Haile, T., M. Olguin, and M. Solache-Rios, *Removal of mercury ions from mixed aqueous metal solutions by natural and modified zeolitic minerals*. Water, Air, & Soil Pollution, 2003. **148**(1): p. 179-200.
28. Chojnacki, A., et al., *The application of natural zeolites for mercury removal: from laboratory tests to industrial scale*. Minerals Engineering, 2004. **17**(7): p. 933-937.
29. Doula, M.K., *Simultaneous removal of Cu, Mn and Zn from drinking water with the use of clinoptilolite and its Fe-modified form*. Water Research, 2009. **43**(15): p. 3659-3672.
30. Oliveira, L.C., et al., *Magnetic zeolites: a new adsorbent for removal of metallic contaminants from water*. Water Research, 2004. **38**(17): p. 3699-3704.
31. Athanasiadis, K. and B. Helmreich, *Influence of chemical conditioning on the ion exchange capacity and on kinetic of zinc uptake by clinoptilolite*. Water Research, 2005. **39**(8): p. 1527-1532.

32. Pitcher, S., R. Slade, and N. Ward, *Heavy metal removal from motorway stormwater using zeolites*. Science of the Total Environment, 2004. **334**: p. 161-166.
33. Lee, M.-G., et al., *Conversion of coal fly ash into zeolite and heavy metal removal characteristics of the products*. Korean Journal of Chemical Engineering, 2000. **17**(3): p. 325-331.
34. Molina, A. and C. Poole, *A comparative study using two methods to produce zeolites from fly ash*. Minerals Engineering, 2004. **17**(2): p. 167-173.
35. Hollman, G., G. Steenbruggen, and M. Janssen-Jurkovičová, *A two-step process for the synthesis of zeolites from coal fly ash*. Fuel, 1999. **78**(10): p. 1225-1230.
36. Hui, K. and C.Y.H. Chao, *Effects of step-change of synthesis temperature on synthesis of zeolite 4A from coal fly ash*. Microporous and Mesoporous Materials, 2006. **88**(1): p. 145-151.
37. Park, M., et al., *Molten-salt method for the synthesis of zeolitic materials: II. Characterization of zeolitic materials*. Microporous and Mesoporous Materials, 2000. **37**(1): p. 91-98.
38. Tanaka, H., Y. Sakai, and R. Hino, *Formation of Na-A and-X zeolites from waste solutions in conversion of coal fly ash to zeolites*. Materials Research Bulletin, 2002. **37**(11): p. 1873-1884.

39. Chang, H.-L. and W.-H. Shih, *Synthesis of zeolites A and X from fly ashes and their ion-exchange behavior with cobalt ions*. Industrial & Engineering Chemistry Research, 2000. **39**(11): p. 4185-4191.
40. El-Kamash, A., A. Zaki, and M.A. El Geleel, *Modeling batch kinetics and thermodynamics of zinc and cadmium ions removal from waste solutions using synthetic zeolite A*. Journal of Hazardous Materials, 2005. **127**(1): p. 211-220.
41. Liu, L., et al., *Adsorption of Au (III), Pd (II), and Pt (IV) from aqueous solution onto graphene oxide*. Journal of Chemical & Engineering Data, 2012. **58**(2): p. 209-216.
42. Yu, Y., et al., *Benzene carboxylic acid derivatized graphene oxide nanosheets on natural zeolites as effective adsorbents for cationic dye removal*. Journal of hazardous materials, 2013. **260**: p. 330-338.
43. Zhu, J., et al., *Facile one-pot synthesis of novel spherical zeolite-reduced graphene oxide composites for cationic dye adsorption*. Industrial & Engineering Chemistry Research, 2014. **53**(35): p. 13711-13717.
44. Somerset, V., L. Petrik, and E. Iwuoha, *Alkaline hydrothermal conversion of fly ash precipitates into zeolites 3: the removal of mercury and lead ions from wastewater*. Journal of environmental management, 2008. **87**(1): p. 125-131.

45. Yin, M., et al., *Magnetic self-assembled zeolite clusters for sensitive detection and rapid removal of mercury (II)*. ACS applied materials & interfaces, 2011. **4**(1): p. 431-437.
46. Wan, S., et al., *Rapid and highly selective removal of lead from water using graphene oxide-hydrated manganese oxide nanocomposites*. Journal of hazardous materials, 2016. **314**: p. 32-40.
47. Kim, D.-G., T.T. Nhung, and S.-O. Ko, *Enhanced adsorption of heavy metals with biogenic manganese oxide immobilized on zeolite*. KSCE Journal of Civil Engineering, 2016. **20**(6): p. 2189-2196.
48. Zendehtdel, M., B. Shoshtari-Yeganeh, and G. Cruciani, *Removal of heavy metals and bacteria from aqueous solution by novel hydroxyapatite/zeolite nanocomposite, preparation, and characterization*. Journal of the Iranian Chemical Society, 2016. **13**(10): p. 1915-1930.
49. Shaw, R., et al., *Surface engineered zeolite: An active interface for rapid adsorption and degradation of toxic contaminants in water*. ACS applied materials & interfaces, 2016. **8**(19): p. 12520-12527.
50. Sharifipour, F., et al., *Kinetics and thermodynamics of lead adsorption from aqueous solutions onto Iranian sepiolite and zeolite*. International Journal of Environmental Research, 2015. **9**(3): p. 1001-1010.

51. Gupta, S.S. and K.G. Bhattacharyya, *Immobilization of Pb (II), Cd (II) and Ni (II) ions on kaolinite and montmorillonite surfaces from aqueous medium*. Journal of environmental management, 2008. **87**(1): p. 46-58.
52. Potgieter, J., S. Potgieter-Vermaak, and P. Kalibantonga, *Heavy metals removal from solution by palygorskite clay*. Minerals Engineering, 2006. **19**(5): p. 463-470.
53. Bektaş, N., B.A. Ağım, and S. Kara, *Kinetic and equilibrium studies in removing lead ions from aqueous solutions by natural sepiolite*. Journal of Hazardous materials, 2004. **112**(1): p. 115-122.
54. Shaheen, S.M., A.S. Derbalah, and F.S. Moghanm, *Removal of heavy metals from aqueous solution by zeolite in competitive sorption system*. International Journal of Environmental Science and Development, 2012. **3**(4): p. 362.
55. Kabwadza-Corner, P., E. Johan, and N. Matsue, *pH Dependence of Lead Adsorption on Zeolites*. Journal of Environmental Protection, 2015. **6**(1): p. 45.
56. Buasri, A., et al., *Use of natural clinoptilolite for the removal of lead (II) from wastewater in batch experiment*. Chiang Mai J Sci, 2008. **35**(3): p. 447-456.
57. Payne, K.B. and T.M. Abdel-Fattah, *Adsorption of divalent lead ions by zeolites and activated carbon: effects of pH, temperature, and ionic strength*. Journal of Environmental Science and Health, Part A, 2004. **39**(9): p. 2275-2291.

58. Dursun, S. and A. Pala, *Lead pollution removal from water using a natural zeolite*. J Int Envir Appli & Sci, 2007. **2**(1&2): p. 11-19.
59. Agulanna Albert Chibuzo, C.O.A., Onoh Maxwell Ikechukwu ,Azubuike.K Arinze, *Kinetics and Isotherm Studies on Divalent Lead Ions Adsorption by Zeolite Solution*. International Journal of Novel Research in Engineering and Science, 2016. **3**(1): p. 49-61.
60. Attari, M., *Mercury Removal from Aqueous Solution Using Natural, Synthetic, and Modified Zeolites*. 2015.
61. Kyzas, G.Z., N.A. Travlou, and E.A. Deliyanni, *The role of chitosan as nanofiller of graphite oxide for the removal of toxic mercury ions*. Colloids and Surfaces B: Biointerfaces, 2014. **113**: p. 467-476.
62. Kulkarni, S.J., *Studies and Research on Mercury Removal from Water A Review*. International Journal of Research, 2015. **2**(2): p. 221-225.
63. Tawabini, B., et al., *Removal of mercury from water by multi-walled carbon nanotubes*. Water science and technology, 2010. **61**(3): p. 591-598.
64. Rengaraj, S., K.-H. Yeon, and S.-H. Moon, *Removal of chromium from water and wastewater by ion exchange resins*. Journal of hazardous materials, 2001. **87**(1): p. 273-287.
65. Alyüz, B. and S. Veli, *Kinetics and equilibrium studies for the removal of nickel and zinc from aqueous solutions by ion exchange resins*. Journal of Hazardous Materials, 2009. **167**(1): p. 482-488.

66. Ohzeki, K., et al., *Enrichment of trace amounts of copper as chelate compounds using a finely divided ion-exchange resin*. Analyst, 1990. **115**(1): p. 23-28.
67. Clevenger, T. and J.T. Novak, *RECOVERY OF METALS FROM ELECTROPLATING WASTES*.
68. Veli, S. and B. Pekey, *Removal of copper from aqueous solution by ion exchange resins*. Fresenius Environmental Bulletin, 2004. **13**(3): p. 244-250.
69. Untea, I., E. Tudorache, and C. Florea, *Thermodynamic aspects regarding the ion exchange equilibrium in a system Lewatit MP 500A-K₂CrO₄ solutions*. Revista de Chimie, 2000. **51**(2): p. 123-126.
70. Pabalan, R.T., *Thermodynamics of ion exchange between clinoptilolite and aqueous solutions of Na⁺ K⁺ and Na⁺ Ca²⁺*. Geochimica et Cosmochimica Acta, 1994. **58**(21): p. 4573-4590.
71. <https://www.chemguide.co.uk/inorganic/complexions/whatis.html>.
72. Martell, E., *Chemistry of the metal chelate compounds*. 1952.
73. Farkas, E. and P. Buglyó, *Lead (II) Complexes of Amino Acids, Peptides, and Other Related Ligands of Biological Interest*. Lead: Its Effects on Environment and Health, 2017. **17**: p. 201.
74. Persson, I., et al., *Coordination chemistry study of hydrated and solvated lead (II) ions in solution and solid state*. Inorganic chemistry, 2011. **50**(3): p. 1058-1072.

75. Allen, F.H., *The Cambridge Structural Database: a quarter of a million crystal structures and rising*. Acta Crystallographica Section B: Structural Science, 2002. **58**(3): p. 380-388.
76. Shimoni-Livny, L., J.P. Glusker, and C.W. Bock, *Lone pair functionality in divalent lead compounds*. Inorganic Chemistry, 1998. **37**(8): p. 1853-1867.
77. Mos-Hummel, A., M. Ströbele, and H.-J. Meyer, *A journey through ternary lead chlorido tungstates by thermal scanning*. Dalton Transactions, 2017. **46**(24): p. 7743-7749.
78. Faulconer, E.K., N.V.H. von Reitzenstein, and D.W. Mazyck, *Optimization of magnetic powdered activated carbon for aqueous Hg (II) removal and magnetic recovery*. Journal of hazardous materials, 2012. **199**: p. 9-14.
79. Malamis, S. and E. Katsou, *A review on zinc and nickel adsorption on natural and modified zeolite, bentonite and vermiculite: Examination of process parameters, kinetics and isotherms*. Journal of hazardous materials, 2013. **252**: p. 428-461.
80. Boparai, H.K., M. Joseph, and D.M. O'Carroll, *Kinetics and thermodynamics of cadmium ion removal by adsorption onto nano zerovalent iron particles*. Journal of hazardous materials, 2011. **186**(1): p. 458-465.
81. Dada, A., et al., *Langmuir, Freundlich, Temkin and Dubinin–Radushkevich isotherms studies of equilibrium sorption of Zn²⁺ unto phosphoric acid modified rice husk*. IOSR Journal of Applied Chemistry, 2012. **3**(1): p. 38-45.

82. Gupta, S.S. and K.G. Bhattacharyya, *Kinetics of adsorption of metal ions on inorganic materials: a review*. Advances in Colloid and Interface Science, 2011. **162**(1): p. 39-58.
83. Raji, F. and M. Pakizeh, *Kinetic and thermodynamic studies of Hg (II) adsorption onto MCM-41 modified by ZnCl₂*. Applied Surface Science, 2014. **301**: p. 568-575.
84. Robati, D., *Pseudo-second-order kinetic equations for modeling adsorption systems for removal of lead ions using multi-walled carbon nanotube*. Journal of nanostructure in Chemistry, 2013. **3**(1): p. 55.
85. Hodaifa, G., et al., *Kinetic and thermodynamic parameters of iron adsorption onto olive stones*. Industrial Crops and Products, 2013. **49**: p. 526-534.
86. Armbruster, T., *Clinoptilolite-heulandite: applications and basic research*. Studies in surface science and catalysis, 2001. **135**: p. 13-27.
87. Langella, A., et al., *NH₄⁺, Cu²⁺, Zn²⁺, Cd²⁺ and Pb²⁺ exchange for Na⁺ in a sedimentary clinoptilolite, North Sardinia, Italy*. Microporous and Mesoporous Materials, 2000. **37**(3): p. 337-343.
88. Largitte, L. and R. Pasquier, *A review of the kinetics adsorption models and their application to the adsorption of lead by an activated carbon*. Chemical Engineering Research and Design, 2016. **109**: p. 495-504.
89. Qiu, H., et al., *Critical review in adsorption kinetic models*. Journal of Zhejiang University-Science A, 2009. **10**(5): p. 716-724.

90. Jafari-zare, F. and A. Habibi-yangjeh, *Competitive adsorption of methylene blue and rhodamine B on natural zeolite: thermodynamic and kinetic studies*. Chinese Journal of Chemistry, 2010. **28**(3): p. 349-356.
91. Di Natale, F., et al., *Mercury adsorption on granular activated carbon in aqueous solutions containing nitrates and chlorides*. Journal of hazardous materials, 2011. **192**(3): p. 1842-1850.
92. Hadi, P., et al., *Aqueous mercury adsorption by activated carbons*. Water research, 2015. **73**: p. 37-55.
93. Rodríguez, O., et al., *Concerns on liquid mercury and mercury-containing wastes: A review of the treatment technologies for the safe storage*. Journal of environmental management, 2012. **101**: p. 197-205.
94. Rio, S. and A. Delebarre, *Removal of mercury in aqueous solution by fluidized bed plant fly ash*. Fuel, 2003. **82**(2): p. 153-159.
95. Zhang, F.-S., J.O. Nriagu, and H. Itoh, *Mercury removal from water using activated carbons derived from organic sewage sludge*. Water research, 2005. **39**(2): p. 389-395.
96. Nabais, J.V., et al., *Mercury removal from aqueous solution and flue gas by adsorption on activated carbon fibres*. Applied Surface Science, 2006. **252**(17): p. 6046-6052.

97. Liu, M., et al., *Synthesis, characterization, and mercury adsorption properties of hybrid mesoporous aluminosilicate sieve prepared with fly ash*. Applied surface science, 2013. **273**: p. 706-716.
98. Manohar, D., K.A. Krishnan, and T. Anirudhan, *Removal of mercury (II) from aqueous solutions and chlor-alkali industry wastewater using 2-mercaptobenzimidazole-clay*. Water Research, 2002. **36**(6): p. 1609-1619.
99. Chiarle, S., M. Ratto, and M. Rovatti, *Mercury removal from water by ion exchange resins adsorption*. Water Research, 2000. **34**(11): p. 2971-2978.
100. Nooney, R.I., et al., *Heavy metal remediation using functionalized mesoporous silicas with controlled macrostructure*. Langmuir, 2001. **17**(2): p. 528-533.
101. <https://en.wikipedia.org/wiki/Cystamine>.
102. https://www.wqpmag.com/sites/wqpmag.com/files/16_filtration%20media.indd.pdf.
103. Xu, Q. and W. Zhang, *Next-Generation Graphene-Based Membranes for Gas Separation and Water Purifications*, in *Advances in Carbon Nanostructures*. 2016, InTech.
104. Gehrke, I., A. Geiser, and A. Somborn-Schulz, *Innovations in nanotechnology for water treatment*. Nanotechnology, science and applications, 2015. **8**: p. 1.

105. Rao, G.P., C. Lu, and F. Su, *Sorption of divalent metal ions from aqueous solution by carbon nanotubes: a review*. Separation and Purification Technology, 2007. **58**(1): p. 224-231.
106. Khajeh, M., S. Laurent, and K. Dastafkan, *Nanoadsorbents: classification, preparation, and applications (with emphasis on aqueous media)*. Chemical reviews, 2013. **113**(10): p. 7728-7768.
107. Diallo, M.S., et al., *Dendrimer enhanced ultrafiltration. 1. Recovery of Cu (II) from aqueous solutions using PAMAM dendrimers with ethylene diamine core and terminal NH₂ groups*. Environmental science & technology, 2005. **39**(5): p. 1366-1377.
108. Sadeghi-Kiakhani, M., M. Arami, and K. Gharanjig, *Dye removal from colored-textile wastewater using chitosan-PPI dendrimer hybrid as a biopolymer: Optimization, kinetic, and isotherm studies*. Journal of Applied Polymer Science, 2013. **127**(4): p. 2607-2619.
109. Qu, X., P.J. Alvarez, and Q. Li, *Applications of nanotechnology in water and wastewater treatment*. Water research, 2013. **47**(12): p. 3931-3946.
110. Chiang, A. and K.-j. Chao, *Membranes and films of zeolite and zeolite-like materials*. Journal of Physics and Chemistry of Solids, 2001. **62**(9): p. 1899-1910.
111. Treacy, M.M. and J.B. Higgins, *Collection of simulated XRD powder patterns for zeolites fifth (5th) revised edition*. 2007: Elsevier.

112. Wang, S. and Y. Peng, *Natural zeolites as effective adsorbents in water and wastewater treatment*. Chemical Engineering Journal, 2010. **156**(1): p. 11-24.
113. Bukhari, S.S., et al., *Conversion of coal fly ash to zeolite utilizing microwave and ultrasound energies: a review*. Fuel, 2015. **140**: p. 250-266.
114. Sepehr, M.N., et al., *Removal of hardness agents, calcium and magnesium, by natural and alkaline modified pumice stones in single and binary systems*. Applied Surface Science, 2013. **274**: p. 295-305.
115. Kazemian, H., H. Zakeri, and M. Rabbani, *Cs and Sr removal from solution using potassium nickel hexacyanoferrate impregnated zeolites*. Journal of radioanalytical and nuclear chemistry, 2006. **268**(2): p. 231-236.
116. Bukhari, S.S., et al., *A comparative study using direct hydrothermal and indirect fusion methods to produce zeolites from coal fly ash utilizing single-mode microwave energy*. Journal of materials science, 2014. **49**(24): p. 8261-8271.
117. Hui, K., C.Y.H. Chao, and S. Kot, *Removal of mixed heavy metal ions in wastewater by zeolite 4A and residual products from recycled coal fly ash*. Journal of Hazardous Materials, 2005. **127**(1): p. 89-101.
118. Katsou, E., et al., *Regeneration of natural zeolite polluted by lead and zinc in wastewater treatment systems*. Journal of hazardous materials, 2011. **189**(3): p. 773-786.

119. Turan, N.G. and O. Ozgonenel, *The design and implementation of adsorptive removal of Cu (II) from leachate using ANFIS*. The Scientific World Journal, 2013. **2013**.
120. Lagadic, I.L., M.K. Mitchell, and B.D. Payne, *Highly effective adsorption of heavy metal ions by a cystamine-functionalized magnesium phyllosilicate clay*. Environmental science & technology, 2001. **35**(5): p. 984-990.
121. Trgo, M., et al. *Mercury ions capture by natural and iron-modified zeolite-influence of solid/liquid ratio*. in *5th Serbian-Croatian-Slovenian Symposium on Zeolites*. 2013.
122. White, R.J., et al., *Supported metal nanoparticles on porous materials. Methods and applications*. Chemical Society Reviews, 2009. **38**(2): p. 481-494.
123. Stefanović, Š.C., et al., *Structural investigation of Zn 2+ sorption on clinoptilolite tuff from the Vranjska Banja deposit in Serbia*. Microporous and Mesoporous Materials, 2007. **105**(3): p. 251-259.
124. Li, Z., et al., *Chromate transport through columns packed with surfactant-modified zeolite/zero valent iron pellets*. Chemosphere, 2007. **68**(10): p. 1861-1866.
125. Stefanakis, A.I., et al., *Effluent quality improvement of two pilot-scale, horizontal subsurface flow constructed wetlands using natural zeolite*

- (*clinoptilolite*). *Microporous and Mesoporous Materials*, 2009. **124**(1): p. 131-143.
126. Bosinceanu, R. and N. Sulitanu, *Synthesis and characterization of FeO(OH)/Fe₃O₄ nanoparticles encapsulated in zeolite matrix*. *J. Optoelectron. Adv. Mater*, 2008. **10**(12): p. 3482-3486.
127. Celis, R., M.C. Hermosin, and J. Cornejo, *Heavy metal adsorption by functionalized clays*. *Environmental science & technology*, 2000. **34**(21): p. 4593-4599.
128. Mercier, L. and T.J. Pinnavaia, *Heavy metal ion adsorbents formed by the grafting of a cystamine functionality to mesoporous silica molecular sieves: factors affecting Hg (II) uptake*. *Environmental Science & Technology*, 1998. **32**(18): p. 2749-2754.
129. Ritchie, S.M., et al., *Polycysteine and other polyamino acid functionalized microfiltration membranes for heavy metal capture*. *Environmental science & technology*, 2001. **35**(15): p. 3252-3258.
130. <http://www.water-research.net/index.php/standards/primary-standards>.
131. Pearson, R.G., *Hard and soft acids and bases, HSAB, part I: Fundamental principles*. *Journal of Chemical Education*, 1968. **45**(9): p. 581.
132. Pearson, R.G., *Hard and soft acids and bases, HSAB, part II: Underlying theories*. *Journal of Chemical Education*, 1968. **45**(10): p. 643.

133. Castaldi, P., et al., *Thermal and spectroscopic studies of zeolites exchanged with metal cations*. Journal of Molecular Structure, 2005. **734**(1-3): p. 99-105.
134. Gebremedhin-Haile, T., M. Olguin, and M. Solache-Rios, *Removal of mercury ions from mixed aqueous metal solutions by natural and modified zeolitic minerals*. Water, air, and soil pollution, 2003. **148**(1-4): p. 179-200.
135. Erdem, E., N. Karapinar, and R. Donat, *The removal of heavy metal cations by natural zeolites*. Journal of colloid and interface science, 2004. **280**(2): p. 309-314.
136. Langmuir, I., *The adsorption of gases on plane surfaces of glass, mica and platinum*. Journal of the American Chemical society, 1918. **40**(9): p. 1361-1403.
137. Foo, K.Y. and B.H. Hameed, *Insights into the modeling of adsorption isotherm systems*. Chemical engineering journal, 2010. **156**(1): p. 2-10.
138. Zeldowitsch, J., *Adsorption site energy distribution*. Acta phys. chim. URSS, 1934. **1**: p. 961-973.
139. Edzwald, J.K., *Water Quality and Treatment A Handbook on Drinking Water*. 2010: McGrawHill.
140. Crittenden, J.C., et al., *MWH's water treatment: principles and design*. 2012: John Wiley & Sons.

141. Giles, C.H., D. Smith, and A. Huitson, *A general treatment and classification of the solute adsorption isotherm. I. Theoretical*. Journal of colloid and interface science, 1974. **47**(3): p. 755-765.
142. Limousin, G., et al., *Sorption isotherms: a review on physical bases, modeling and measurement*. Applied Geochemistry, 2007. **22**(2): p. 249-275.
143. Helfferich, F.G., *Ion exchange*. 1995: Courier Corporation.
144. Helfferich, F.G., *Ion exchange*. 1962: Courier Corporation.
145. Collins, F.C. and G.E. Kimball, *Diffusion-controlled reaction rates*. Journal of colloid science, 1949. **4**(4): p. 425-437.
146. Beyki, M.H. and F. Shemirani, *Dual application of facilely synthesized Fe₃O₄ nanoparticles: fast reduction of nitro compound and preparation of magnetic polyphenylthiourea nanocomposite for efficient adsorption of lead ions*. RSC Advances, 2015. **5**(28): p. 22224-22233.
147. Suslick, K.S. and W.L. Nyborg, *Ultrasound: its chemical, physical and biological effects*. 1990, ASA.
148. Dhas, N.A., A. Zaban, and A. Gedanken, *Surface synthesis of zinc sulfide nanoparticles on silica microspheres: sonochemical preparation, characterization, and optical properties*. Chemistry of materials, 1999. **11**(3): p. 806-813.
149. Suslick, K.S., et al., *Sonochemical synthesis of amorphous iron*. nature, 1991. **353**(6343): p. 414.

150. Wang, H., et al., *Preparation of copper monosulfide and nickel monosulfide nanoparticles by sonochemical method*. Materials Letters, 2002. **55**(4): p. 253-258.
151. Arul Dhas, N., H. Cohen, and A. Gedanken, *In situ preparation of amorphous carbon-activated palladium nanoparticles*. The Journal of Physical Chemistry B, 1997. **101**(35): p. 6834-6838.
152. Hyeon, T., M. Fang, and K.S. Suslick, *Nanostructured molybdenum carbide: sonochemical synthesis and catalytic properties*. Journal of the American Chemical Society, 1996. **118**(23): p. 5492-5493.
153. Shafi, K.V., et al., *Sonochemical preparation of nanosized amorphous NiFe₂O₄ particles*. The Journal of Physical Chemistry B, 1997. **101**(33): p. 6409-6414.
154. Gorai, S. and S. Chaudhuri, *Sonochemical synthesis and characterization of cage-like β -indium sulphide powder*. Materials chemistry and physics, 2005. **89**(2-3): p. 332-335.
155. Dhas, N.A. and A. Gedanken, *Characterization of sonochemically prepared unsupported and silica-supported nanostructured pentavalent molybdenum oxide*. The Journal of Physical Chemistry B, 1997. **101**(46): p. 9495-9503.
156. Anderson, P. and T.H. Christensen, *Distribution coefficients of Cd, Co, Ni, and Zn in soils*. Journal of soil science, 1988. **39**(1): p. 15-22.

157. Gomes, P.C., et al., *Selectivity sequence and competitive adsorption of heavy metals by Brazilian soils*. Soil Science Society of America Journal, 2001. **65**(4): p. 1115-1121.
158. Shaheen, S.M., et al., *Distribution coefficient of copper in different soils from Egypt and Greece*. Communications in soil science and plant analysis, 2009. **40**(1-6): p. 214-226.
159. Shaheen, S. and C. Tsadilas, *Sorption of cadmium and lead by acidic Alfisols as influenced by fly ash and sewage sludge application*. Pedosphere, 2010. **20**(4): p. 436-445.
160. Tsadilas, C., et al., *Influence of fly ash application on copper and zinc sorption by acidic soil amended with sewage sludge*. Communications in soil science and plant analysis, 2009. **40**(1-6): p. 273-284.
161. Covelo, E., F. Vega, and M. Andrade, *Competitive sorption and desorption of heavy metals by individual soil components*. Journal of Hazardous Materials, 2007. **140**(1-2): p. 308-315.
162. Shaheen, S.M., *Sorption and lability of cadmium and lead in different soils from Egypt and Greece*. Geoderma, 2009. **153**(1-2): p. 61-68.
163. Shaheen, S.M., C.D. Tsadilas, and K.M. Eskridge, *Effect of common ions on phosphorus sorption and lability in Greek Alfisols with different pH*. Soil Science, 2009. **174**(1): p. 21-26.

164. Saha, U., S. Taniguchi, and K. Sakurai, *Simultaneous adsorption of cadmium, zinc, and lead on hydroxyaluminum-and hydroxyaluminosilicate-montmorillonite complexes*. Soil Science Society of America Journal, 2002. **66**(1): p. 117-128.
165. Appel, C. and L. Ma, *Concentration, pH, and surface charge effects on cadmium and lead sorption in three tropical soils*. Journal of Environmental Quality, 2002. **31**(2): p. 581-589.
166. Lata, S., P. Singh, and S. Samadder, *Regeneration of adsorbents and recovery of heavy metals: a review*. International journal of environmental science and technology, 2015. **12**(4): p. 1461-1478.
167. Bolster, C.H. and G.M. Hornberger, *On the use of linearized Langmuir equations*. Soil Science Society of America Journal, 2007. **71**(6): p. 1796-1806.
168. Bothwell, M. and L. Walker, *Evaluation of parameter estimation methods for estimating cellulase binding constants*. Bioresource technology, 1995. **53**(1): p. 21-29.
169. Azizian, S. and H. Bashiri, *Adsorption kinetics at the solid/solution interface: statistical rate theory at initial times of adsorption and close to equilibrium*. Langmuir, 2008. **24**(20): p. 11669-11676.

170. Ward, C., R. Findlay, and M. Rizk, *Statistical rate theory of interfacial transport. I. Theoretical development*. The Journal of Chemical Physics, 1982. **76**(11): p. 5599-5605.
171. *CRC Handbook of Chemistry and Physics. 92nd Edition*. 2012, International Institute of Anticancer Research.
172. Umpleby II, R.J., et al., *Application of the Freundlich adsorption isotherm in the characterization of molecularly imprinted polymers*. Analytica Chimica Acta, 2001. **435**(1): p. 35-42.

Curriculum vitae

MOHSEN HAJIPOUR MANJILI

(BSc, MSc, Ph.D.)

Cell Phone: (414) 204 3719

Email: hajipou2@uwm.edu

EDUCATION

Ph.D. in Materials Science and Engineering (2013-2018)

Material Science and Engineering Department,
University of Wisconsin-Milwaukee, USA.

Master of Science in Extractive Metallurgy (2010-2012)

Material Science and Engineering Department,
Sharif University of Technology, Tehran, Iran.

Bachelor of Materials Science and Engineering (2005-2010)

Material Science and Engineering Department,
Sharif University of Technology, Tehran, Iran.

JOURNAL PAPERS

- Mohsen H. Manjili, Mohammad Halal. "Removal of Non-Metallic Inclusion from Nickel Based Superalloys by Electromagnetic Levitation Melting in Slag", *Metallurgical and Materials Transactions B*, 2017.
- Chang-SooKim, Kyu Cho, Mohsen H Manjili, and Marjan Nezafati , " Mechanical performance of particulate-reinforced Al metal-matrix Composites (MMNs) and Al metal-matrix nanocomposites (MMNCs)", *Journal of materials science*, 2017.

LIST OF PUBLICATIONS AND ATTENDED CONFERENCES

- Mohsen Manjili, M. Silva "Fabrication of Novel Porous Materials for the Removal of Mercury from Wastewater", 6th Annual IEEE Conference on Technologies for Sustainability, Sus Tech 2018, Nov 11-13, Long Beach, CA, USA
- Mohsen Manjili, M. Silva, D. Garman, "Novel Porous Materials for the Removal of Heavy Metals from Water", (poster presentation) Navigating the Future of Water Conference, October 18 – 21, 2017, Milwaukee, Wisconsin
- Amir Kordijazi, Mohsen H. Manjili, "Corrosion Resistance of Ni-P-Zn Alloy Deposit Coated Using a Sulfate Electroless Bath", (Oral Presentation) TMS 146th Annual Meeting & Exhibition, February 26- March 2, 2017, San Diego, California.
- Mohsen H. Manjili, M. Shaker, M. Hosseinzadeh, " TiO₂-CeO₂ Nano Crystalline powders and Thin Films by an Aqueous Sol-Gel Process: Effect of Ce:Ti Molar Ratio on Microstructure and Physical Properties", (Oral Presentation) TMS 145th Annual Meeting & Exhibition, February 14-18,2016, Nashville, Tennessee.
- A. Vahid Mohammadi, M. Halali, M. Hajipour, "Effect of Cooling Gas Type on Synthesis of Ultra-High Pure Titanium Nanoparticles by Electromagnetic Levitation Melting Gas Condensation", 3rd international Conference on nanotechnology: Fundamentals and Applications (ICNFA 2012) proceedings, Paper No.162, Pages 162-1 to 162-6, 2012.

- A. Vahid Mohammadi, M. Halali, M. Hajipour, "Synthesis of Pure Titanium Nanoparticles by Electromagnetic Levitation Melting Gas Condensation" (In Persian), New and Advanced Materials International Congress, Esfahan, Iran, 30-31 May, 2012.
- A. Vahid Mohammadi, M. Halali, M. Hajipour, "Synthesis of Pure Titanium Nanoparticles by Electromagnetic Levitation Melting Gas Condensation" (Poster Presentation), New and Advanced Materials International Congress, Esfahan, Iran, 30-31 May, 2012.
- M. Hajipour, M. Halali, A. Vahid Mohammadi, "Refining the nickel based superalloys by electromagnetic levitation in slag process", (Poster Presentation, in Persian), 1st Int'l Conference on Metallurgy, Foundry Engineering, Tehran, Iran, Nov. 2012.
- M. Shaker, M. Hajipour, N. Soltani, "Synthesis an discussion about structure and properties of TiO₂-CeO₂ nanopowder and nano thin film" , (Poster Presentation, in Persian), 1st Int'l Conference on Metallurgy, Foundry Engineering, Tehran, Iran, Nov. 2012.

TEACHING EXPERIENCES

- **Instructor** in Thermodynamics of materials, Materials Science and Engineering Department, UW-Milwaukee.
- **Teaching assistant** in Engineering Materials Lab, Materials Science and Engineering Department, UW-Milwaukee (achieved highest instructor score in Engineering Department, Fall-2015 semester).
- **Teaching assistant** in Hydrometallurgical Processes in Metal Extraction Lab, Materials Science and Engineering Department, Sharif University of Technology.
- **Teaching assistant** in Pyrometallurgical Processes in Metal Extraction Lab, Materials Science and Engineering Department, Sharif University of Technology.

WORKING EXPERIENCES

- Research assistant at Global Water Center (GWC), US, 2017-now.
- Research engineer at R&D Department, Mehrava Co. IRAN, (2011-2013)
- Metal forming engineer, Saipa Press Co. IRAN, (2010-2011)
- Polymer engineer in medical and laboratory products, PIP, Iran (2007-2010)

CERTIFICATES

- Project Management Essentials, Milwaukee, WI, US (Feb-2017)

EXPERIMENTAL SKILLS

- Materials analysis and characterizations tests: X Ray Diffraction (XRD), X Ray Fluorescence (XRF), atomic Absorption (AA), Induced Coupled Plasma Mass Spectrometry (ICP-MS), TGA, DSC, DMA, Raman Spectroscopy, FTIR, BET, Energy dispersive spectroscopy (EDS).
- Microscopy: Scanning Electron Microscopy (SEM), and Optical Microscope.

COMPUTER SKILLS

- Operating System: **Windows 98/2000/XP/VISTA/Seven, Ten.**
- Other Software: **Abaqus, Ansys, Materials Studio, Microsoft office, AutoCAD, Design X'pert, Minitab, DOE**
- Programming languages: **Matlab, Python**

HONORS

- Among top 1% of the all participants in Concour Exam, 2005.
- Among top 10% of the all participants in Master's Degree Entrance Examination, 2010.
- The 3rd in ranking in Master's program, Extractive Metallurgy, Materials Science and Engineering Department, Sharif University of Technology
- The 3rd place in the college of engineering and applied science's 10th annual Student Research Poster Competition, 2018.

HOBBIES

Sport: Soccer, Volleyball